Aus dem Institut für Molekularbiologie und Tumorforschung
Geschäftsführender Direktor: Prof. Dr. Rolf Müller
des Fachbereichs Medizin der Philipps-Universität Marburg

Functional analysis of the histone arginine methyltransferase PRMT6

Inaugural-Dissertation
zur Erlangung des Doktorgrades der Naturwissenschaften
(Dr. rer. nat.)

dem Fachbereich Medizin der Philipps-Universität Marburg
vorgelegt von

Stefanie Riedl

aus Jena, Deutschland

Marburg, 2014

Angenommen vom Fachbereich Medizin der Philipps-Universität Marburg am:
15.12.2014

Gedruckt mit Genehmigung des Fachbereichs.

Dekan:	Prof. Dr. Helmut Schäfer
Referent:	Prof. Dr. Uta-Maria Bauer
1. Korreferent:	Prof. Dr. Lienhard Schmitz

TABLE OF CONTENTS

LIST OF FIGURES

LIST OF TABLES

1 SUMMARY

1.1 Abstract

Aberrant expression of several PRMTs is linked to the pathogenesis of human cancer. PRMTs catalyse the arginine methylation of many substrates, which are implicated in cancer development, progression and aggressiveness. In this context, only few studies investigated PRMT6 so far and its possible role in tumourigenesis and the control of cellular processes, which could also be deregulated in human cancer by PRMT6. Hence, the present study analysed the expression of PRMT6 in murine lung cancer, tried to reveal the role of PRMT6 in cell proliferation and senescence and continued the validation of putative interaction partners of PRMT6.

In the first part of this thesis, immunohistochemical (IHC) stainings demonstrated that Prmt6 protein levels are predominantly increased in lung tumour cells compared to healthy tissue using the LLC1 and $Kras^{LA2}$ mouse models. The second part of this thesis showed that PRMT6 negatively regulates the transcriptional expression of the tumour suppressor genes *CDKN1A* and *p16-INK4A*. Both are direct target genes of PRMT6, whereby the corresponding histone mark H3R2me2a is exclusively enriched at the *CDKN1A* gene. Knockdown of *PRMT6* results in proliferation defects of several transformed cell lines and induces a senescent phenotype in non-transformed human diploid fibroblasts. Furthermore, PRMT6 was found to inhibit the onset of oncogene-induced senescence (OIS), in which CDKN1A is an activator of the senescent phenotype. In the third part of this thesis, PRMT6 was shown to interact with PCNA, DDB1 and DDB2. These interactors are subunits of the CUL4A-RING ubiquitin E3-ligase complex (CRL4) and hint to possible novel cellular functions of PRMT6 in the ubiquitylation processes either after DNA damage or during replication and transcription.

In summary, the present study reveals that PRMT6 is overexpressed in murine lung cancer. It uncovers novel functional aspects of PRMT6 being a positive regulator of proliferation and negative regulator of senescence by transcriptional repression of

tumour suppressor genes. Finally, it opens up a field of so far undescribed possible functions of PRMT6 by validation of novel interaction partners of PRMT6.

1.2 Zusammenfassung

Die aberrante Expression mehrerer PRMTs ist mit der Entstehung von humanem Krebs verknüpft. PRMTs katalysieren die Arginin-Methylierung vieler Substrate, die in der Krebsentstehung, dessen Verlauf und Aggressivität verwickelt sind. In diesem Zusammenhang untersuchten bisher nur wenige Studien PRMT6 und seine mögliche Rolle in der Tumorgenese und in der Kontrolle zellulärer Prozesse, die ebenfalls in humanem Krebs durch PRMT6 dereguliert sein können. Daher analysierte die vorliegende Arbeit die Expression von PRMT6 in murinem Lungenkrebs, versuchte die Rolle von PRMT6 in der Zell-Proliferation und Seneszenz aufzudecken und setzte die Validierung potentieller PRMT6-Interaktionspartner fort.

Im ersten Teil dieser Arbeit zeigten immunhistochemische Färbungen, dass die Prmt6 Proteinspiegel vorwiegend in Lungen-Tumor-Zellen im Vergleich zu gesundem Gewebe unter Verwendung der LLC1 und $Kras^{LA2}$ Mausmodelle erhöht sind. Der zweite Teil dieser Arbeit bewies, dass PRMT6 die transkriptionelle Expression der Tumorsuppressorgene *CDKN1A* und *p16-INK4A* negativ regulierte. Beides sind direkte Zielgene von PRMT6, wobei das entsprechende Histon-Mark H3R2me2a ausschließlich am *CDKN1A*-Gen angereichert ist. Der Knockdown von *PRMT6* resultiert in Proliferationsdefekten mehrerer transformierter Zelllinien und induziert einen seneszenten Phänotyp in nicht-transformierten humanen diploiden Fibroblasten. Darüber hinaus wurde für PRMT6 gefunden, dass es die Entstehung onkogen-induzierter Seneszenz (OIS) inhibiert, in welcher CDKN1A ein Aktivator des seneszenten Phänotyps ist. Im dritten Teil dieser Arbeit wurde gezeigt, dass PRMT6 mit PCNA, DDB1 und DDB2 interagiert. Diese Interaktionspartner sind Untereinheiten des CUL4A-RING Ubiquitin E3-Ligase Komplexes (CRL4) und deuten auf mögliche neue zelluläre Funktionen von PRMT6 in Ubiquitylierungsprozessen entweder nach DNA-Schaden oder während der Replikation und Transkription hin.

Zusammenfassend deckt die vorliegende Arbeit eine erhöhte Expression von PRMT6 in murinem Lungenkrebs auf. Sie legt neue funktionelle Aspekte von PRMT6 als positiver Regulator der Proliferation und als negativer Regulator der Seneszenz durch die

transkriptionelle Repression von Tumorsuppressorgenen dar. Abschließend erschließt sie aufgrund der Validierung neuer Interaktionspartner von PRMT6 ein Feld bisher unbeschriebener, denkbarer Funktionen von PRMT6.

2 INTRODUCTION

2.1 Chromatin structure and post-translational modifications (PTMs)

The nucleus in eukaryotic cells was first described by the botanist Robert Brown in 1831. It has a distinct, nonetheless very dynamic structure and contains the DNA as carrier of genetic information. Genomic DNA is highly condensed in form of chromatin, which is organised in euchromatin and heterochromatin (Lamond and Earnshaw, 1998). Repeating units of nucleosomes build the platform of chromatin organisation and allow a first degree of chromosomal compaction (Rothbart and Strahl, 2014). The nucleosome consists of 1.65 superhelical turns of 147 bp DNA wrapped around an octamer of core histone proteins, one histone H3/H4 tetramer and two histone H2A/H2B dimers (Harshman et al., 2013; Li et al., 2007; Luger et al., 1997). Binding of the linker histone H1 to the nucleosome and the linker DNA, which enters and exits the core particle, stabilises higher-order chromatin structures (Finch and Klug, 1976; Thoma et al., 1979). Various non-histone proteins, such as DNA polymerase, transcription factors, co-regulators or chromatin remodelers, can bind to the nucleosome and function as structural adapters. For example, the adapter protein HP1 is the best known heterochromatin protein in higher eukaryotes, which was first described in Drosophila (James and Elgin, 1986; Lamond and Earnshaw, 1998). In addition, numerous existing histone variants, such as H2AZ or H3.3, increase dynamics of chromatin structure and are involved in transcriptional regulation (Mariño-Ramírez et al., 2005).

Histones are small basic proteins rich in lysine and arginine residues, which are structured in a flexible, charged histone tail (N-terminal part) and a globular core domain associated with DNA (Jenuwein and Allis, 2001). Post-translational modifications (PTMs) of histones are not restricted to histone tails. They also occur in the core domain of histones (Tropberger and Schneider, 2010). Common types of these PTMs are acetylation, phosphorylation, ubiquitylation and methylation (Bhaumik et al., 2007; Li et al., 2007). Other, less frequent chromatin modifications are SUMOylation, ADP-ribosylation, deimination and proline isomerisation (Kouzarides,

2007). PTMs of histones on the same or adjacent histone tails act in an individual or combinatorial manner. The interplay of PTMs at the same histone is called *cis*-interaction and on adjacent histones *trans*-interaction (Rothbart and Strahl, 2014). This interaction indirectly influences downstream cellular events, such as gene activation or repression by binding of "reader"-proteins harbouring for example PHD fingers or other regulatory domains, such as Tudor-, MBT-, Bromo- or Chromodomains (Maurer-Stroh et al., 2003). Alternatively, PTMs on histones can directly regulate chromatin characteristics, whereby the interaction between DNA and histone octamer is influenced. For example, acetylation of lysine residues generate a recognition site for Bromodomain containing proteins that regulate chromatin structure and gene expression (Dhalluin et al., 1999; Seet et al., 2006). These processes contribute to the shaping of the epigenetic landscape and form the "histone code" (Imhof and Becker, 2001; Jenuwein and Allis, 2001; Strahl and Allis, 2000). Typical histone modifications, which are associated with active transcription, are di- or trimethylation of H3K4 (H3K4me2, H3K4me3) and acetylation of H3K9 (H3K9ac). Trimethylation of H3K27 (H3K27me3) is a mark of repressed genes (Li et al., 2007), while trimethylation of H3K9 and H4K20 (H3K9me3, H4K20me3) occur at pericentric heterochromatin (Muramatsu et al., 2013).

2.2 Protein arginine methyltransferases (PRMTs)

2.2.1 Classification of PRMTs

Protein methylation is a common form of PTMs. It was first described by Paik and Kim (Paik and Kim, 1967, 1968) and typically occurs on substrates with lysine and arginine residues (Lee et al., 2005a). For example, almost 2% of all arginines in nuclear protein fractions isolated from rat liver were found to be methylated (Boffa et al., 1977). Protein methylation on arginine residues is catalysed by the family of protein arginine methyltransferases (PRMTs).

PRMTs are classified into type I, II and III enzymes based on their reaction products as depicted in Figure 1 (Baldwin et al., 2014; Yang and Bedford, 2013). In a first step, they

promote the covalent addition of a methyl group on one of the terminal (or ω) guanidino nitrogen atoms of arginine residues (type III PRMTs). This product is called ω-N^G-monomethylarginine (MMA) and can be converted into ω-N^G,N^G-asymmetric dimethylarginine (ADMA) by type I enzymes, which add another methyl group to the same nitrogen in a second step. Alternatively, a ω-N^G,N'^G-symmetric dimethylarginine (SDMA) can be generated by type II PRMTs, which add another methyl group to a different terminal nitrogen atom. The co-substrate S-adenosyl-L-methionine (AdoMet) functions as methyl group donor and is metabolised to methylarginine and S-adenosylhomocysteine (AdoHcy) (Bedford and Richard, 2005). In yeast, a type IV PRMT (Rmt2) has been reported to catalyse the formation of δ-N^G-monomethylarginine at an internal guanidine nitrogen atom (Wang and Li, 2012; Zobel-Thropp et al., 1998).

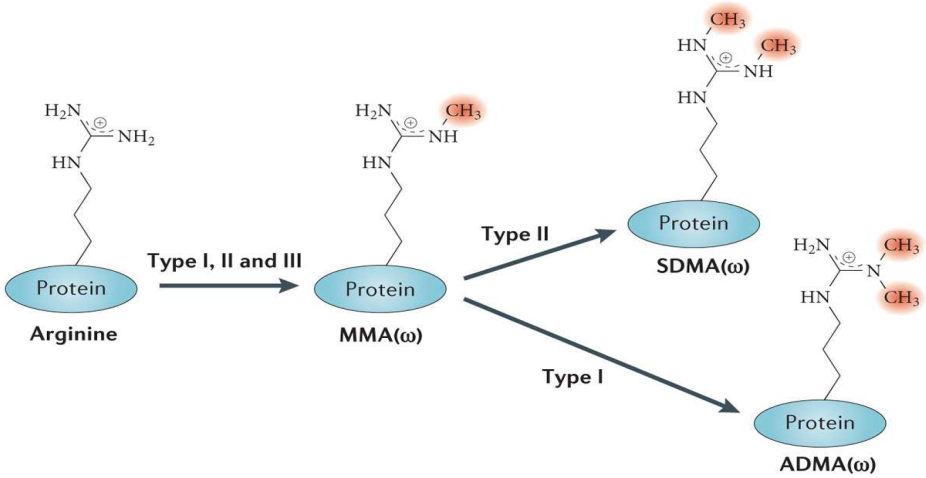

Figure 1: Schematic depiction of arginine methylation performed by PRMTs.

Abbreviations used in the figure are MMA: ω-N^G-monomethylarginine, ADMA: ω-N^G,N^G-asymmetric dimethylarginine and SDMA: ω-N^G,N'^G-symmetric dimethylarginine. Presented from (Yang and Bedford, 2013).

Nine PRMTs (PRMT1 - PRMT9) have been described in mammals to date (Yang and Bedford, 2013). PRMT1, PRMT2, PRMT3, PRMT4 (CARM1), PRMT6 and PRMT8 belong to the class of type I enzymes. PRMT1 possesses the predominant activity (about 85%) in mammalian cells (Tang et al., 2000a). The group of type II PRMTs consists of PRMT5 (JBP1) and potentially PRMT9 (Cook et al., 2006). Recent studies have shown that PRMT7 is the only bona fida type III enzyme without type II activity (Feng et al., 2013;

Miranda et al., 2004; Zurita-Lopez et al., 2012). A study by Cook and colleagues indicated that purified PRMT9 exhibits *in vitro* methylation activity on several substrates by performing SDMA modifications, but an *in vivo* activity for PRMT9 has not been properly clarified (Cook et al., 2006).

PRMTs are evolutionary conserved enzymes in eukaryotes (Pal and Sif, 2007). For example, *Saccharomyces cerevisiae* possesses four PRMTs with HMT1 (also known as Rmt1) being the major type I and HSL7 (also known as Skb1) being a type II enzyme (Boisvert et al., 2005). *Drosophila melanogaster* contains DART1 to DART9 (Boulanger et al., 2004). The protozoan parasite *Trypanosoma brucei* encodes five PRMTs, including two type I (TbPRMT1, TbPRMT6), one type II (TbPRMT5), one type III (TbPRMT7) enzyme, and one enzyme that still remains uncharacterised (Fisk et al., 2010; Wang et al., 2014).

Generally, methylation substrates of PRMTs are not only histones, but also a large amount of non-histone proteins. The majority of methylation events occurs on substrates, such as RNA-binding proteins (including hnRNPs, fibrillarin and nucleolin), enriched in GAR (glycine-arginine-rich) motifs (Liu and Dreyfuss, 1995; Najbauer et al., 1993). However, PRMT4 is not able to methylate arginines within GAR motifs. PRMTs possess various functions in cellular processes, such as transcriptional regulation, mRNA splicing, genomic stability, DNA damage repair as well as signal transduction (Bedford and Clarke, 2009; Bedford and Richard, 2005; Di Lorenzo and Bedford, 2011; Yang and Bedford, 2013).

2.2.2 Structure of PRMTs

All PRMTs contain an AdoMet binding and a substrate binding (barrel-like) domain, as shown in Figure 2. Between the two domains lies the active site pocket that is formed by the double-E (glutamic acid-glutamic acid) and THW (threonine-histidine-tryptophan) loop and captures the target arginine (Zhang and Cheng, 2003). The substrate binding domain is unique for the PRMT family, in contrast to the AdoMet binding domain,

which is also found in other AdoMet-dependent methyltransferases (Cheng and Roberts, 2001). Additionally, the sequence motifs I, post-I, II, double-E loop and III of the AdoMet binding domain are highly conserved between all PRMTs. The same applies to the invariant THW loop within the substrate binding domain at the respective C-terminus. All PRMTs harbour a dimerisation arm that is necessary for the AdoMet binding and enzymatic activity, but it exists a high diversity concerning length and composition of this arm (Cheng et al., 2011). In general, homodimerisation is a conserved feature of PRMTs (Zhang et al., 2000). However, the type III PRMT7 from *Caenorhabditis elegans* possesses an exceptional character because it was found that PRMT7 forms a homodimer-like structure by a single monomer (Hasegawa et al., 2014).

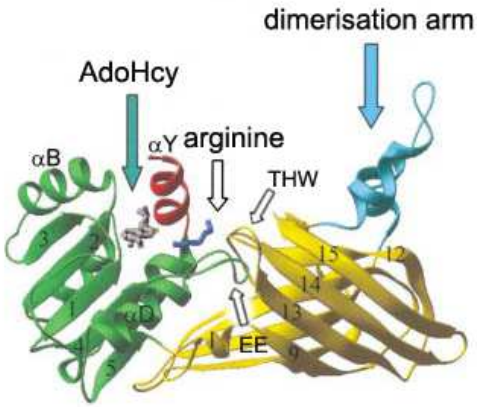

Figure 2: Schematic depiction of the crystal structure of rat PRMT1.

The catalytic structure of rat PRMT1 with its substrate arginine and S-adenosylhomocysteine (AdoHcy) is depicted. The AdoMet binding (green) and substrate binding (yellow) domains are indicated. Additionally, the dimerisation arm (blue), the double-E (EE) and THW loop are shown (see arrows). Adapted from (Zhang and Cheng, 2003).

The N- and C-termini differ between individual PRMTs. For example, PRMT2 contains a SH3-domain in the N-terminus, which is essential for its binding to the hnRNP protein E1B-AP5 (Kzhyshkowska et al., 2001). PRMT3 harbours a single zinc-finger domain in the N-terminal part that recognises RNA-associated substrates (Frankel and Clarke, 2000). PRMT4 contains an autonomous activation domain in the C-terminus, which is required for its co-activator function (Teyssier et al., 2002), while PRMT7 harbours two copies of the central catalytic domain caused by gene duplication (Miranda et al.,

2004). Moreover, PRMT8 possesses an N-terminal myristoylation motif. PRMT8 is exclusively expressed in the brain and is anchored to the plasma membrane by myristoylation (Kousaka et al., 2009; Lee et al., 2005b). In case of PRMT9, four splice variants were identified (Cook et al., 2006). PRMT9 isoform 1 harbours an F-box domain in the N-terminal part to associate with Skp1 and the ubiquitin ligase complex. PRMT9 also contains a zinc-finger domain in the C-terminus, which mediates substrate binding to this complex (Cardozo and Pagano, 2004). Isoform 2 and 3 lack the zinc finger motif, whereas isoform 4 lacks both the N- and C-terminal domains.

To date, the crystal structures of rat PRMT1 and its yeast homologue HMT1, rat PRMT3, rat PRMT4, human PRMT5, PRMT7 in *Mus musculus* and *Caenorhabditis elegans* and AbPRMT10 in *Arabidopsis thaliana* have been analysed (Antonysamy et al., 2012; Cheng et al., 2011; Cura et al., 2014; Ho et al., 2013; Sun et al., 2011; Troffer-Charlier et al., 2007; Weiss et al., 2000; Yue et al., 2007; Zhang and Cheng, 2003; Zhang et al., 2000). Recently, the first crystal structure of PRMT6 from protozoan *Trypanosoma brucei* (apo-TbPRMT6) has been published (Wang et al., 2014). TbPRMT6 shares only a 31% amino acid sequence identity with its human PRMT6 homologue. Although there are numerous unique structural features, the crystal structure of TbPRMT6 reveals a high overlap in all conserved structures with other PRMTs, including its ability to form a homodimer (Figure 3).

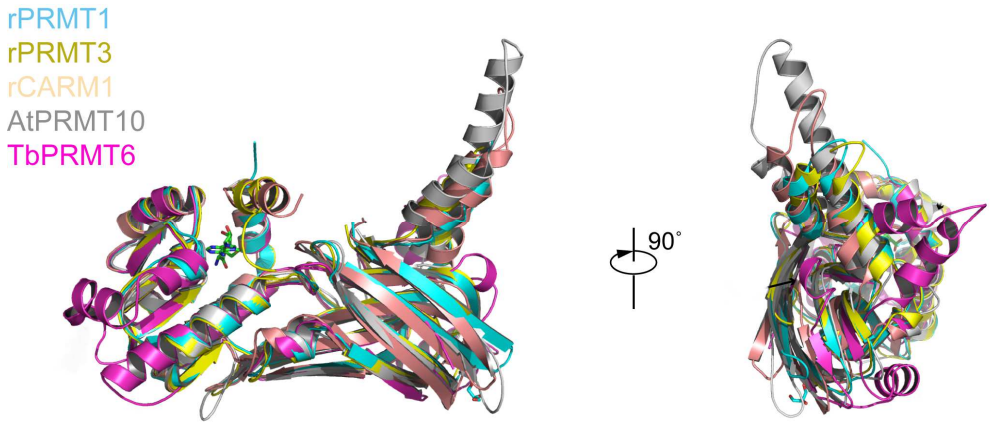

Figure 3: Structural comparison of TbPRMT6 with other type I PRMTs.

Two views of the superpositions of TbPRMT6 (magenta) with rat PRMT1 (cyan), rat PRMT3 (yellow), rat PRMT4 (wheat) and AtPRMT10 (grey), respectively. Adapted from (Wang et al., 2014).

In general, each arginine contains five potential hydrogen bond donors, which are most frequently bound by a plethora of acceptors (Bedford and Clarke, 2009). Addition of a methyl group by PRMTs does not change the overall positive charge of the protein. However, blocking of hydrogen bonding, enhanced bulkiness and increase in local hydrophobicity have a crucial influence on protein-protein interactions (Lee and Stallcup, 2009).

2.2.3 Regulation of arginine methylation

Analysis of PRMTs as recombinant proteins has demonstrated that most PRMTs exhibit an enzymatic activity to methylate different substrates. It is assumed that PRMTs possess a constitutive activity in cells, but regulation of PRMTs by PTMs, cross-talk between arginine methylation sites and adjacent PTMs or by association of PRMTs with other regulatory proteins can influence their activity (Bedford and Clarke, 2009; Yang and Bedford, 2013).

One example of the regulation of PRMTs by PTMs is the automethylation of arginine residues in PRMT4, PRMT6 and PRMT8. In case of PRMT4, the automethylation at R551 (position in murine PRMT4, isoform 1) has no influence on the substrate specificity or enzymatic activity of PRMT4. Nevertheless, its automethylation impairs PRMT4-mediated mRNA splicing and has a negative influence on transcription of several PRMT4-responsive ERα target genes (Kuhn et al., 2011). PRMT6 was first identified by Frankel et al. (2002) to perform automethylation. Later the auto-methylation site was mapped to arginine residue R35, which is very important for PRMT6 stability and inhibition of HIV-1 replication (Singhroy et al., 2013). For PRMT8, the biological role of automethylation still remains unknown. However, there is evidence that automethylation of PRMT8 has an autoregulatory effect on its ability to recognise substrates (Sayegh et al., 2007). Even PRMT1 shows weak automethylation as demonstrated by *in vitro* analyses (Frankel et al., 2002; Sayegh et al., 2007). A second example for PRMT regulation by PTMs is the phosphorylation of human PRMT4 at serine residues S216 and S228. As a result, AdoMet binding is impaired and PRMT4

methyltransferase activity is blocked (Feng et al., 2009; Higashimoto et al., 2007). Furthermore, S216 phosphorylation of PRMT4 reinforces its translocation to the cytoplasm primarily during mitosis (Feng et al., 2009). PRMT4 phosphorylation at S228 leads to the disruption of its homodimerisation and co-activator complex formation. This could not be demonstrated for the S216 phosphorylation. Both, S216 and S228 phosphorylation of PRMT4, have a negative influence on ER-dependent transcription. The kinase responsible for the phosphorylation of PRMT4 still remains unknown.

PTMs of amino acid residues adjacent to arginine methylation sites can either positively or negatively influence the methylation event. For example, the core MLL complex (MLL, WDR5, RBBP5, ASH2) mediated H3K4 trimethylation inhibits, but not totally blocks the dimethylation of H3R2 by PRMT6 (Guccione et al., 2007; Hyllus et al., 2007; Iberg et al., 2008). As a consequence, both marks are mutually exclusive in their genome-wide location (Guccione et al., 2006). In contrast to this negative cross-talk, H3R2me2a positively correlates with the repressive mark H3K27me3, mediated by the EZH2 (enhancer of zeste 2) containing PRC2 complex (polycomb repressive complex 2) (Cao and Zhang, 2004; Cao et al., 2002). Here, it was demonstrated that H3K27me3 correlates with the appearance of H3R2me2a (Guccione et al., 2006) and that PRMT6 activity was enhanced in the presence of H3K27me3 shown by i*n vitro* methylation assays (Hyllus et al., 2007). Other examples for PTMs at residues in the proximity of arginine methylation sites are H3K9ac and H3K14ac. Both acetylated residues inhibit PRMT5-mediated arginine methylation at H3R8 (Pal et al., 2004), which then blocks H3K9 methylation mediated by the protein methyltransferase G9a (Rathert et al., 2008).

Protein-protein interaction is another mechanism to regulate the enzymatic activity of PRMTs. The association of PRMTs with other regulatory proteins can activate, inhibit or change their activity. BTG1 and TIS21, also known as BTG2, are two related proteins, which bind PRMT1 and positively modulate its catalytic activity (Berthet et al., 2002; Lin et al., 1996). A binding partner of BTG1, hCAF1, also interacts with PRMT1 and can regulate its activity on several substrates (Robin-Lespinasse et al., 2007). Passeri and colleagues have revealed that the interaction between BTG2 and PRMT1 promotes

gene-specific methylation of H4R3 by PRMT1 during hematopoietic differentiation of myeloid leukemia cells (Passeri et al., 2006). Furthermore, as an integral component of the NUMAC complex (nucleosomal methylation activator complex), PRMT4 methylates nucleosomal histone H3, whereas recombinant PRMT4 prefers to methylate free core histone H3 (Xu et al., 2004). PRMT5 is able to change its substrate specificity from H3R8 towards H4R3 when it interacts with CORP5 (Lacroix et al., 2008). Additionally, COPR5 is essential for the recruiting of PRMT5 to its target gene *CCNE1*. PRMT5 also associates with BRG1 and BRM, which are the catalytic subunits of the human SWI/SNF remodeling complex (Pal et al., 2004). As a result, PRMT5-mediated methylation of H3R8 and H4R3 is significantly increased. Interaction between different PRMTs influences also their catalytic activity. It was shown that PRMT1 is able to interact with PRMT8 and PRMT2. The heterodimerisation of PRMT1 and PRMT8 promotes the localisation of PRMT1 to the plasma membrane, which causes a shift of the substrate specificity and enzymatic activity of PRMT1 (Lee et al., 2005b). The interaction between PRMT1 and PRMT2 leads to an enhanced enzymatic activity of PRMT1 to perform ADMA catalysis (Pak et al., 2011).

Beside the mechanisms mentioned above, arginine methylation might also be counteracted by enzymes, which block methylation or remove methyl groups from arginine residues (Lee and Stallcup, 2009; Yang and Bedford, 2013). In 2007, JMJD6 (jumonji domain containing 6) was identified as a putative demethylase of methylated arginines. It was shown that JMJD6 demethylates histone H3 at arginine 2 (H3R2me2) and histone H4 at arginine 3 (H4R3me2), which are either asymmetrically or symmetrically dimethylated (Chang et al., 2007). However, further studies of JMJD6 demonstrated that this enzyme is a lysine-hydroxylase without demethylation activity (Hahn et al., 2010; Webby et al., 2009). These findings were supported by the published crystal structure of JMDJ6 in 2010 (Hong et al., 2010; Mantri et al., 2010). Therefore, the question still remains whether arginine demethylases exist.

In 2004, two scientific groups described PADI4 (peptidyl arginine deiminase, type IV) as a nuclear enzyme, which counteracts PRMT-mediated methylation at H3 and H4 histone tails by deimination of MMA and unmodified arginines to citrulline (Cuthbert

et al., 2004; Wang et al., 2004). Presumably, PADI4 cannot convert dimethylated arginines into citrullin because asymmetrically and symmetrically dimethylated arginines can not be accommodated in its substrate-binding site (Holbert and Marmorstein, 2005). PADIs block PRMT-mediated methylation, but are not able to perform a full reversal, where citrulline residues are converted back to arginines (Denman, 2005).

2.2.4 PRMT6, its substrates and functions

In 2002, sequence analysis of the human genome identified PRMT6 as a novel methyltransferase gene on chromosome 1p13.3. PRMT6 is predominantly located in the nucleus as identified by immunofluorescence (Frankel et al., 2002). PRMT6 belongs to the type I class of PRMTs and prefers ADMA catalysis of already monomethylated substrates (Hyllus et al., 2007; Lakowski and Frankel, 2008). Similar to other PRMTs, PRMT6 requires homodimerisation for the transfer of a methyl group from AdoMet to its substrate (Thomas et al., 2010).

PRMT6 is capable of catalysing arginine methylation within GAR as well as non-GAR motifs. GST-GAR was described as the first substrate of PRMT6 (Frankel et al., 2002). *In vitro* studies reported that the histones H3 at R2 as well as H4 and H2A at R3 are further methylation sites for PRMT6 (Hyllus et al., 2007). Additionally, *in vivo* studies have shown that the primary target of PRMT6 is H3R2. The enzyme catalyses the asymmetric dimethylation of H3R2 (H3R2me2a) in mammals (Guccione et al., 2007; Hyllus et al., 2007; Neault et al., 2012). Interestingly, the analysis of MEFs (mouse embryonic fibroblasts) isolated from $Prmt6^{-/-}$ mice revealed that the global asymmetrical dimethylation of H3R2 was not fully lost after *Prmt6* knockout. This oberservation implies that other PRMTs are also able to methylate H3R2 to a certain degree (Neault et al., 2012).

H3R2me2a was demonstrated to inversely correlate with the methylation mark H3K4me3 in the promoter regions of MYC-dependent genes (Guccione et al., 2006).

H3K4 trimethylation is mediated by the core MLL complex (MLL, WDR5, RBBP5, ASH2) and correlates with transcriptional activation of several genes, such as *HOX* genes and MYC-dependent genes (Hughes et al., 2004; Hyllus et al., 2007; Milne et al., 2002). The PRMT6-mediated H3R2 dimethylation prevents binding of the MLL complex through WDR5 to the N-terminal H3 tail (WDR5 recognises A1, R2 and T3 in histone H3) and thereby inhibits H3K4 trimethylation (Couture et al., 2006; Han et al., 2006; Hyllus et al., 2007; Iberg et al., 2008; Ruthenburg et al., 2006; Schuetz et al., 2006). As a result, H3K4 trimethylation mediated by the core MLL complex is globally reduced and thus contributes to gene repression. Apart from an asymmetric dimethylation of H3R2 (H3R2me2a) mediated by PRMT6, H3R2 can also be symmetrically dimethylated by PRMT5 or PRMT7 (H3R2me2s). This enhances WDR5 binding and, as a consequence, supports euchromatin maintenance (Migliori et al., 2012).

In addition to H3R2, PRMT6 is able to catalyse the methylation of H2AR29 (H2AR29me2). This modification is specifically enriched at genes repressed by PRMT6 (Waldmann et al., 2011). The methyltransferase does not only methylate arginine residues within the histone tail, but also within core histones. A study by Casadio and colleagues has shown that PRMT6 and PRMT4 are able to methylate the core histone residue H3R42 (Casadio et al., 2013). The thereby created H3R42me2a mark has a positive effect on transcription caused by direct disruption of the interaction between DNA and the histone octamer.

PRMT6 is not only capable of methylating histones, but also non-histone proteins. To date, several PRMT6-specific non-histone substrates have been described implicating a role of PRMT6 in various cellular processes. For example, PRMT6 is involved in base excision repair (BER) mediated by the DNA polymerase ß (Pol ß). Here, it was shown that Pol ß forms a complex with PRMT6, which methylates Pol ß at positions R83 and R152 (El-Andaloussi et al., 2006). As a result, enhanced DNA binding and processivity of Pol ß significantly increased the polymerase activity, which lead to more efficient BER. Therefore, PRMT6 has a positive effect on BER. Several studies have demonstrated that the chromatin-associated factors HMGA1a and HMGA1b (high mobility group AT-hook 1a/b) are further PRMT6 substrates (Miranda et al., 2005; Sgarra et al., 2006; Zou

et al., 2007). PRMT6 methylates these non-histone chromatin proteins mainly at arginines in the second AT-hook, which is important for protein-DNA and protein-protein interactions. Additionally, PRMT6 is a negative regulator of viral transcription and replication of the human immunodeficiency virus (HIV) (Boulanger et al., 2005; Invernizzi et al., 2006, 2007). For example, PRMT6 is able to directly methylate the arginine-rich transactivation motif (ARM) in the transactivator protein (Tat) encoded by HIV type I (Boulanger et al., 2005). Upon methylation of Tat by PRMT6, the interaction between Tat and the Tat transactivation region (TAR) of viral RNA and cyclin T1 is lost (Xie et al., 2007). As a consequence, viral replication activity is impaired. Interestingly, PRMT6 automethylation regulates its own stability and is indispensable for its antiretroviral activity (Singhroy et al., 2013).

PRMT6 also functions as a transcriptional co-activator or co-repressor. Synergistically with PRMT4, PRMT6 enhances SHR/NR-(steroid hormone receptor/nuclear receptor) dependent transcriptional activity in a hormone-dependent manner (Harrison et al., 2010). As a co-activator PRMT6 supports *ER*α- and *ER*β- (estrogen receptor α and β), *GR* (glucocorticoid receptor) and *PR*- (progesterone receptor) mediated target gene expression (Harrison et al., 2010). Another study showed that PRMT6 specifically interacts with ERα via its ligand-binding domain. This interaction leads to methylation of ERα and thereby enhanced ERα activity (Sun et al., 2014). Additionally, Herglotz and colleagues demonstrated that PRMT6 interacts with the transcription factor RUNX1 (Herglotz et al., 2013). RUNX1 recruits PRMT6 to a subset of megakaryocytic target genes, such as *CD41* and *miR27a*, in human hematopoietic progenitor cells. Here, dimethylation of H3R2 by the co-repressor PRMT6 (H3R2me2a) and concomitant H3K27 trimethylation (H3K27me3), keep RUNX1 target genes in a repressed state. This transcriptional block of RUNX1 target genes is disrupted upon megakaryocytic differentiation.

In order to identify novel interaction partners of PRMT6, which possibly hint to new cellular functions of PRMT6 a MS/MS analysis with TAP (tandem affinity purification)-tagged *PRMT6* protein lysates from MCF7 cells was performed in our group. Thereby, 43 co-purifying proteins were identified, which are putative new interaction partners

of PRMT6 (PhD thesis, Claudia Stein). The interaction between PRMT6 and the two transcription factors ILF2 (interleukin enhancer binding factor 2) and ILF3, the histone-binding protein RBBP7 (retinoblastoma binding protein 7) and its homolog RBBP4 could be confirmed by CoIP/Western blot analyses. PRMT6 also associated with AURKB (aurora kinase B), which is implicated in cell cycle regulation (bachelor thesis, Lisa Schubert).

Further interesting putative interaction partners of PRMT6 were DDB1 (damage-specific DNA binding protein 1) and PCNA (proliferating cell nuclear antigen). DDB1 and DDB2 form the damaged DNA binding protein complex (UV-DDB) that detects UV-induced DNA lesions and recruits the global genome nucleotide excision repair (GG-NER) machinery to repair the damage (Iovine et al., 2011a; Lee and Zhou, 2007). DDB1 and PCNA physically associate with the CUL4A-RING ubiquitin E3-ligase complex (CRL4). This complex targets various substrates for ubiquitylation and subsequent degradation including the cell cycle regulator proteins CDKN1A and E2F1 (Jackson and Xiong, 2009).

2.3 PRMTs in lung cancer

Several publications demonstrated that nearly every PRMT is aberrantly expressed in one or more types of human cancer, such as breast, prostate, colorectal or lung cancer (Baldwin et al., 2014; Yang and Bedford, 2013). Moreover, PRMTs catalyse the arginine methylation of a variety of substrates, which have been linked to cancer development, progression and aggressiveness. This relatively novel connection between arginine methylation and cancer opens a new field for the development of anti-cancer drugs and therapies. Moreover, PRMTs are implicated in cell proliferation and survival or resistance of cancer cells to DNA damaging agents. The first part of this thesis focuses on the deregulation of PRMTs and especially of PRMT6 in lung cancer to further elucidate the role of PRMT6 in this cancer type. Since the method of choice was mainly IHC the next chapters will briefly describe the structure and functions of a normal lung

(2.3.1) as well as the histology and pathology of a lung tumour (2.3.2). Afterwards, the deregulation of PRMTs in lung cancer is described (2.3.3).

2.3.1 Structure and functions of the lung

The main functions of the respiratory system are air conduction, filtration and respiration. The trachea divides into the paired main bronchi and each bronchus enters the hilum of the lung and is subdivided into additional bronchial branches, which divide into smaller tubes (Figure 4). The segmental bronchi further devide into smaller terminal bronchi followed by the respiratory bronchioles. These ducts form the beginning of the respiratory passage, in which gas exchange occurs. The wall of a bronchiole consists of bundles of smooth muscles and adjacent blood vessels. These arteries supply the lung with oxygenated blood and nutrients. Respiratory bronchioles divide into alveolar ducts, which terminate in alveolar sacs. Alveolar sacs are enlarged spaces surrounded by clusters of alveoli, the primary site of gas exchange.

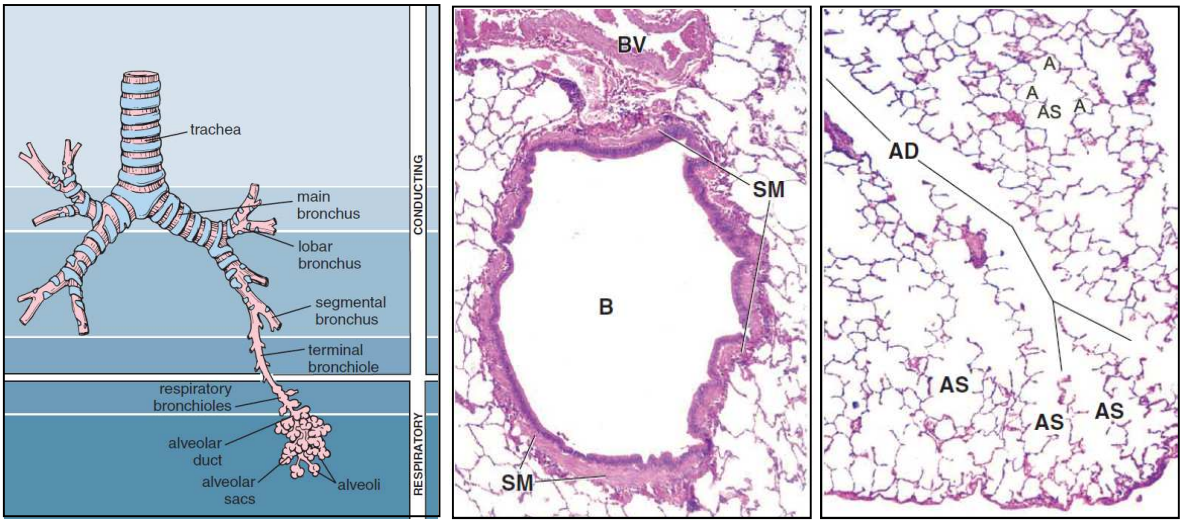

Figure 4: Diagram of the divisions of the bronchial tree (left). H&E stainings (75 x) of a bronchiole (middle) and an alveolar structure in the human lung (right panel).

Abbreviations used in the figure are H&E: Hematoxylin and eosin, A: alveolus, AD: alveolar duct, AS: alveolar sac, B: bronchiole, BV: blood vessel, SM: smooth muscle. Adapted from "Histology, a text and atlas" by Michael H. Ross, Wojciech Pawlina, sixth Edition, Lippincott Williams & Wilkins.

2.3.2 Lung cancer, its key features and pathology

Lung cancer is the leading cause of cancer-related death in humans worldwide. In 85% of all lung cancer cases, patients suffer from non-small cell lung carcinoma (NSCLC) (Ramalingam et al., 2011). The five-year survival rate of these patients is poor (5 - 15%) due to having no symptoms in the early stages and a high metastasis rates in advanced stages (Zakrzewicz et al., 2012). Conventional chemotherapy alone cannot sufficiently cure the disease in the majority of patients. Novel therapeutic options and targets are urgently required for earlier detection of this disease. In this context, PRMTs could be attractive targets for the development of drugs (Baldwin et al., 2014).

In humans, lung cancer is histological divided into two groups, non-small cell lung cancer (NSCLC) and small cell lung cancer (SCLC) depending on their pathological appearance and presumed cellular origin. NSCLC is subclassified into adenocarcinoma, squamous cell carcinoma and large cell carcinoma (Zakrzewicz et al., 2012). Additionally, the different malignant lung tumour stages are classified into TNM (tumour-node-metastasis) subsets to facilitate diagnosis and clinical research (Mirsadraee et al., 2012).

2.3.3 Deregulation of PRMTs in lung cancer

Several PRMTs are deregulated in lung cancer. For example, expression of PRMT5 is increased in several human lung cancer cell lines and tissues. Depletion of *PRMT5* causes proliferation defects accompanied by a G1-arrest in A549 cells (Gu et al., 2012). Furthermore, the silencing of *PRMT5* prevents the growth of A549 lung tumour xenografts in mice. In this context it was demonstrated that PRMT5 is involved in FGFR signaling, a pathway whose activation is needed for efficient tumour growth. For example, *PRMT5*-depleted A549 cells show a reduced expression of FGFR3, an important component of the FGFR pathway (Gu et al., 2012). Further studies demonstrated that PRMT5 regulates the HIF-1 signaling pathway. Particularly, it

enhanced the expression of several HIF-1 target genes, such as *VEGF* or *PDK1* (Lim et al., 2012).

Moreover, PRMT4 is an important regulator of lung development. In *Prmt4* knockout mice, pulmonary epithelial cell proliferation and differentiation are impaired. Newborn mice, which are deficient for *Prmt4*, are smaller than their wild type littermates and die just after birth (Yadav et al., 2003). These mice have defects in lung unfolding accompanied by respiratory problems caused by hyperproliferation of alveolar type II cells (O'Brien et al., 2010). Additionally, PRMT4 as well as PRMT1 are deregulated in lung tumour tissues from NSCLC patients (Elakoum et al., 2014).

Besides *PRMT1*, the expression of *PRMT6* was demonstrated to be increased in several cancer tissues, such as bladder, lung and prostate cancer (Vieira et al., 2014; Yoshimatsu et al., 2011). Both, PRMT6 and PRMT1 are required for proper cell cycle progression and proliferation of certain cancer cell lines. For example, siRNA-mediated depletion of *PRMT6* or *PRMT1* impaired growth of several cancer cell lines by affecting G1-S cell cycle transition (G0/G1 arrest). This was shown for several lung cancer (such as A549) and bladder cancer cell lines (such as SW780) (Yoshimatsu et al., 2011).

PRMT6 represses the natural inhibitor of angiogenesis and endothelial cell migration *THBS1* (thrombospondin 1), which supports the idea that PRMT6 can contribute to the unimpeded growth of tumour cells (Michaud-Levesque and Richard, 2009). In this study, PRMT6 associated with the *THBS1* promoter and directly regulated *THBS1* transcription in a repressive manner through dimethylation of H3R2. *PRMT6* depletion also caused cell migration and invasion defects in U2OS cells (Michaud-Levesque and Richard, 2009). Moreover, it was found that THBS1 is deregulated in several human and murine cancers, such as invasive cervical cancer or hepatocellular carcinoma (Kodama et al., 2001; Poon et al., 2004). Additionally, Harrison and colleagues revealed that *PRMT6* knockdown inhibits the estrogen-stimulated proliferation of breast cancer cells (MCF7) (Harrison et al., 2010). This effect was even enhanced in a double knockdown of *PRMT6* and *PRMT4*. These data imply an important role of PRMT6 in tumourigenesis.

2.4 PRMTs in cellular senescence

Cellular senescence is a protective mechanism against unlimited cell proliferation and therefore presents a barrier to tumourigenesis (Prieur and Peeper, 2008). There is first evidence that PRMTs are implicated in the regulation of proliferation and senescence in different cell types. The following chapters will first describe key features and causes of cellular senescence (2.4.1) and then, the role of PRMTs and especially of PRMT6 in this process (2.4.2).

2.4.1 Cellular senescence, its key features and causes

The process of aging at the cellular level was first described more than five decades ago by Hayflick and colleagues (Hayflick, 1965; Hayflick and Moorhead, 1961). They observed a spontaneous proliferative arrest of normal untransformed cells (human diploid fibroblasts) in the course of serial passaging in *in vitro* culture. Later, this process was termed replicative cellular senescence, in which the lack of endogenous telomerase causes telomere attrition and triggers a DNA damage response (DDR) (Bodnar et al., 1998; Prieur and Peeper, 2008). Senescent cells undergo a growth arrest in G1-phase. They remain viable and metabolically active, but show an enlarged, flattened morphology accompanied by enhanced activity of senescence-associated ß-galactosidase (SA-ß-gal), resistance to apoptosis (in some cells) and characteristic changes in gene expression (Campisi and d'Adda di Fagagna, 2007; Dimri et al., 1995). Additionally, cells exhibit an altered chromatin structure through developing SAHF (senescence-associated heterochromatin foci) (Narita et al., 2003) and SDF (senescence-associated DNA damage foci) (d'Adda di Fagagna et al., 2003; Takai et al., 2003). Both are also used as cytological markers of senescent cells.

Independently of replicative cellular senescence caused by telomere shortening permanent growth arrest can be induced by other conditions. This process is called premature cellular senescence and can be triggered by oxidative stress (ROS - reactive oxygen species), DNA damage (such as UV light, γ-irradiation), mitogenic oncogenes

(e.g. BRAF), chemotherapeutic drugs or even inadequate culturing conditions (Michaloglou et al., 2005; Parrinello et al., 2003; Toussaint et al., 2002). Here, oncogene-induced senescence (OIS) provides a link between senescence and cancer.

At the molecular level, cellular senescence is induced by the tumour suppressor proteins p53 (TP53) and pRb (RB1) and the increased expression of the CDK (cyclin-dependent kinase) inhibitors p21 ($p21^{CIP/WAF1}$, CDKN1A) and p16 (p16-INK4A, CDKN2A). Stress as well as oncogenes activate the TP53-CDKN1A-RB1 and/or p16-INK4A-RB1 cascade dependent on the cell strain and severity of one or even combined stimuli (Ben-Porath and Weinberg, 2005; Kuilman et al., 2010). p16-INK4A blocks the phosphorylation of RB1 by specifically binding to CDK4 and CDK6 (Serrano et al., 1993; Wang et al., 2012a). RB1 is kept in a hypophosphorylated state that binds and inactivates the transcription factor E2F. As a result, E2F-target genes, which stimulate or support S-phase progression, are repressed in senescent cells (Narita et al., 2003). Similarly, the TP53-dependent target gene CDKN1A is increased, particularly binds to and inactivates CCNE-CDK2 complexes and thereby causes an arrest in G1-phase in these cells (Brugarolas et al., 1995).

2.4.2 Role of PRMTs in cellular senescence

Evidence has emerged that PRMTs play an important role in cell cycle progression and senescence of different cells. Kim and colleagues showed that in synchronised HeLa cells PRMT6 protein levels were increased during cell cycle from G0/G1- to G1-phase (Kim et al., 2010). Another study demonstrated that protein levels of PRMT6, PRMT1, PRMT4 and PRMT5 as well as asymmetric dimethylation of arginines decreased during replicative and H_2O_2-induced premature senescence in human diploid fibroblasts (Lim et al., 2008). In contrast, global levels of CDKN1A were reduced in these cells. Another example are primary MEFs isolated from *Prmt6* knockout mice. These cells showed proliferation defects and an elevated senescence phenotype (Neault et al., 2012). Similarly, MEFs isolated from *Prmt1* knockout mice exhibited a delay in cell cycle progression and spontaneous DNA damage (Yu et al., 2009).

Moreover, the CDK inhibitor p16-INK4A interacts with and is methylated by PRMT6 at arginines R22, R131 and R138 (Wang et al., 2012a). Here, overexpression of *PRMT6* counteracted the cell cycle arrest at G1 phase induced by p16-INK4A in the NSCLC cell line A549. Normally, the INK4A-ARF locus is repressed mediated by the binding of several Polycomb group (PcG) proteins in pre-senescent fibroblasts (Bracken et al., 2007; Dietrich et al., 2007; Jacobs et al., 1999). PcG proteins form the two protein complexes PRC1 (polycomb repressive complex 1) and PRC2, whose function is to maintain transcriptional repression (Dietrich et al., 2007). In senescence cells these proteins are displaced. This is accompanied by reduced levels of H3K27me3, while the INK4A-ARF locus is actively transcribed (Bracken et al., 2007). Previous studies demonstrated that PRMT6 co-purifies and interacts with a subset of PRC core subunits, such as CBX8 (chromobox homolog 8) or EZH2, which is the catalytically active subunit of PRC2 (PhD thesis, Claudia Stein and personal communication, René Reiner Nötzold). These data strengthen the idea that PRMT6 plays an important role in the regulation of proliferation and senescence of normal human cells as well as tumour cells.

2.5 Objectives

To date, only a few studies have investigated PRMT6 and its possible role in tumourigenesis. Here, cDNA microarray analysis and siRNA-mediated *PRMT6* depletion experiments gave an inital hint that PRMT6 is overexpressed in bladder and lung cancer tissues and that PRMT6 might positively affect the growth of these cancer cells (Yoshimatsu et al., 2011). This study aims to further investigate the deregulation of PRMT6 in lung cancer. Therefore, it analyses the expression of PRMT6 in the two murine lung cancer models LLC1 and $Kras^{LA2}$ by IHC. Moreover, this study investigates several human and murine lung cancer cell lines in their PRMT6 expression by RT-qPCR and Western blot and analyses whether the clonogenic growth of two human cell lines is impaired by depletion of *PRMT6*.

Several publications demonstrated that PRMTs are implicated in cell proliferation and survival, transformation, invasion of cancer cells and that they contribute to the resistance to DNA damaging agents (Baldwin et al., 2014; Yang and Bedford, 2013). Furthermore, Lim and colleagues demonstrated that the protein level of PRMT6 is strongly reduced in senescent fibroblasts (Lim et al., 2008). These data gave an initial hint that PRMT6 plays an important role in the regulation of proliferation and senescence in different cell types. To gain a better understanding of PRMT6 and its functions in cell proliferation and senescence, this study investigates transformed (U2OS) as well as non-transformed cells (TIG3-T) in *PRMT6* knockdown experiments. Beside the characterisation of phenotypical effects, possible transcriptional downstream target genes of PRMT6 should be detected in these cells. Furthermore, this study analyses PRMT6 in an oncogene-inducible senescence model (OIS) to unravel whether it is implicated in the process of premature cellular senescence triggered by the oncogene Braf (TIG3 BRAF-ER cells) (Agger et al., 2009; Woods et al., 1997).

Previously, PRMT6 was demonstrated to increase the activity of the DNA polymerase ß (Pol ß) in base excision repair (El-Andaloussi et al., 2006). Another study showed that PRMT6 stimulates *CCDN1* expression upon DNA damage presumably through

dimethylation of H3R2 (Iberg et al., 2008). A previous MS/MS analysis of MCF7 cells overexpressing TAP-tagged PRMT6 in our group revealed that the two proteins DDB1 and PCNA are putative interaction partners of PRMT6 (Claudia Stein, PhD thesis). Both proteins are implicated in DNA damage repair, where DDB1 forms a complex with DDB2 in UV-DDB (Essers et al., 2005; Iovine et al., 2011b) and strengthen the hypothesis that PRMT6 possesses additional features in DNA repair. Therefore, this study examines the interaction between PRMT6 with PCNA, DDB1 and DDB2 by Co-IP studies in MCF7 cells. The validation of putative interaction partners of PRMT6 might serve as basis for the future characterisation of PRMT6 and its functional role in various cellular processes.

3 MATERIALS

3.1 Material sources

3.1.1 Enzymes

Benzonase Nuclease HC, 250 U/µl	Merck
M-MLV Reverse Transcriptase, 200 U/µl	Life Technologies
Proteinase K, 20 µg/µl	AppliChem
Restriction Endonucleases, 10 U/µl (*Bgl*II, *Hind*III)	Thermo Scientific
Ribonuclease A (RNase A) DNase free, 10 µg/µl	AppliChem
T4 DNA Ligase, 30 U/µl	Thermo Scientific

3.1.2 Enzyme inhibitors

Aprotinin, 10 µg/µl in ddH_2O	AppliChem
Leupeptin, 10 µg/µl in ddH_2O	AppliChem
PMSF, 10 µg/µl in ddH_2O in isopropanol	Sigma-Aldrich
Protease Inhibitor Cocktail Tablets (PICs)	Roche
RiboLock RNase Inhibitor, 40 U/µl	Thermo Scientific

3.1.3 Agarose gel electrophoresis

Ethidium bromide 1% , 10 mg/ml	Roth
GeneRuler DNA Ladder Mix	Thermo Scientific
Orange G	Sigma-Aldrich
SeaKem LE Agarose	Lonza

3.1.4 SDS-PAGE and Western blot

APS	AppliChem
BSA (Albumin Fraction V, Protease-free)	AppliChem
Coomassie Brilliant Blue G 250	Sigma-Aldrich
p-Coumaric acid	
Roth Hydrogen peroxide 30%	Roth
Immobilon-P (PVDF membrane)	Millipore
Luminol	Roth
Medical X Ray Film Super RX	Fujifilm
PageRuler Prestained Protein Ladder	Thermo Scientific
TEMED	AppliChem
Ultra Pure ProtoGel	Biozym
(Acrylamide:Bis-Acrylamide 37.5:1)	
Whatman paper	Schleicher and Schuell

3.1.5 Immunohistochemical staining (IHC)

Antibody diluent	Dako
Dako Pen	Dako
Mayer´s hemalum solution	Merck
Mowiol 4-88	Roth
Peroxidase solution (30%)	Roth
Roticlear	Roth
Streptavidin peroxidase	KPL
Staining boxes and racks (made of lime-soda-glass)	Roth
Staining boxes (made of PMP plastic)	Roth
Staining chamber (for up to 20 microscope slides)	Roth
Steam cooker	Braun
Tissue sections from murine lungs	Rajkumar Savai (MPI, Bad Nauheim)
(HealthyCon #1 - #3, LLC1 #1 - #3, 59s Lung #1, #2, #4)	

3.1.6 Other chemicals, reagents and consumables

4-Hydroxytamoxifen (4-OHT)	Sigma-Aldrich
Polybrene (Hexadimethrine bromide)	Sigma-Aldrich
Potassium ferricyanide(III) ($K_3Fe(CN)_6$)	AppliChem
Potassium ferrocyanide ($K_4Fe(CN)_6$)	AppliChem
Protein A Sepharose 4 Fast Flow	GE Healthcare
Salmon Sperm	AppliChem
X-gal	Roth
Clear Seal Diamond Heat Sealing Film	Thermo Scientific
Clear Seal sheets	4titude
qPCR 96-well plates	Sarstedt

3.1.7 Kits

Table 1: Kits with corresponding application and supplier.

Kit	Application	Supplier
ABsolute qPCR SYBR Green Mix Plus ROX Vial	RT-qPCR analysis (cDNA or ChIP-chromatin)	Thermo Scientific
AEC (red) Substrate Kit	Immunohistochemical staining (IHC) of tissue sections	Life Technologies
JETQUICK Gel Extraction Spin Kit	Agarose gel purification	Genomed
JETSTAR Plasmid Maxiprep Kit	Plasmid-DNA isolation from prokaryotic cells	Genomed
RNA Mini Kit	RNA isolation from eukaryotic cells	Seqlab
RNeasy Micro Kit	RNA isolation from eukaryotic cells (from very small cell numbers)	Qiagen
peqGOLD DNase I Digest Kit	DNA digest (RNA isolation)	Peqlab
QIAquick PCR Purification Kit	DNA purification (ChIP analysis)	Qiagen
Senescence Cells Histochemical Staining Kit	SA-ß-gal staining of eukaryotic cells	Sigma-Aldrich

3.2 Standard solutions and buffers

Standard solutions and buffers were prepared according to standard protocols. Additional buffers are listed in the individual subsections of section 4, METHODS.

PBS	2 mM KH_2PO_4 - pH 7.4 (NaOH)
	10 mM Na_2HPO_4
	137 mM NaCl
	2.7 mM KCl
TBE	89 mM TRIS - pH 7.9 (NaOH)
	2 mM EDTA
	89 mM Boric acid
TBS	10 mM TRIS - pH 7.9 (HCl)
	150 mM NaCl
TBS-T (0.05%)	TBS - pH 7.9
	0.05% (v/v) Tween 20
TBS-T (0.5%)	TBS - pH 7.9
	0.5% (v/v) Tween 20

3.3 Bacteria strain, culture medium and supplements

DH5α	*E. coli* strain	for plasmid-DNA amplification
LB medium	1% (w/v)	peptone (from casein)
	0.5% (w/v)	yeast extract
	1% (w/v)	NaCl
Agar plates	1.5% (w/v)	agar in LB medium
Ampicillin	100 µg/ml	(final concentration)
Kanamycin	50 µg/ml	(final concentration)

3.4 Cell lines, tissue culture media and antibiotics

Different eukaryotic cell lines of either human or murine origin were used and are listed in Table 2.

Table 2: Eukaryotic cell lines with corresponding medium and antibiotic.

Cell line	Cell type	Tissue culture media and antibiotics [data in (v/v)]	Source/Reference
Beas2B	human transformed bronchial epithelial cell line	DMEM/F-12 + 5% FCS + 1% PS	Rajkumar Savai
H1299	human lung, carcinoma (NSCLC)	DMEM + 10% FCS + 1% PS	Thorsten Stiewe
H1650	human lung, bronchoalveolar adenocarcinoma (NSCLC)	RPMI 1640 (ATCC modification) + 10% FCS + 1% PS	Rajkumar Savai
A549	human lung, carcinoma (NSCLC)	DMEM + 10% FCS + 1% PS	Thorsten Stiewe
H358	human lung, bronchoalveolar adenocarcinoma (NSCLC)	RPMI 1640 + 10% FCS + 1% PS	Sylvie Gazzeri
MLE12	murine transformed lung epithelial cell line	DMEM/F-12 + 5% FCS + 1% PS	Rajkumar Savai
LLC1	mouse Lewis lung carcinoma line 1	RPMI 1640 + 10% FCS + 1% PS	Rajkumar Savai
U2OS	human osteosarcoma cell line (epithelial-like)	DMEM + 10% FCS + 1% PS	Uta-Maria Bauer
Phoenix-Eco	human second-generation retrovirus producer cell line for generation of ecotropic (*Eco*) retroviruses	DMEM + 10% FCS + 1% PS	(Grignani et al., 1998)
TIG3-T	human diploid embryonic fibroblasts, h*TERT*-immortalised, express ecotropic murine receptor (*EcoR*)	DMEM + 10% FCS + 1% PS	Kristian Helin (Bracken et al., 2007; Dietrich et al., 2007)

TIG3 BRAF-ER	human diploid embryonic fibroblasts, h*TERT*-immortalised, stably expressing a pMSCV-Blast-*BRAF-ER* plasmid (oncogenic *Braf* kinase domain is fused to a mutant form of ligand binding domain (LBD) of estrogen receptor (*ER*), which is 4-OHT inducible)	DMEM + 10% FCS + 1% PS	Kristian Helin (Agger et al., 2009)
MCF7	human breast adenocarcinoma cell line	DMEM + 10% FCS + 1% PS	Uta-Maria Bauer

All tissue culture media and supplements, such as FCS, PS and Trypsin-EDTA (0.05%), used in this study were purchased from Life Technologies. The most commonly used DMEM contained 4.5 g/l glucose, L-glutamine, phenol red and sodium pyruvate. Cells were cultivated at 37°C and 5% CO_2. TIG3 BRAF-ER cells were treated every second day with 200 nM 4-OHT (Sigma-Aldrich) for the indicated time intervals. Antibiotics required for plasmid selection of TIG3-T or TIG3 BRAF-ER cells are listed in Table 3.

Table 3: Eukaryotic cell lines with corresponding antibiotics for plasmid selection.

Cell line	Antibiotics	Final concentration
TIG3-T	Neomycin (G418) - for *EcoR* Hygromycin - for h*TERT* Puromycin - for Puromycin resistence gene (infection with pSUPER.retro.puro constructs)	500 µg/ml 100 µg/ml 1 µg/ml
TIG3 BRAF-ER	Blasticidin - for *BRAF-ER* Neomycin (G418) - for h*TERT*	5 µg/ml 50 µg/ml

3.5 Transfection reagents

Table 4: Transfection reagents with corresponding application.

Transfection reagent	Application
Calcium phosphate	transfection of Phoenix-Eco cells (ecotropic retroviruses generation)
FuGENE HD (Roche)	plasmid-DNA transfection of TIG3 BRAF-ER cells
Lipofectamine RNAiMax (Life Technologies)	siRNA transfection of U2OS, H1299 and H358 cells
Polyethylenimine (PEI), 0.1% (v/v) (Sigma-Aldrich)	siRNA transfection of TIG3 BRAF-ER cells, plasmid-DNA transfection of MCF7 cells

3.6 Eukaryotic expression plasmids

3.6.1 Empty plasmids

Table 5: Eukaryotic empty plasmids used in this study.

Plasmid	Resistance	Comments	Source/Reference
pcDNA3.1	Ampicillin, Neomycin	control plasmid for pcDNA3.1-h*PRMT6*, myc-his C-terminal (5500 bp)	Invitrogen
pSUPER.retro.puro	Ampicillin, Puromycin	retroviral pSUPER-shRNA plasmid (originally from OligoEngine), with RNA Polymerase III-dependent H1-RNA promoter and Puromycin resistence gene	(Brummelkamp et al., 2002)

3.6.2 Expression plasmids

Table 6: Eukaryotic expression plasmids used in this study.

Plasmid	Resistance	Comments	Source/Reference
p3xFLAG10-Hs*PCNA*	Ampicillin, Neomycin	interaction analysis of PCNA with PRMT6 (IPs)	Kyungjae Myung (Motegi et al., 2006)
pcDNA3-flag-*DDB1*	Ampicillin	interaction analysis of DDB1 with PRMT6 (IPs)	Francesca Bernassola (Malatesta et al., 2013)

pcDNA3.1-h*PRMT6*	Ampicillin, Neomycin	h*PRMT6*-ORF was generated by *Bam*HI/*Eco*RI restriction of pGEX-2T-h*PRMT6* and cloned into pcDNA3.1 (Invitrogen)	Uta-Maria Bauer (Stein et al., 2012)

3.6.3 Retroviral expression plasmids

Ecotropic retroviral supernatants were produced in Phoenix-Eco cells by transfection of pSUPER.retro.puro plasmids encoding several shRNAs.

Table 7: Retroviral expression plasmids used in this study.

Plasmid	Resistance	Comments (depleted gene)	Source/Reference
pSUPER.retro.puro-shLuci	Ampicillin, Puromycin	plasmid for shLuci expression	Uta-Maria Bauer (Stein et al., 2012)
pSUPER.retro.puro-shPRMT6_1	Ampicillin, Puromycin	plasmid for shPRMT6_1 expression (*PRMT6*)	Uta-Maria Bauer (Stein et al., 2012)
pSUPER.retro.puro-shPRMT6_2	Ampicillin, Puromycin	plasmid for shPRMT6_2 expression (*PRMT6*)	Uta-Maria Bauer (Stein et al., 2012)
pSUPER.retro.puro-shPRMT6_3	Ampicillin, Puromycin	plasmid for shPRMT6_3 expression (*PRMT6*)	Uta-Maria Bauer (Stein et al., 2012)

3.7 Oligonucleotides

All oligonucleotides were ordered from Eurofins MWG/Operon and dissolved to a concentration of 100 pmol/µl.

3.7.1 Sequencing primers and sequence analysis

The pSUPER.retro.puro plasmid constructs were sequenced with the sequencing primer 5´-pRS GGAAGCTTGGCTTTTG. The DNA sequence analysis was performed by LGC Genomics. Other plasmids were sequenced by standard primer pairs available at the same company.

3.7.2 Reverse transcription (RT) primer

An oligo(dT)$_{17}$ primer was used to transcribe 10 ng - 2 µg RNA into cDNA.

3.7.3 Real-time quantitative PCR (RT-qPCR) primers

RT-qPCR primers were designed with the help of the Universal ProbeLibrary from Roche using an intron spanning assay to avoid the amplification of genomic DNA.

3.7.3.1 Human RT-qPCR primers

Table 8: Human primers for RT-qPCR gene expression analysis.

Gene	NCBI number (detected transcript variants, TV)	Sequence (5´→3´) **forward**/reverse
CCNA2	NM_001237.3	**ATGAGACCCTGCATTTGGCTG** TTGAGGTAGGTCTGGTGAAGG
CCND1	NM_053056.2	**GACCTCCTCCTCGCACTTC** CCCTCGGTGTCCTACTTCAA
CDKN1A (p21)	NM_000389.4 (TV1) NM_078467.2 (TV2) NM_001291549.1 (TV3) NM_001220778.1 (TV4) NM_001220777.1 (TV5)	**GGCAGACCAGCATGACAGATTTC** CGGATTAGGGCTTCCTCTTGG
CDKN1B (p27)	NM_004064.4	**CCCTAGAGGGCAAGTACGAGT** AGTAGAACTCGGGCAAGCTG
CDKN1C (p57)	NM_000076.2 (TV1) NM_001122630.1 (TV2) NM_001122631.1 (TV3)	**CACGATGGAGCGTCTTGTC** GCTCAGCTCCTCGTGGTC
EZH2	NM_004456.4 (TV1) NM_152998.2 (TV2) NM_001203247.1 (TV3) NM_001203248.1 (TV4) NM_001203249.1 (TV5)	**TCAAAACCGCTTTCCGGG** TGTCCCAATGGTCAGCG
p16-INK4A (CDKN2A)	NM_000077.4 (TV1) NM_001195132.1 (TV5)	**CCCCTTGCCTGGAAAGATAC** AGCCCCTCCTCTTTCTTCCT
THBS1	NM_003246.2	**AATGCTGTCCTCGCTGTTG** GCCACAGCTCGTAGAACAGG

TP53 (P53)	NM_000546.5 (TV1) NM_001126112.2 (TV2) NM_001126114.2 (TV3) NM_001126113.2 (TV4) NM_001126115.1 (TV5) NM_001126116.1 (TV6) NM_001126117.1 (TV7) NM_001126118.1 (TV8)	**AGGCCTTGGAACTCAAGGAT** CCCTTTTTGGACTTCAGGTG
PRMT6	NM_018137.2	**AGACACGGACGTTTCAGGAG** CCACTTTGTAGCGCAGCAG
RPLP0	NM_001002.3 (TV1) NM_053275.3 (TV2)	**GTCGGAGGAGTCGGACGAG** GCCTTTATTTCCTTGTTTTGCAAA
RPS14	NM_001025071.1 (TV1) NM_001025070.1 (TV2) NM_005617.3 (TV3)	**GGCAGACCGAGATGAATCCTCA** CAGGTCCAGGGGTCTTGGTCC
UBC	NM_021009.6	**CACTTGGTCCTGCGCTTGA** CAATTGGGAATGCAACAACTTTAT

3.7.3.2 Human/murine RT-qPCR primers

Primer pairs were designed for detection of both the human and murine transcript levels of *PRMT6/Prmt6* or the corresponding controls *RPLP0/Rplp0* and *RPS14*/*Rps14*.

Table 9: Human/murine primers for RT-qPCR gene expression analysis.

Genes	NCBI number (detected transcript variants, TV)	Sequence (5´→3´) **forward**/reverse
PRMT6/Prmt6	NM_018137.2 NM_178891.5	**TCGCCTTTTCACCCGGCCAC** GTCTCCCACTTTGTAGCGCA
RPLP0/Rplp0	NM_001002.3 (TV1) NM_053275.3 (TV2) NM_007475.5	**ACACCATGATGCGCAAGGC** GTGAGGTCCTCCTTGGTGAAC
RPS14/*Rps14*	NM_001025071.1 (TV1) NM_001025070.1 (TV2) NM_005617.3 (TV3) NM_020600.4	**TGACTGGTGGGATGAAGG** CAGGTCCAGGGGTCTTGGTC

3.7.4 Human ChIP-qPCR primer

ChIP-qPCR primer pairs were designed using the Primer3 program.

Table 10: Human primers for ChIP analysis by qPCR.

Gene (region)	Sequence (5´→3´) **forward**/reverse
CDKN1A (-6.8kb)	**GGAGGGCAAAGTACAGTGGA** CACATGTGACTTGGGGTGAG
CDKN1A (-1.0kb)	**TACGGGCTATGTGGGGAGTA** AAGGGGAGGATTTGACGAGT
CDKN1A (TSS)	**CCGAAGTCAGTTCCTTGTGG** CGCTCTCTCACCTCCTCTGA
CDKN1A (+0.5kb)	**GTGGGGATGAAGTCCGTGTC** ACTTACTCCACTCCGCTTTC
CDKN1A (+8.6kb)	**CTGTAAACCTCTCGAGGGCA** GCACCTGCTGTATATTCAGC
p16-INK4A (-1.8kb)	**CTTTTACCTCCTTGCGCTTG** TGGGAGACAAGAGCGAAACT
p16-INK4A (-0.5kb)	**AGGGGAAGGAGAGAGCAGTC** CTACCCCCTCAACCCTTGAT
p16-INK4A (TSS)	**CCCCTTGCCTGGAAAGATAC** AGCCCCTCCTCTTTCTTCCT
p16-INK4A (+0.5kb)	**TCAGGTAGCGCTTCGATTCT** GGCTCCTCATTCCTCTTCCT
p16-INK4A (+1.0kb)	**CCCTTCACTTTGGGAGATCA** CCCCCGGCTACTTTTTGTAT

3.7.5 siRNA oligonucleotids

The depletion of specific or unspecific mRNAs was achieved by transient transfection of siRNAs. The siRNA sequences were provided from Dharmacon, Sigma-Aldrich and reordered from Eurogentec (20 µM stock solutions).

Table 11: siRNA oligonucleotides used in this study.

Name (depleted gene)	NCBI number (detected transcript variants, TV)	Sequence (5´→3´) **sense**/antisense	Source/Reference
siGFP	--	**GCAAGCUGACCCUGAAGUU** AACUUCAGGGUCAGCUUGC	--
siLuci	--	**GAUUAUGUCCGGUUAUGUA** UACAUAACCGGACAUAAUC	Dharmacon
siNon	--	**AUGAACGUGAAUUGCUCAA** UUGAGCAAUUCACGUUCAU	Dharmacon
siScr	--	**CAUAAGCUGAGAUACUUCA** UGAAGUAUCUCAGCUUAUG	Martin Eilers
siPRMT6_1 (*PRMT6*)	NM_018137.2	**GAGCAAGACACGGACGUUU** AAACGUCCGUGUCUUGCUC	Dharmacon
siPRMT6_2 (*PRMT6*)	NM_018137.2	**GCAAGACACGGACGUUUCA** UGAAACGUCCGUGUCUUGC	Dharmacon
siPRMT6_3 (*PRMT6*)	NM_018137.2	**GGAGGGAGAGUGACUUCAU** AUGAAGUCACUCUCCCUCC	--
siPRMT6_4 (*PRMT6*)	NM_018137.2	**GACGUUUCAGGAGAGAUCA** UGAUCUCUCCUGAAACGUC	Sigma-Aldrich
siPRMT6_5 (*PRMT6*)	NM_018137.2	**CGGAACAGGUGGAUGCCAU** AUGGCAUCCACCUGUUCCG	Sigma-Aldrich
siCDKN1A (pool of 3 sequences) (*CDKN1A*)	NM_000389.4 (TV1) NM_078467.2 (TV2) NM_001220778.1 (TV4) NM_001220777.1 (TV5)	**CGAUGGAACUUCGACUUUG** CAAAGUCGAAGUUCCAUCG **GCGAUGGAACUUCGACUUU** AAAGUCGAAGUUCCAUCGC **GAUGGAACUUCGACUUUGU** ACAAAGUCGAAGUUCCAUC	Dharmacon

3.7.6 shRNA oligonucleotids

The cloning strategy was based on manufacturer's instructions (OligoEngine) and resulted in the production of retroviral expression plasmids (chapter 3.6.3) for the selective suppression of one of the displayed human mRNAs listed in Table 12. Each oligo pair (sense and antisense) was designed with a *Bgl*II restriction site (GATC) at the 5´-end of the sense oligo and a *Hind*III restriction site (AGCT) at the 5´-end of the antisense oligo. All used shRNAs were identical to siRNA sequences as described above.

Table 12: Specific and unspecific oligonucleotides used for shRNA production.

Name	Depleted gene	Sequence (5´→3´)
shLuci (sense)	--	GATCCCC**GATTATGTCCGGTTATGTA**TTCAA GAGA**TACATAACCGGACATAATC**TTTTTA
shLuci (antisense)		AGCTTAAAAA**GATTATGTCCGGTTATGTA**TC TCTTGAA**TACATAACCGGACATAATC**GGG
shPRMT6_1 (sense)	*PRMT6*	GATCCCC**GAGCAAGACACGGACGTTT**TTCAA GAGA**AAACGTCCGTGTCTTGCTC**TTTTTA
shPRMT6_1 (antisense)		AGCTTAAAAA**GAGCAAGACACGGACGTTT**TC TCTTGAA**AAACGTCCGTGTCTTGCTC**GGG
shPRMT6_2 (sense)	*PRMT6*	GATCCCC**GCAAGACACGGACGTTTCA**TTCAA GAGA**TGAAACGTCCGTGTCTTGC**TTTTTA
shPRMT6_2 (antisense)		AGCTTAAAAA**GCAAGACACGGACGTTTCA**TC TCTTGAA**TGAAACGTCCGTGTCTTGC**GGG
shPRMT6_3 (sense)	*PRMT6*	GATCCCC**GGAGGGAGAGTGACTTCAT**TTCAA GAGA**ATGAAGTCACTCTCCCTCC**TTTTTA
shPRMT6_3 (antisense)		AGCTTAAAAA**GGAGGGAGAGTGACTTCAT**TC TCTTGAA**ATGAAGTCACTCTCCCTCC**GGG

3.8 Antibodies and antisera

3.8.1 Primary antibodies

Table 13: Antibodies and antisera used in this study.

Primary antibody	Type of antibody	Dilution/Amount (Application)	Source/Reference
α-CDK2 (M2)	rabbit, polyclonal IgG	1:5.000 (Wb)	Santa Cruz (sc-163)
α-DDB1 (clone ZD001)	mouse, monoclonal IgG1κ	1:500 (Wb)	Invitrogen (39-9901)
α-DDB2 (2246C4a)	mouse, monoclonal IgG1	1:800 (Wb)	Santa Cruz (sc-81246)
α-H3	rabbit, polyclonal IgG	1:1.000 (Wb) 2 µl (ChIP)	Abcam (ab1791)
α-H3R2me2a	rabbit, polyclonal IgG	5 µl (ChIP)	Millipore (07-585)
α-IgG	rabbit, polyclonal	6 µg (ChIP) 45 µg (IP)	Sigma-Aldrich (I5006)
α-p16 (JC8) (= p16-INK4A)	mouse, monoclonal IgG	1:5 (Wb)	Gordon Peters
α-p21 (N-20) (= CDKN1A)	rabbit, polyclonal IgG	1:400 (Wb)	Santa Cruz (sc-469)
α-PCNA (PC10)	mouse, monoclonal IgG2a	1:1.000 (Wb)	Santa Cruz (sc-56)
α-PRMT1_milli	rabbit, polyclonal IgG	1:2.000 (Wb) 1:1.000 (IHC)	Millipore (07-404)
α-PRMT1_affi	rabbit, polyclonal IgG (affinity-purified)	1:50 (IHC)	Uta-Maria Bauer
α-PRMT6_2affi (full-length His-tagged PRMT6 antigen)	rabbit, polyclonal IgG (affinity-purified)	1:8.000 (Wb) 30 µl (ChIP) 1:100 (IHC)	affinity-purified from crude serum using GST-tagged PRMT6 protein, Uta-Maria Bauer
α-PRMT6_3affi (full-length GST-tagged PRMT6 antigen)	rabbit, polyclonal IgG (affinity-purified)	1:50 (IHC)	affinity-purified from crude serum using His-tagged PRMT6 protein, Uta-Maria Bauer
α-PRMT6_1 (His-tagged) α-PRMT6_2 (His-tagged) α-PRMT6_3 (GST-tagged) α-PRMT6_4 (GST-tagged)	rabbit, polyclonal IgG (crude sera)	45 µg (IP)	Uta-Maria Bauer
α-PRMT6_1 (His-tagged) α-PRMT6_3 (Gst-tagged)	rabbit, polyclonal IgG (preimmune sera)	45 µg (IP)	Uta-Maria Bauer
α-PRMT6_bethyl	rabbit, polyclonal IgG	1:100 (IHC)	Bethyl Laboratories (A300-929A)

3.8.2 Secondary antibodies

Table 14: Secondary antibodies used for Western blot and IHC analysis.

Secondary antibody	Type of antibody	Dilution (Application)	Source
α-mouse IgG	from sheep, polyclonal, HRP-conjugated	1:5.000 (ECL, Wb)	GE Healthcare
α-rabbit IgG	from donkey, polyclonal, HRP-conjugated	1:5.000 (ECL, Wb)	GE Healthcare
α-mouse Lambda light chain	from goat, polyclonal, HRP-conjugated	1:5.000 (ECL, Wb)	Bethyl Laboratories
α-rabbit IgG	from goat, polyclonal, biotinylated	1:500 (IHC)	Dako

4 METHODS

4.1 Cell biological methods

4.1.1 Cultivation of eukaryotic cells

Adherent eukaryotic cell lines were cultivated at a confluence of 70 - 100% in complete medium (plus FCS and antibiotics) at 37°C, 5% CO_2 and 100% humidity. Cells were splitted every two to four days depending on their growth rate.

In order to split cells the old medium was aspirated from a 145 cm^2 cell culture dish. Cells were washed once with 10 ml PBS and incubated with 2 ml Trypsin-EDTA (0.05%) at 37°C for several minutes. Upon detaching of the cells from the plastic surface of the vessel trypsin activity was stopped by adding 8 ml complete medium. After resuspension of the cells the appropriate amount of splitted cells was transferred into a new dish (145 cm^2) and supplemented with fresh complete medium to a total volume of 20 ml.

4.1.2 Freezing and thawing of eukaryotic cells

A 145 cm^2 dish was trypsinised as described in chapter 4.1.1 at a cell confluence of about 70 - 80%. Cell suspension was transferred into a 50 ml falcon, centrifuged (1.200 rpm, 3 minutes, RT) and the cell pellet was quickly resuspended in 1 ml freezing medium and transferred into a cryotube. To achieve gentle freezing of the cells, the cryotube was wrapped in paper towels and stored in a polystyrene box several days at -80°C until long term storage in the liquid nitrogen tank.

Freezing medium	30% (v/v) FCS
	10% (v/v) DMSO
	60% (v/v) complete medium

Cells were thawed quickly in a water bath at 37°C and resupended in 10 ml of fresh complete medium to avoid possible cell damage by DMSO. After centrifugation

(1.200 rpm, 3 minutes, RT), cells were transferred into a new cell culture flask depending on the cell pellet size (25 cm^2 - 175 cm^2) and cultivated.

4.1.3 Cell counting (Neubauer chamber)

In every cell culture experiment a defined cell number was needed. For this purpose cells were trypsinised (chapter 4.1.1) and diluted in a sufficient quantity of complete medium. Cell number was determined by counting at least 4 of 8 big squares of a Neubauer chamber and cell concentration was calculated using the following formula.

$$\text{concentration (cells/ml)} = \frac{\text{number of cells}}{\text{number of big squares}} \times 10^4 \times \text{dilution factor}$$

If the cell suspension was diluted before counting for example 1:10, the dilution factor of 10 was considered in the calculation of the total cell number.

4.1.4 Transient transfection of eukaryotic cells with plasmid-DNA

The choice of the best transfection method including transfection reagent was dependent on the cell line and highest transfection efficiency with lowest toxicity for the cells. The amount of transfection reagent and other supplements in the mix was adapted to the size of the dish used in an experiment.

4.1.4.1 FuGENE HD transfection

A FuGENE HD transfection in a FuGENE HD transfection reagent:DNA ratio of 2:1 was the most efficient way to transfect TIG3 BRAF-ER cells with plasmid-DNA. Therefore, 180.000 cells were seeded in a 6-well plate one day before transfection. On the next day 100 µl Opti-MEM/GlutaMAX (Life Technologies) was mixed with 1 µg DNA in a tube and 2 µl FuGENE HD was added. After an incubation of 15 minutes at RT the mix was added dropwise to a 6-well plate in a total volume of 2 ml complete medium.

4.1.4.2 Polyethylenimine (PEI) transfection

Polyethylenimine (PEI) is a linear cationic polymer. The negative charge of nucleic acids associates with PEI whereby plasmid-DNA gets a neutral charge, which is easily ingested by eukaryotic cells.

A 0.1% (v/v) PEI-solution was used to transfect MCF7 cells with plasmid-DNA seeded at a density of 3.0 x 10^6 cells in a 145 cm^2 dish. Therefore, the medium of the cell dish (50% confluent) was replaced by 18 ml fresh complete medium directly before the transfection. The DNA and PEI solution were mixed upon separate incubation (5 minutes, RT). After another 15 minutes of incubation the transfection mix was carefully added to the cell dish and the complete medium was replaced after 4 hours with 20 ml fresh complete medium. Cells were harvested 48 hours post-infection for co-immunoprecipitation (co-IP) analysis (chapter 4.3.6).

DNA solution	40 µg DNA in 900 µl PBS
PEI solution	40 µl PEI in 900 µl PBS

4.1.5 Transfection of eukaryotic cells with siRNA

For transfection of eukaryotic cells with plasmid-DNA the most efficient siRNA transfection method was used for each individual eukaryotic cell line.

4.1.5.1 LipofectamineRNAiMAX (LipoRNAiMAX) transfection

Cells were seeded 24 hours before transfection in the appropriate complete medium. NSCLC cell lines (H1299, H358) were seeded at a density of 1.1 x 10^6 cells and U2OS were seeded at a density of 0.93 x 10^6 cells in a 56 cm^2 dish. The transfection mix, Opti-MEM/GlutaMAX with siRNA and Opti-MEM/GlutaMAX with LipoRNAiMAX, was incubated for 5 minutes at RT and then combined/gently mixed in one tube for another incubation of 20 minutes at RT. The DNA-LipoRNAiMAX complexes were

added dropwise to the dish and gently mixed. After siRNA-mediated knockdown cells were harvested either for RT-qPCR (chapter 4.2.9) and Western blot analysis (chapter 4.3.5) or were replated for colony formation assay (chapter 4.1.8). All volumina of the components used in the LipoRNAiMAX transfection are listed in Table 15.

Table 15: Amounts of siRNA and LipoRNAiMAX for siRNA-mediated depletion in different cell lines.

56 cm^2 dish (10 ml):	H1299, H358 (50 nM siRNA final concentration)	U2OS (20 nM siRNA final concentration)
siRNA solution	1 ml Opti-MEM/GlutaMAX + 25 µl siRNA	1 ml Opti-MEM/GlutaMAX + 10 µl siRNA
LipoRNAiMAX solution	1 ml Opti-MEM/GlutaMAX + 15 µl LipoRNAiMAX	1 ml Opti-MEM/GlutaMAX + 6 µl LipoRNAiMAX

4.1.5.2 Polyethylenimine (PEI) transfection

The transfection reagent 0.1% (v/v) PEI was used for transient overexpression of plasmid-DNA in eukaryotic cells and siRNA-mediated depletion (20 µM stock solutions) in TIG3 BRAF-ER cells. One day before transfection, 180.000 cells were seeded in a 6-well plate (2 ml final volume) and transfected on the following day.

Solution A 5 µl siRNA (50 nM final concentration) in 75 µl PBS

Solution B 4 µl PEI in 75 µl PBS

Both solutions (A+B) were incubated for 5 minutes at RT, gently mixed, incubated another 15 minutes at RT and added dropwise to the cells. In accordance with the respective experiment cells were harvested for RT-qPCR analysis (chapter 4.2.9) or stained in a SA-ß-gal assay (chapter 4.1.7).

4.1.6 Retrovirus production and infection of eukaryotic cells

Retroviral infection of eukaryotic cells with shRNA constructs is a common method that allows stable integration of these shRNA genes into host cell genome. The Phoenix-Eco cell line is a second-generation ecotropic retrovirus producer cell line based on HEK 293T, which is capable of producing *gag*, *pol* and *env* proteins to generate recombinant retroviruses. Thereby, foreign DNA, such as shRNA-encoding plasmids (pSUPER.retro.puro), can be easily packaged in their virus particles by transfection of these constructs with calcium phosphate (Brummelkamp et al., 2002). Human TIG3-T cells that stably express the ecotropic murine receptor allow infection by ecotropic retroviruses.

4.1.6.1 Retrovirus production using Phoenix-Eco cells

The calcium phosphate method was used for efficient transfection of Phoenix-Eco cells with pSUPER.retro.puro constructs encoding for shRNAs. The produced precipitates of calcium cations and the anionic phosphate groups of the DNA were internalised by endocytosis of the Phoenix-Eco cells and production of retroviral supernatants was achieved. In the following, a transfection of a 56 cm^2 dish is described. All used buffers were dissolved in ddH_2O and sterile-filtered through a 0.2 µm syringe filter.

Cells were seeded at a density of 5.5 x 10^6 cells in a 56 cm^2 dish. On the next day they were transfected using 30 µg plasmid-DNA in 1 ml transfection solution. Therefore, DNA was filled up to 450 µl with TE (1:10 dilution), vortexed and mixed with 50 µl of 2.5 mM $CaCl_2$. Then, 500 µl 2 x HBS was added dropwise to the suspension while vortexing. This step is very crucial and important for the transfection efficiency because of the formation of very fine microcrystalline precipitates. The DNA-calcium-precipitate mix was incubated for 20 minutes at RT and added dropwise to the dish. The dish was carefully swayed. After incubation for 16 - 20 hours cells were washed with PBS to remove precipitates and 7 ml of fresh complete medium was added. After additional 24 hours the virus supernatant was collected, centrifuged (1.200 rpm,

3 minutes, RT), quickly frozen in liquid nitrogen and stored at -80°C. Again 7 ml of fresh complete medium was added to the dish. On the next day the second virus supernatant was collected as before.

TE	10 mM TRIS - pH 8.0
	1 mM EDTA
$CaCl_2$	2.5 mM
2 x HBS	1.5 mM Na_2HPO_4 - pH 6.95
	273 mM NaCl
	54 mM HEPES

4.1.6.2 Infection of TIG3-T cells

At the day of infection the virus was quickly thawed in a water bath at 37°C before adding to TIG3-T cells. For a 56 cm^2 dish, 1.2 x 10^6 TIG3-T cells were seeded 24 hours before infection. 3 ml virus, 2 ml complete medium and 10 µl Polybrene (8 µg/ml final concentration) were gently mixed. The medium was aspirated and the virus solution was added to the dish. The plate was moved to distribute the virus on the plate and cultured. After 14 - 16 hours the procedure was repeated and after additional 8 - 10 hours, 5 ml of fresh complete medium was added for recovery of the cells. 48 hours post-infection with the first virus supernatant TIG3-T cells were selected with puromycin (1 µg/ml) for 72 hours. As a control TIG-3 T cells without infection were selected with puromycin. After 3 days of puromycin selection the day counting of the experiment started and corresponded to day 0.

Polybrene	4 µg/µl in ddH_2O

4.1.7 Senescence-associated ß-galactosidase (SA-ß-gal) staining

Senescent cells have an increased activity of ß-galactosidase (ß-gal), which is detectable by histochemical staining at pH 6.0. Enhanced levels of this biomarker are associated with aging or other senescence inducing-stimuli (e.g. mitogenic oncogenes, oxidative stress), but not detectable in pre-senescent cells (early passage, proliferating cells) (Dimri et al., 1995; Storer et al., 2013).

ß-gal staining was done using the "Senescence Cells Histochemical Staining Kit" from Sigma-Aldrich. It contained the chromogenic substrat X-gal (5-bromo-4-chloro-3-indolyl-β-D-galactopyranoside), which was hydrolysed into galactose and 5-bromo-4-chloro-3-hydroxyindole by ß-galactosidase and later converted into a microscopical detectable blue, water-insoluble dye. Based on manufacturer's instructions, senescence-induced TIG3 BRAF-ER cells (200 nM 4-OHT at the indicated time points) were stained for SA-ß-gal activity. For each condition, 180.000 cells were seeded in triplicates using 6-well plates with a grid. SA-ß-gal-positive TIG3 BRAF-ER cells were photographed for qualitative analysis and the total number was quantified by counting 300 cells per condition and calculation of the mean values ± standard deviation.

After puromycin selection TIG3-T cells were incubated another 6 days in culture for efficient shRNA-mediated depletion, replated and stained at day 7 for SA-ß-gal activity (Dimri et al., 1995). Therefore, 150.000 cells were seeded in 6-well plates. After 24 hours cells were washed twice with PBS, fixed with 3% formaldehyde (in PBS) for 3 - 5 minutes at RT, washed twice in PBS and stained with SA-ß-gal staining solution (2 ml per 6-well plate) for 12 - 14 hours at 37°C incubator (without CO_2).

SA-ß-gal staining solution	1 mg/ml X-gal (in DMF)
	40 mM citric acid/sodium phosphate buffer
	($C_6H_8O_7$ x H_2O (0.1 M), Na_2HPO_4 (0.2 M) - pH 6.0)
	5 mM potassium ferricyanide(III) ($K_3Fe(CN)_6$)
	5 mM potassium ferrocyanide ($K_4Fe(CN)_6$)
	150 mM NaCl
	2 mM $MgCl_2$

4.1.8 Colony formation assay (CFA)

A colony formation assay (CFA) or clonogenic assay provides a method to determine the ability of cells to form clones without close contact to neighbour cells due to their transformational character indicated by unlimited division potential. The examined cells were transfected with siRNAs using LipoRNAiMAX as described in chapter 4.1.5.1. 48 hours post-transfection cells were replated in triplicates using a very high cell dilution depending on the cell size.

Table 16: Number of cells seeded per 6-well plate for CFA analysis.

cell line	cell number/6-well plate
H1299	400
H358	40.000
U2OS	400

After an incubation of 10 or 14 days cells were fixed in 70% (v/v) ethanol at 4°C ON, washed twice with PBS and colonies were stained with crystal violet [0.1% (w/v) in 20% ethanol] for 20 minutes. Cells were thoroughly washed several times with ddH_2O, dishes were air-dried and photographed. The quantification of crystal-violet stained colonies was performed by counting the relative colony number (in %) or by "Colony Area", an ImageJ plugin for automatically generated quantification of the colony area (in %) of each dish (Guzmán et al., 2014).

4.2 Molecular biological methods

4.2.1 Hybridisation of oligonucleotides

The 60-mer complementary oligonucleotides used for shRNA production were dissolved in ddH_2O (nuclease free) to a final concentration of 100 pmol/µl and hybridised in the following annealing reaction. The control of efficient hybridisation was achieved by agarose gel electrophoresis.

Annealing mix	1 nmol oligo (sense)
	1 nmol oligo (antisense)
	1 µl 100 mM NaCl
	1 µl 20 mM TRIS pH 7.5
	add 50 µl ddH_2O
Annealing reaction	10 minutes 95°C
	5 minutes 80°C
	3 minutes 75°C
	5 minutes, 70°C - slowly cooling-down phase to RT

4.2.2 Restriction digest of plasmid-DNA

The pSUPER.retro.puro plasmid (7195 bp) possesses amongst others a unique/single *Bgl*II and *Hind*III restriction site. The plasmid was restricted with both restriction enzyme sites, purified (chapter 4.2.3) and ligated with annealed double stranded oligo nucleotides encoding shRNAs (chapter 4.2.4), which were designed with these two restriction sites at their termini. According to manufacturer's instructions, restriction enzymes were used in their provided restriction buffers with highest enzyme activity.

Restriction I	20 µg plasmid-DNA (pSUPER.retro.puro)
	4 µl enzyme (*Hind*III, 10 U/µl)
	5 µl 10 x R restriction buffer
	add 50 µl ddH_2O - 2h at 37°C
Restriction II	Restriction I
	4 µl enzyme (*Bgl*II, 10 U/µl)
	3 µl 10 x O restriction buffer
	add 80 µl ddH_2O - 2h at 37°C

4.2.3 Agarose gel extraction of DNA fragments

Separation of DNA fragments according to their size was achieved by agarose gel electrophoresis (150 V, 1 - 2 hours) using 1 - 3% (w/v) agarose in TBE buffer depending on their expected size and 1 - 3 µl ethidium bromide, a fluorescence marker for nucleic acids. For quantification, 7 µl of "GeneRuler DNA Ladder Mix" (Thermo Scientific) was loaded on the agarose gel. Samples were mixed with 6 x Orange G sample buffer.

6 x Orange G sample buffer	60 mM TRIS - pH 7.5
	30 mM NaAc
	12 mM EDTA
	60% (v/v) glycerol
	0.36% (w/v) Orange G

The purification of DNA fragments from agarose gels was performed with the "JETQUICK Gel Extraction Spin Kit" (Genomed) according to the manufacturer`s instructions.

4.2.4 Ligation of DNA fragments

The linearised, purified pSUPER.retro.puro plasmid was ligated with the annealed 60-mer oligonucleotides using T4 DNA ligase.

Ligation reaction	20 ng plasmid-DNA (pSUPER.retro.puro)
	1 µl insert DNA (annealed oligos)
	1 µl T4 DNA ligase (5 U/µl)
	1 µl 10 x ligation buffer
	add 10 µl ddH_2O (nuclease free) - 16°C water bath, ON

4.2.5 Transformation of competent bacteria

Standard bacteria transformation was performed by heat shock. Therefore, chemical competent DH5α bacteria were thawed on ice and 100 µl cells were mixed with either 1 µg recombinant plasmid-DNA or 5 - 10 µl ligation. Cells were incubated for 20 minutes on ice. Heat shock was achieved by incubation of the cells at 42°C for 1 - 2 minutes, followed by incubation for 2 minutes on ice. In case of kanamycin-resistance plasmids, 400 µl LB medium (without antibiotic) was mixed with the bacterial cell suspension and incubated for 30 minutes up to 1 hour on a 37°C shaker. The transformation was plated on a LB dish plus antibiotic or transferred into a LB liquid culture plus antibiotic for Mini-/Maxiprep (chapter 4.2.6.1) and was incubated ON at 37°C.

4.2.6 Isolation and purification of nucleic acids

4.2.6.1 Plasmid-DNA isolation from prokaryotic cells

Miniprep - analytical scale

Plasmid-DNA was isolated from a 1.5 ml ON bacteria culture. Cells were pelleted by centrifugation (13.000 rpm, 5 minutes, RT) and supernatant was aspirated. The buffers E1 (cell resuspension), E2 (cell lysis) and E3 (neutralisation) applied in the Miniprep were components of the "JETSTAR Plasmid Maxiprep Kit" (Genomed). Cell pellet was dissolved in 300 µl cold E1 buffer. Afterwards 200 µl E2 buffer was added to the cell suspension, inverted 5 times and incubated for 5 minutes at RT. In the next step 200 µl E3 buffer was mixed with the lysed cells for neutralisation by invertion (10 times) and incubation on ice for 5 minutes. Cell debris and denatured/precipitated cell components were centrifuged (13.000 rpm, 5 minutes, RT) and the supernatant (plasmid-DNA) was mixed with 500 µl 100% ethanol, inverted 5 times and centrifuged again. The supernatant was carefully removed. The DNA pellet was dissolved in 200 µl ddH_2O, vortexed and the solution was treated with 200 µl 9 M LiCl, incubated at -20°C for 15 minutes. After centrifugation supernatant was transferred in a new tube, mixed with 300 µl isopropanol and incubated at -20°C (15 minutes) for DNA precipitation. The

solution was centrifuged, the pellet was dried, washed in 200 µl 70% (v/v) ethanol, centrifuged and washed again in 200 µl 100% ethanol. The DNA pellet was completely dried and dissolved in 50 µl ddH_2O. The DNA concentration was measured using the NanoDrop (chapter 4.2.8).

Maxiprep - preparative scale

A 300 ml ON culture was centrifuged (5.000 rpm, 15 minutes, 4C). Cell lysis and extraction of plasmid-DNA was achieved according to manufacturer's instructions using buffers E1 - E6 from the "JETSTAR Plasmid Maxiprep Kit" (Genomed). Afterwards 10ml isopropanol was added to the eluted DNA for precipitation, mixed by inverting (approximately 10 times), incubated for 5 minutes at RT and centrifuged again (5.000 rpm, 30 minutes, RT). The supernatant was discarded. After air-drying DNA pellet was dissolved in 300 µl ddH_2O. DNA was added to 15 µl 5 M NaCl (0.25 M final concentration) and mixed. In the next step 900 µl 100% ethanol was carefully added to the DNA solution and mixed until a DNA flake appeared. The DNA flake was washed twice in 900 µl 75% (v/v) ethanol and was air-dried at RT. According to the size of the flake, DNA was dissolved in 100 - 400 µl ddH_2O and concentration was measured by NanoDrop (chapter 4.2.8).

4.2.6.2 Total RNA isolation from eukaryotic cells

Adherent cells were scraped in 400 µl RL lysis buffer after aspirating the medium. The following isolation and purification of RNA from eukaryotic cells was performed according to manufacturer's instructions from the "RNA Mini Kit" (Seqlab). Additionally, after RNA binding to the column a DNase digest was performed using 1 µl DNase I in 45 µl digest buffer (RNase free) from the "peqGOLD DNase I Digest Kit" (Peqlab). After an incubation of 20 minutes at RT the column was washed and RNA was eluted in 50 µl ddH_2O (RNase free) as described in the kit. After freezing at -20°C the RNA concentration was measured by NanoDrop (chapter 4.2.8).

RNA from dishes with very small cell numbers, as seeded in the colony formation assay (CFA) in U2OS cells, was isolated according to the "RNeasy Micro Kit" (Qiagen). Before direct cell lysis buffer RLT was mixed with ß-mercaptoethanol (10 µl per 1 ml buffer). Then cell-culture medium was completely aspirated from the 6-well plate, 350 µl buffer RLT was added to the cells and cell lysat was collected in a tube. Lysate was homogenised by vortexing for 1 minute. Afterwards 1 volume of 70 % ethanol was added to the homogenised lysate, mixed and pipetted into an RNeasy spin column. After centrifugation (13.000 rpm, 15 seconds, RT) the flow-trough was discarded. As described above on-column DNA digestion was performed using the "peqGOLD DNase I Digest Kit" (Peqlab). In the next step 700 µl buffer RW1 was added to the RNeasy spin column and centrifuged to wash the spin column membrane. Again the flow-through was discarded. Two additional washing steps were performed using buffer RPE (500 µl). Spin column membrane was dried by centrifugation (13.000 rpm, 2 minutes, RT) and RNA was eluted in 11 µl ddH_2O (RNase free).

4.2.7 Control digest of DNA fragments

After ligation of the shRNA-encoding oligonucleotides into the pSUPER.retro.puro plasmid (chapter 4.2.4), DH5α bacteria transformation (chapter 4.2.5) and Miniprep (chapter 4.2.6.1), a control digest was performed.

Control digest	0.5 - 1 µg DNA
	0.5 µl enzyme (*Bgl*II, 10 U/µl)
	1.5 µl restriction buffer
	add 15 µl ddH_2O - 2h at 37°C incubation
	plus 1% (w/v) agarose gel electrophoresis

4.2.8 Concentration determination of nucleic acids (NanoDrop)

RNA and DNA concentration was determined by the NanoDrop ND-1000 spectrophotometer. The absorption of 1.5 µl of a RNA- or DNA-solution was measured at 260 nm after adjustment to the solvent ddH_2O. The additional measurement of the absorbance at 280 nm and thereby the calculation of the absorbance ratio of 260 nm and 280 nm provided information about the purity of the DNA or RNA. A ratio of $\geq$1.8 for DNA and $\geq$2.0 for RNA indicated a good purity.

4.2.9 cDNA synthesis (Reverse transcription of mRNA into cDNA)

Total RNA isolation from eukaryotic cells is explained in chapter 4.2.6.2. Amounts of 10 ng - 2 µg RNA were applied to reverse transcription after determination of RNA concentration using the NanoDrop (chapter 4.2.8). All RNA samples were equalised with ddH_2O (nuclease free) to a final volume of 10 µl. In a first reaction step, RNA was mixed with 5 µl of MasterMix I. Thereby, RNA secondary structures were removed by heating the samples to 65°C for 5 minutes followed by a fast cooling-down phase (2 minutes, 4°C). In a second step, 10 µl of MasterMix II was added to each sample. M-MLV Reverse Transcriptase contained in this mix performed cDNA synthesis using the included dNTPs (mix of dATP, dCTP, dGTP and dTTP, each 10 mM). The reaction was performed at 37°C for 1 - 2 hours in the thermocycler, stopped at 75°C for 15 minutes, followed by 4°C and storage at -20°C until RT-qPCR analysis, in which new synthesised cDNA served as template (chapter 4.2.10).

Mastermix I	1 µl 10 mM dNTP Mix
	1 µl oligo$(dT)_{17}$ primer (0.5 µg/µl)
	4 µl ddH_2O (nuclease free)

MasterMix II	2 µl 0.1 M DTT
	0.5 µl RiboLock (RNase inhibitor)
	5 µl 5 x First strand (FS) buffer
	2.5 µl ddH_2O (nuclease free)
	0.7 µl M-MLV Reverse Transcriptase

4.2.10 Real time-quantitative PCR (RT-qPCR)

RT-qPCR analysis was performed with synthesised cDNA (chapter 4.2.9) or DNA from ChIP (chapter 4.3.7) using the "ABsolute qPCR SYBR Green Mix Plus ROX Vial" (Thermo Scientific) and the Mx3000P qPCR system (Agilent Technologies). DNA polymerase, reaction buffer, dNTPs, SYBR Green I (fluorescence dye activated after binding to dsDNA) and additionally ROX (passive reference dye for normalisation of data) were provided within the kit.

In a first step, cDNA or chromatin was diluted 1:6 - 1:12 and the primer pair (100 pmol/µl, 1:1 mixture of fwd and rev primer) was diluted 1:20 - 1:40 with ddH_2O (nuclease free) depending on the performed experiment. The cDNA or chromatin dilution was pipetted in triplicates, each 6 µl, into the wells of the 96-well qPCR plate. The qPCR mix was prepared with 5 - 2.5 pmol/µl of each primer pair as well as 30 nM ROX (reference dye) and was added to the cDNA/chromatin dilution in a total volume of 25 µl.

qPCR mix	12.5 µl SYBR Green mix
	8.0 µl ddH_2O (nuclease free)
	1 µl primer pair mix (5 - 2.5 pmol/µl)
	30 nM ROX - 19 µl in 96-well

The PCR reaction was performed according the following program:

Initial denaturation	95°C	15 minutes	
Denaturation	95°C	15 seconds	45 - 55 cycles
Annealing	60°C	20 seconds	
Elongation	72°C	15 seconds	
Denaturation	95°C	1 minute	
Dissociation curve	55°C	30 seconds	
	55°C → 95°C	gradually	
	95°C	30 seconds	

The thermal profile included an amplification curve and a dissociation curve. In this second phase, the dsDNA product was melted in ssDNA by a stepwise increase in temperature from 55°C → 95° to discriminate between specific and non-specific PCR products. Additionally, a no template control (NTC), qPCR mix without DNA, was included for each primer pair to monitor contaminating template or the presence of primer dimers in the reaction.

The Mx3000P software measured for each sample the Ct value (threshold cycle), a defined cycle, in which the fluorescence increase has exceeded a specific threshold, a background signal measured in the early rounds of amplification by the software. The relative quantification of the gene expression difference between two conditions was determined by the $\Delta\Delta Ct$-method, in which the mRNA expression of a specific target gene ($Ct_{target\ gene}$) was normalised to the mRNA expression of a constant, non-regulated housekeeping gene ($Ct_{\text{housekeeping gene}}$), such as *RPS14*, *RPLP0* or *UBC*. In the context of a knockdown experiment the $\Delta\Delta Ct$ value was calculated from the ΔCt value of the specific knockdown and the ΔCt value of the control condition.

$$\Delta\Delta Ct = \Delta Ct_{knockdown} - \Delta Ct_{control} \qquad [\Delta Ct = Ct_{target\ gene} - Ct_{housekeeping\ gene}]$$

The relative expression between both conditions was presented in the following formula, in which it was presumed that a doubling in cDNA amount has taken place in each cycle.

$$relative\ expression = 2^{-\Delta\Delta Ct}$$

The standard deviation (s) was calculated by the mean value of the triple measurement of each sample. The calculation of the relative standard deviation ($s_{relative}$) according to the law of error propagation was as follows:

$$s_{relative} = 2^{-\Delta\Delta Ct} \times ln2 \times \sqrt{s(knockdown)^2 + s(control)^2}$$

In ChIP-qPCR analysis immunoprecipitated chromatin was analysed in triplicates, in which mean values were relative expressed as % input of chromatin or fold IgG, which was equated to 1. The calculation was done as follows (left panel) provided that 1% input and same IP dilutions were taken. The calculation of the relative standard deviation ($s_{relative}$) for % input and fold IgG is shown on the right panel.

$$\%\ input = \frac{1}{2^{(Ct\ IP\ -Ct\ input)}} \qquad s_{relative} = \%\ input\ \times ln2 \times \sqrt{s(IP)^2 + s(input)^2}$$

$$fold\ IgG = \frac{1}{2^{(Ct\ IP - Ct\ IgG)}} \qquad s_{relative} = fold\ IgG\ \times ln2 \times \sqrt{s(IP)^2 + s(IgG)^2}$$

Histone modifications, such as H3R2me2a, were calculated relative to histone H3 instead of normalisation to IgG. However, this is identical to the calculation of fold IgG.

4.3 Protein biochemical methods

4.3.1 Preparation of protein whole cell extracts

4.3.1.1 Protein extraction from eukaryotic cells - FT lysis

FT (freeze and thaw) lysis is a method for extraction of histones, which are released from chromatin using a high salt concentration and Benzonase digest. After removal of the medium from a confluent 145 cm^2 dish cells were washed two times in ice-cold PBS and scraped in 3 ml ice-cold PBS. Cells were pelleted (2.000 rpm, 3 minutes, 4°C) and resupended in 200 - 400 µl FT lysis buffer plus freshly added protease inhibitors. After three freeze and thaw cycles by transferring the tube into liquid nitrogen and subsequently thawing in a water bath, the cell lysate was incubated with Benzonase (250 nM) in 7 mM $MgCl_2$ for at least 30 - 45 minutes at 4°C on a rotating wheel to digest the DNA. The sample was centrifuged (13.000 rpm, 10 - 15 minutes, 4 °C) and a Bradford assay of the supernatant was performed (chapter 4.3.2).

FT lysis buffer	20 mM TRIS - pH 8.0
	600 mM NaCl
	20% (v/v) glycerol
Protease inhibitors (1:1000)	Aprotinin
	Leupeptin
	PMSF (each 10 µg/µl)

4.3.1.2 Protein extraction from eukaryotic cells - IPH lysis

A confluent cell culture dish (145 cm^2) was washed twice with ice-cold PBS. Cells were collected in 3 ml ice-cold PBS into a falcon, centrifuged (2.000 rpm, 5 minutes, 4°C) and cell pellet was stored ON at -20°C. On the next day the cell pellet was resuspended in 200 µl IPH buffer (400 mM NaCl) with protease inhibitors and incubated at least 30 minutes at 4°C on a rotating wheel. Protein extracts were diluted with IPH Buffer (0 mM NaCl) to a final lysis buffer concentration of 200 nM NaCl. Benzonase (250 U)

and 7 mM $MgCl_2$ were added to the suspension and incubated for 1 hour at 4°C on a rotating wheel. After centrifugation (13.000 rpm, 15 minutes, 4°C) the supernatant was centrifuged again. Protein concentration of the second supernatant was determined by Bradford (chapter 4.3.2) for the following Co-IP (chapter 4.3.6) or Western blot (chapter 4.3.5) analysis.

IPH buffer (400 mM NaCl)	50 mM TRIS - pH 8.0
	400 mM NaCl
	5 mM EDTA
	0.5% (v/v) igepal
Protease inhibitors (1:1000)	Aprotinin
	Leupeptin
	PMSF (each 10 µg/µl)

4.3.2 Determination of protein concentration (Bradford)

Colorimetric protein assay is a spectroscopic method to measure the protein concentration in a solution using Coomassie Brilliant Blue G described by Bradford in 1976 (Bradford, 1976). Each protein sample was measured in duplicates. Therefore, 100 µl ddH_2O was provided in semi-micro cuvettes and the protein sample (1 µl) was added. After addition of 900 µl Bradford solution and an incubation of 5 minutes at RT the extinction/OD at 595 nm of each sample was measured in the photometer relative to a blank solution without protein extract. Quantification of protein concentration was realised by an additional calculated standard curve using a BSA standard series with a range of 0 - 8 µl BSA (1 µg/µl).

Bradford solution	0.01% (w/v) Coomassie Brilliant Blue G 250
	in 4.75% (v/v) ethanol,
	10% (v/v) ortho-phosphoric acid (85%)

4.3.3 SDS-polyacrylamide gel electrophoresis (SDS-PAGE)

SDS-polyacrylamide gel electrophoresis (SDS-PAGE) is a technique to separate proteins in an electrical field according to their molecular weight. The addition of the detergent SDS causes a denaturation of proteins. In detail, SDS interacts with aa side chains and removes secondary and tertiary structures. It creates an equal negative charge of the unfolded polypeptide chains. Proteins with a smaller size run faster and larger proteins run slowier in the polymer grid structure. After SDS-PAGE several other techniques, such as Coomassie staining (chapter 4.3.4) or Western blot analysis (chapter 4.3.5), were performed.

The following Table 17 shows the formula of the separation and stacking gel for one SDS gel with a size of 1.5 mm. The amount of 30% (w/v) acrylamide/0.8% (w/v) bis-acrylamide in a separation gel is depending on the percentage of the gel or the size of the polymer grid structure, respectively.

Table 17: Composition of the separation and stacking gel used in SDS-PAGE.

Data for 1 x gel (1.5 mm)	Separation gel	Stacking gel (4%)
30% (w/v) acrylamide / 0.8% (w/v) bis-acrylamide	x ml	0.85 ml
1M TRIS pH 8.8	2.8 ml	--
1M TRIS pH 6.8	--	0.625 ml
20% (w/v) SDS	37.5 µl	25 µl
ddH_2O	4.68 ml - x ml	3.5 ml
20% (w/v) APS	20 µl	10 µl
TEMED	10 µl	5 µl

Each protein sample was mixed with an appropriate volume of 4 x SDS sample buffer and was incubated for 5 minutes at 95°C to denature the proteins. Proteins were

loaded into the pockets of a SDS gel in the running chamber, which was filled up with 1 x SDS running buffer. The "PageRuler Prestained Protein Ladder" (Thermo Scientific) served as molecular weight standard. Proteins were separated for 1 hour 15 minutes up to 3 hours at 160 volts depending on the percentage of the separation gel.

4 x SDS sample buffer	250 mM TRIS - pH 6.8
	2% (w/v) SDS
	40% (v/v) glycerol
	0.1% (w/v) bromophenol blue
	20% (v/v) ß-mercaptoethanol
1 x SDS running buffer	25 mM TRIS
	192 mM glycine
	0.1% (w/v) SDS

4.3.4 Coomassie staining

Visualisation of protein bands after separation in a polyacrylamide gel was possible using the Coomassie staining method. This staining technique is used to estimate protein amounts in the gel in comparison to a (e.g.) BSA standard series. After gel electrophoresis the polyacrylamide gel was incubated in staining solution for approximately 10 minutes depending on the gel size (RT, shaker). Remains of the dye were removed by rinsing the gel in tap water. The gel was bleached by incubation three times in the destaining solution (each 10 minutes, RT, shaker) until the desired contrast against the background of the gel was received.

Staining solution	25% (v/v) ethanol
	10% (v/v) acetic acid
	0.25% (w/v) Coomassie Brilliant Blue G 250
Destaining solution	25% (v/v) ethanol
	10% (v/v) acetic acid

4.3.5 Western blot

4.3.5.1 Transfer of proteins from SDS-PAGE on PVDF membrane

Western blot is a technique to transfer and immobilise proteins from a polyacrylamide gel on a PVDF membrane for later antibody detection. Here, tank blotting was performed.

The hydrophobic surface of the PVDF membrane had to be activated by incubation in 100% methanol for approximately 10 seconds. The setup of a Western blot from the cathode (-) to the anode (+) was as follows: blotting sponge, 2 x Whatman paper layers, SDS gel, PVDF membrane, 2 x Whatman paper layers and blotting sponge. All components were soaked in transfer buffer. The tank blotting duration differed from 30 minutes up to 2 hours at 45 volts depending on the size of the proteins.

Tank blotting buffer	384 nM glycine
	50 nM TRIS
	0.2% (w/v) SDS
	20% (v/v) methanol

4.3.5.2 Immunodetection of proteins immobilsed on PVDF membranes

Immunodetection is a method to identify proteins from a given sample, which are immobilised on a PVDF membrane within and detectable using a primary antibody specifically targeting the protein of interest.

After saturation of the membrane with blocking buffer (1 hour, RT, shaker) to saturate unspecific binding sites of PVDF membrane, the blot was incubated with primary antibody (chapter 3.8.1) ON at 4°C or at least 2 - 3 hours at RT on a shaker. Then, the membrane was washed three times with TBS-T (0.5%), each 10 minutes at RT on a shaker to remove excess of antibody. Subsequently the blot was incubated with HRP-conjugated secondary antibody (1 hour, RT, shaker) (chapter 3.8.2). After three washing steps twice TBS-T (0.5%) and once TBS (each 10 minutes, RT, shaker) to

remove unbound secondary antibody antibody bound HRP was detected using ECL (enhanced chemi-luminescence). 10 ml of each ECL solution (A and B), were mixed and poured on the membrane (5 minutes, RT). Thereby Luminol is oxidised by HRP using H_2O_2 (oxidising reagent) leading to emission of light, which blackens the X-ray film, when exposed with the membrane in an X-Ray cassette.

Blocking buffer	4% (w/v) milk powder in TBS-T (0.5%)
ECL (solution A)	100 mM TRIS - pH 8.5 2.5 mM Luminol (in DMSO) 0.4 mM p-Coumaric acid (in DSMO) in ddH_2O
ECL (solution B)	100 mM TRIS - pH 8.5 0.036% H_2O_2

4.3.5.3 Stripping of PVDF membranes

Stripping of PVDF membranes is a method to remove primary and secondary antibodies bound on a membrane either under mild conditions with a pH shift or under harsh conditions using ß-mercaptoethanol.

Mild strip

The membrane was incubated in 50 - 100 ml freshly prepared mild stripping buffer for 5 - 10 minutes under shaking. The buffer was discarded and the mild strip was repeated. The membrane was washed twice with PBS for each 10 minutes, washed twice with TBS-T (0.5%) for each 5 minutes and was reblocked with blocking buffer as described in chapter 4.3.5.2.

Mild stripping buffer	1.5% (w/v) glycine 0.1% (w/v) SDS 1% (v/v) Tween 20 - pH 2.2

Harsh strip

The blot was incubated in 100 ml harsh stripping buffer for 30 minutes at 65°C in a water bath. Afterwards the membrane was rinsed several times in TBS-T (0.5%), washed twice in TBS-T (0.5%) for 30 minutes at RT and reblocked for the following antibody staining (chapter 4.3.5.2).

Harsh stripping buffer	50 mM TRIS - pH 6.8
	4% (w/v) SDS
	1% (v/v) ß-mercaptoethanol

4.3.6 Co-Immunoprecipitation (Co-IP)

Protein-protein-interactions were analysed by semi-endogenous or endogenous Co-IPs using whole cell extracts from MCF7 cells. These protein extracts were incubated with a specific or control rabbit antibody and were precipitated with protein A sepharose. Then, blotting (chapter 4.3.5.1) and immunodetection (chapter 4.3.5.2) were performed with the corresponding antibody such as recognising potential interaction partners.

48 hours after PEI transfection (chapter 4.1.4.2) cells were harvested, lysed and protein extracts were prepared as described in chapter 4.3.1.2. 1 mg precleared extract of each sample with overexpressed or endogenous interaction partners was subjected to IP with PRMT6 crude serum (5 µl) in parallel to PRMT6 preimmune serum (5 µl) or IgG rabbit (45 µg) as controls (ON, 4°C, on a rotating wheel). All samples were adapted to the same sample volume, at least to 500 µl in total. Either 2% or 10% of inputs were prepared from the precleared extracts in parallel to the IPs. The required amount of protein A sepharose, resuspended in IPH buffer (200 mM NaCl) was blocked with BSA (20 µg/ml; ON, 4°C, on a rotating wheel) to minimise unspecific binding to the beads. On the next day 20 µl blocked beads were added to the extracts and incubated for 2 hours at 4°C on a rotating wheel. After extensive washing (5 x each 1 ml) with IPH buffer (200 mM NaCl; plus protease inhibitors) and centrifugation (5.000 rpm,

1 minute, RT) precipitates and inputs were analysed by SDS-PAGE (chapter 4.3.3) and Western blot (chapter 4.3.5) after solving them in 2 x SDS sample buffer (chapter 4.3.3) and incubation for 10 minutes at 95°C.

IPH buffer (200 mM NaCl)	50 mM TRIS - pH 8.0
	200 mM NaCl
	5 mM EDTA
	0.5% (v/v) igepal
Protease inhibitors (1:1000)	Aprotinin
	Leupeptin
	PMSF (each 10 µg/µl)

4.3.7 Chromatin immunoprecipitation (ChIP)

Chromatin immunoprecipitation (ChIP) is an efficient tool to examine binding of nuclear proteins to specific chromatin regions as well as to analyse the occurence of histone modifications. ChIP analysis was performed with U2OS and TIG3-T wild type cells, which were seeded at a density of 2.4 x 10^6 and 2.7 x 10^6 cells in a 145 cm^2 dish, respectively.

Day 1 (Chromatin crosslink and sonication): 72 hours after seeding confluent dishes were treated with 36.5% (v/v) formaldehyde solution (1% final concentration) for 10 minutes at RT in the fume hood for covalent DNA-protein-crosslink. The reaction was stopped by adding 2.5 M glycine (125 mM final concentration) to the medium for 5 minutes at RT. Cell dishes were washed twice with ice-cold PBS and scraped with 1 ml ice-cold PBS per dish into a falcon. After centrifugation (1.200 rpm, 5 minutes, 4°C) the pellet was dissolved in lysis buffer I (1 ml per 145 cm^2 dish) and incubated for 20 minutes on ice. Lysed cells were centrifuged again (1.200 rpm, 5 minutes, 4°C) to remove cell membranes and organelles. The resulting nuclear pellet was resuspended in lysis buffer II (20 x 10^6 cells/ml) for another 10 minutes on ice and aliquots of 1 ml per 15 ml falcon were prepared. In the next step a sonication of the lysats cooled in a

water-ice mixture was performed using the microtip from Branson as follows:

U2OS cells	80 x 1 second pulse, 3 seconds pause, 15% amplitude
TIG3-T cells	60 x 1 second pulse, 3 seconds pause, 20% amplitude

Chromatin was centrifuged (13.000 rpm, 15 minutes, 4°C), supernatants were pooled, stored on ice ON and a 50 µl aliquot was used for reversion of the crosslink with 0.4 µg/µl RNase A and 0.4 µg/µl proteinase K in the thermocycler (3 hours at 55°C, ON at 65°C). The required amount of protein A sepharose was washed and centrifuged twice in lysis buffer II (1.800 rpm, 3 minutes, 4°C). Afterwards the beads were blocked with BSA (1 µg/µl) and salmon sperm (400 µg/ml final concentration) ON at 4°C on a rotating wheel for minimising unspecific bindings.

Day 2 (Preclearing and IPs): 50 µl reversed chromatin was purified according to manufacturer's instructions ("QIAquick PCR Purification Kit"). Sonication efficiency was estimated on a 1% (w/v) agarose gel (110 V, 30 - 50 minutes) with 10 µl of this sample. Sheared DNA fragments should have a size between 500 - 1000 bp. Then the reversed chromatin was used to measure chromatin concentration by NanoDrop for later IP preparation (chapter 4.2.8).

The blocked beads were washed twice in lysis buffer II and beads were added to chromatin (not reversed) for preclearing (2 hours, 4°C, on a rotating wheel) depending on the number of IPs (20 µl per IP). Afterwards precleared chromatin was centrifuged (1.200 rpm, 5 minutes, 4°C) splitted into the planned IP reactions with equivalent amounts of chromatin and minimum of 500 µl volume. Chromatin was incubated with the corresponding antibodies (ON, 4°C, on a rotating wheel). Therefore, 80 - 100 µg chromatin was used for an IP with the PRMT6 or IgG rabbit antibody and 25 - 40 µg chromatin was used for IP with an antibody against H3R2me2a or H3. Triple input (1%) of each chromatin sample was transferred in separate tubes.

Day 3 (Washing and elution of IPs): Each IP was incubated with 28 µl sepharose A for 2 hours at 4°C on a rotating wheel. Subsequently the beads were centrifuged (2.000 rpm, 2 minutes, RT) and washed with 1 ml buffer under centrifugation as follows:

2 x wash buffer I, 2 x wash buffer II, 4 x wash buffer II, 2 x TE buffer

Beads were mixed with 250 µl freshly prepared elution buffer, incubated for 15 - 30 minutes at RT on a rotating wheel, boiled (4 minutes, 65°C) and centrifuged as before. Supernatants were transferred into a new tube and elution was repeated. In parallel, 500 µl elution buffer was added to each 1% input sample. Per sample 52 µl reversion buffer was added and incubated for 3 hours at 55°C and ON at 65°C in the thermocycler.

Day 4 (Purification and ChIP-qPCR): Based on the manufacturer's instructions of the "QIAquick PCR Purification Kit" (Qiagen), chromatin samples were purified and dissolved in 50 µl EB elution buffer of the kit and stored at -80°C. ChIP-qPCR analysis was performed as described in chapter 4.2.10, in which chromatin and input was diluted 1:6 - 1:8 in ddH_2O (nuclease free).

Formaldehyde	36.5% (v/v) in ddH_2O (Sigma)
Glycine	2.5 M (Roth)
Lysis buffer I	5 mM PIPES - pH 8.0 85 mM KCl 0.5% (v/v) igepal (plus protease inhibitors: Aprotinin, Leupeptin, PMSF 1:1000 and PIC tablet)
Lysis buffer II	10 mM TRIS - pH 7.5 150 mM NaCl 1% (v/v) igepal 1% (w/v) sodium deoxycholate 0.1% (w/v) SDS 1 mM EDTA (plus protease inhibitors: Aprotinin, Leupeptin, PMSF 1:1000 and PIC tablet)

Salmon Sperm	sonicated, phenol-chloroform extraction
	4-6 µg/µl in ddH_2O
Wash buffer I	20 mM TRIS - pH 8.0
	150 mM NaCl
	2 mM EDTA
	0.1% (w/v) SDS
	1% (v/v) Triton X-100
Wash buffer II	20 mM TRIS - pH 8.0
	500 mM NaCl
	2 mM EDTA
	0.1% (w/v) SDS
	1% (v/v) Triton X-100
Wash buffer III	10 mM TRIS - pH 8.0
	1 mM EDTA
	250 mM LiCl
	1% (v/v) igepal
	1% (w/v) sodium deoxycholate
TE buffer	10 mM TRIS - pH 8.0
	1 mM EDTA
Elution buffer	1% (w/v) SDS
	0.1 M $NaHCO_3$
Reversion buffer	400 mM TRIS - pH 6.8
	2 M NaCl
	100 mM EDTA
	0.4 µg/µl Proteinase K
	0.2 µg/µl RNase A

4.3.8 Immunohistochemical staining (IHC) of tissue sections

Immunohistochemistry allows the detection of antigens in biological tissue sections by specific antibody staining directed against the antigen and visualisation with a staining dye. Images were taken by NanoZoomer, a digital slide scanner from Hamamatsu using the software NDP.view. All used lung tumour sections in this study and usage of the NanoZoomer were kindly provided by Rajkumar Savai from the MPI in Bad Nauheim. Deparaffinisation (alcohol series), peroxidase block and washing steps of tissue sections were performed in staining boxes with racks made of glass and a capacity of 200 ml. Washing steps in TBS-T (0.05%), TBS or ddH_2O were conducted on the magnetic stirrer under slow stirring.

Tissue sections were deparaffined twice for 8 minutes with Roticlear and incubated in a descending alcohol series for hydrogenation (3 minutes in each solution).

alcohol series	isopropanol
	96% (v/v) ethanol
	80% (v/v) ethanol
	70% (v/v) ethanol

In the meantime 1 x TRIS retrieval (200 ml) was filled into a plastic staining box (with lid) and preheated in the steam cooker (bottom filled with tap water) for 20 minutes. After washing the slides for 3 minutes in ddH_2O rack with slides was transferred into this staining box. Samples were boiled in TRIS retrieval for 20 minutes in the steam cooker to unmask protein epitopes. Subsequently slides were cooled by stepwise addition of tap water within the next 15 minutes. Afterwards slides were washed again with ddH_2O. Tissue sections were blocked with 3% (v/v) peroxidase solution for 10 minutes at RT (blockage of endogenous peroxidases), washed two times for each 3 minutes with TBS-T (0.05%) and once in TBS. A staining chamber (Roth) was prepared with tap water. Primary antibody (chapter 3.8.1) was diluted in "antibody diluent" depending on the total number of sections (100 - 150 µl antibody dilution/slide). Excess solution was removed from each slide and each tissue section was circled with a

"Dako Pen" for providing a barrier to liquids. Thereby, the sensitive sections should never desiccate to avoid tissue damage. Each section was incubated with primary antibody in the staining chamber ON at 4°C. On the next day slides were washed twice with TBS-T (0.05%), once with TBS and were incubated with biotinylated secondary antibody α-rabbit IgG (chapter 3.8.2) in "antibody diluent" (100 - 150 µl/slide) for 30 minutes at RT. After another washing round 1 - 2 drops of undiluted streptavidin peroxidase was added to the slides for the next 30 minutes at RT. Slides were washed again and kept in ddH_2O until AEC staining using the "AEC (red) Substrate Kit" (Life Technologies). Preparation of AEC solution was performed according manufacturer's instructions. Subsequently each tissue section was stained with this AEC solution until the desired staining grade was reached (1 - 15 minutes) and then, transferred into ddH_2O to stop the staining reaction. For nuclear counterstaining, slides were incubated in "Mayer´s hemalum solution" for 8 - 15 seconds under shaking and rinsed intensively in tap water for the next 5 minutes, which was necessary for the pH shift to achieve the "blueing" of the slices. Tissue sections were washed another time in ddH_2O and embedded in Mowiol solution using cover slips for later microscopic analysis.

10 x TRIS retrieval	100 mM TRIS - pH 9.0 10 mM EDTA (stock and 1 x solution - storage at 4°C)
Peroxidase block solution	3% (v/v) H_2O_2 in ddH_2O (20 ml 30% peroxidase stock solution + 180 ml ddH_2O, (storage at 4°C)
Washing buffers	TBS-T (0.05%): TBS - pH 7.9 (HCl), 0.05% (v/v) Tween 20 TBS: TRIS (10 mM) - pH 7.9 (HCl), NaCl (150 mM)
Mayer´s hemalum solution	25% (v/v) in ddH_2O (60 ml hemalum stock solution + 180 ml ddH_2O)

Mowiol solution	60 g (w/v) glycerol
	24 g (w/v) mowiol 4-88
	add 60 ml ddH_2O
	add 120 ml 0.2 M TRIS - pH 8.5, dissolving at 53°C ON
	10 ml aliquots at -20°C, used aliquots at 4°C

5 RESULTS

5.1 PRMT6 is deregulated in lung cancer

PRMTs are deregulated in a variety of human cancers, such as breast, colorectal and lung cancer (Baldwin et al., 2014; Yang and Bedford, 2013). Lung cancer is the single largest cause of cancer-related death in humans mostly caused by non-small cell lung carcinoma (NSCLC) (Ramalingam et al., 2011). Relatively little is known about the deregulation of PRMT6 in lung tumourigenesis. So far, only Yoshimatsu and colleagues performed a cDNA microarray expression analysis, in which few tumour tissues were compared with corresponding non-neoplastic tissues derived from the same patient (Yoshimatsu et al., 2011). Here, gene expression of *PRMT6* was shown to be elevated in lung cancer (NSCLC, SCLC) and PRMT6 positively influences growth of different lung cancer cell lines (e.g. A549) demonstrated by siRNA knockdown of *PRMT6.* Similar results were found for *PRMT1*. However, since no PRMT6 antibody was available, an increase in PRMT6 protein levels could not be validated in cancer tissues by tissue microarray analysis.

5.1.1 Prmt6 protein levels are increased in murine lung tumour sections

In order to get a better insight into the deregulation of PRMT6 in lung cancer immunohistochemical (IHC) analysis of Prmt6 was performed in murine lung tumour sections. Therefore, Prmt6 protein levels in tissue sections of two murine lung cancer models, a LLC1 (Figure 6, LLC1 #1 - #3) and $Kras^{LA2}$ mouse model (Figure 7, 59s Lung #1, #2, #4), were compared to healthy C57BL/6 mice (Figure 5, HealthyCon #1 - #3). Both tumour models are based on this healthy C57BL/6 mouse strain. In each of these cases (C57BL/6, LLC1 or $Kras^{LA2}$ strain), fixed lung tissue sections from three different mice were used in each staining procedure with one specific PRMT antibody in this study. All murine lung tissue sections were kindly provided by Rajkumar Savai (MPI, Bad Nauheim).

Lewis lung carcinoma cells were derived from a spontaneous lung carcinoma and used for allotransplantation, whereas a suspension of LLC1 cells was intravenously injected into the tail of healthy C57BL/6 mice. These treated mice develop lung tumours within one month (Henneke et al., 2010). In contrast to LLC1, the $Kras^{LA2}$ mouse harbours a targeted, latent *Kras* G12D allele that is capable of spontaneous somatic activation *in vivo* (Johnson et al., 2001; Mise et al., 2012). These mice form tumours in numerous organs within several months, in which especially an early onset of lung cancer is detectable. All fixed murine lung tumour sections were stained with an affinity-purified PRMT6 antibody, which was raised against human, full-length PRMT6 (PRMT6_2affi) (Stein et al., 2012). Thereby, PRMT6_2affi is able to cross-react with murine Prmt6 because of their 91.5% amino acid sequence identity. Moreover, all sections were counterstained with Hematoxylin to achieve blue stained cell nuclei.

Typical structures of the lung, such as bronchioles (B) adjacent to blood vessels (BV), alveolar ducts (AD) and alveolar sacs (AS) with its alveoli (A), were visualised by counterstaining in the sections of three healthy C57BL/6 mice (HealthyCon #1 - #3) (Figure 5). Similarly, in the tumour tissues, areas of healthy alveolar and bronchiolar structures (healthy tissue: HT) were clearly distinguishable from proliferating tumour cells (tumour tissue: TT, in Figure 6, 7). The control tissues showed only a few Prmt6-positive stained lung cells, which were mostly located in the epithelium of the bronchioles or in their vicinity. The identity of these positively stained cells is unknown and has to be further analysed. In contrast to tissues of healthy C57BL/6 mice, the IHC stainings of two LLC1 mice (LLC1 #1 and #2) revealed that Prmt6 levels were elevated in the enlarged nuclei and surrounding cytoplasms of cells embedded in the lung tumour tissues (Figure 6A, 6B). The same applied to the PRMT6 stainings of three $Kras^{LA2}$ mice (59s Lung #1, #2 and #4). Here, cells were positively stained for Prmt6 in the tumour mass and the epithelium of bronchioles (Figure 7). However, sections from the third LLC1 mouse (LLC1 #3) differed from the two other LLC1 sections (Figure 6C). Distinct tumour areas could not be detected in this mouse. Prmt6-positive stainings were located everywhere within the bronchiolar and alveolar structures. Presumably,

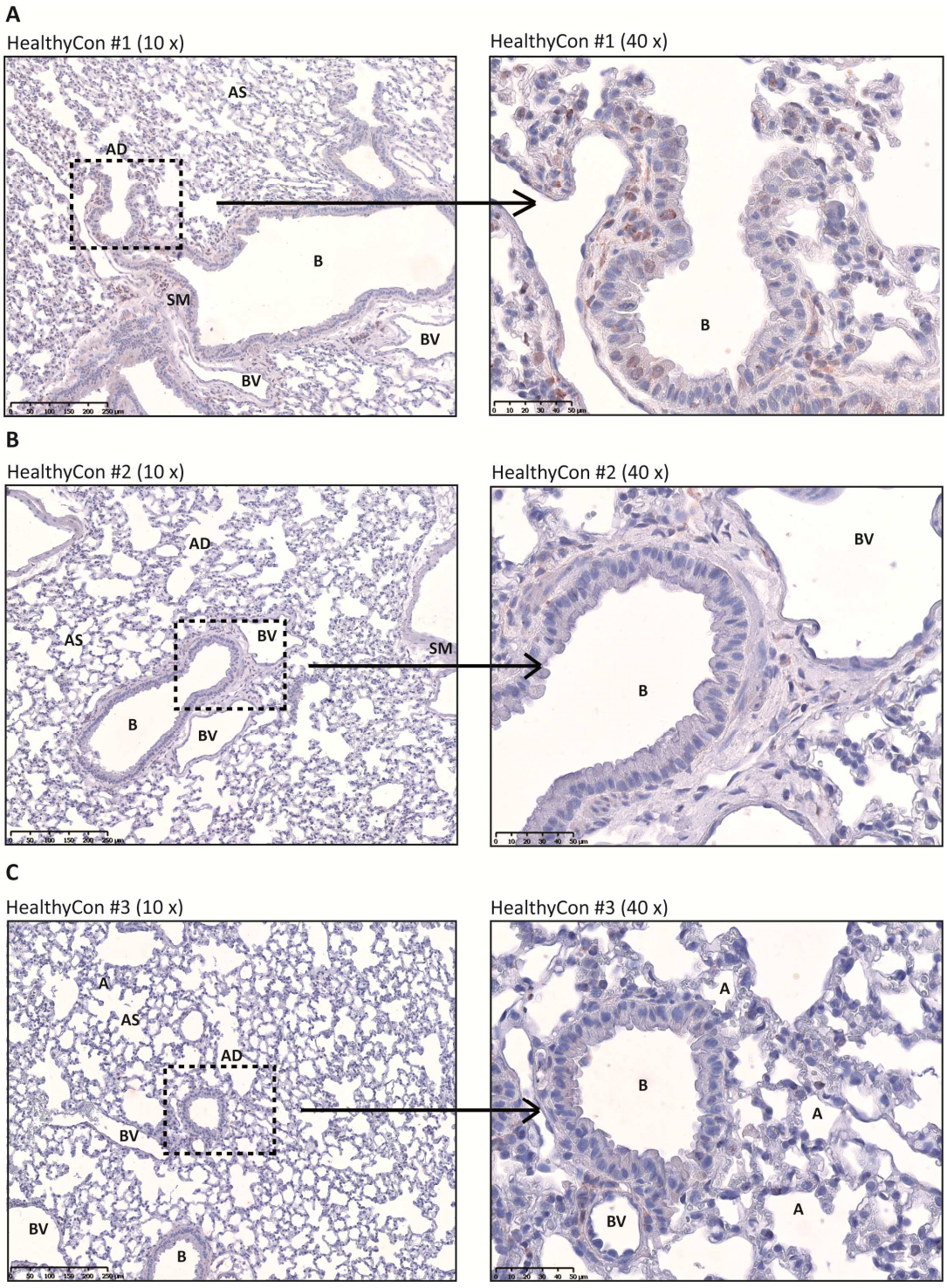

Figure 5: IHC stainings of Prmt6 in lung sections from C57BL/6 mice (PRMT6_2affi).

(**A** - **C**) Paraffin embedded lung tissue sections from healthy C57BL/6 mice (HealthyCon #1 - #3) were stained with a PRMT6-specific antibody (PRMT6_2affi) in a 1:100 dilution (AEC, red). Hematoxylin served for counterstaining (blue). Shown are representative image parts of three individual murine lungs from C57BL/6 mice (HealthyCon #1, #2 and #3) either in a 10 x magnification (left panel, maximal scale bar length: 250 µm) and 40 x magnification (right panel, maximal scale bar length: 50 µm). A: alveolus, AD: alveolar duct, AS: alveolar sac, B: bronchiole, BV: blood vessel, SM: smooth muscle.

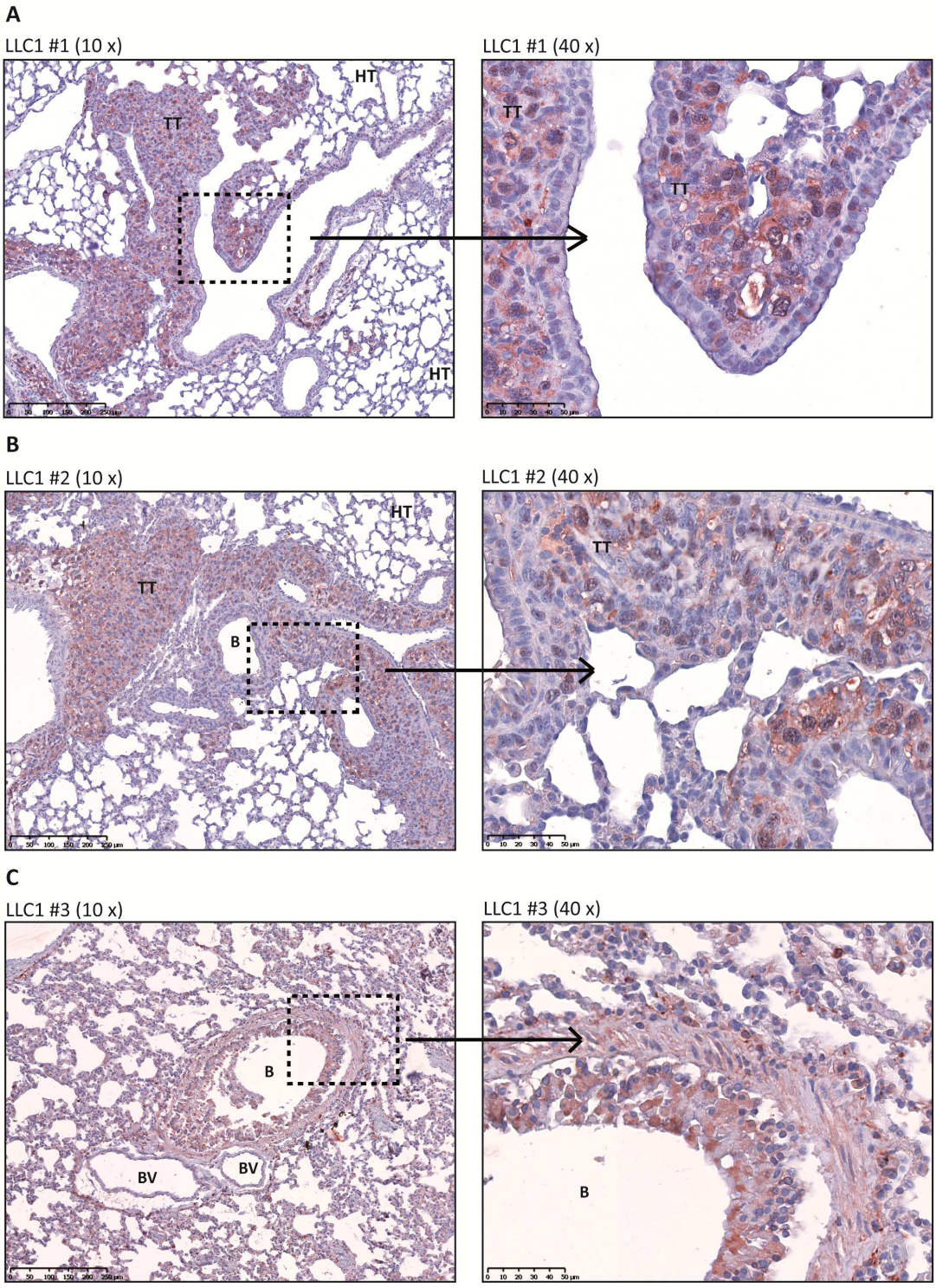

Figure 6: IHC stainings of Prmt6 in murine LLC1 lung specimen (PRMT6_2affi).

(**A** - **C**) IHC analysis of Prmt6 protein levels in paraffin embedded lung tissue sections from LLC1 mice (LLC1 #1 - #3), in which AEC was used for detection of PRMT6 (PRMT6_2affi, 1:100, red) and Hematoxylin for counterstaining (blue). LLC1 #3 was little overstained in the Prmt6 staining. Representative images are depicted in a 10 x magnification (left panel, maximal scale bar length: 250 µm) and 40 x magnification (right panel, maximal scale bar length: 50 µm). B: bronchiole, BV: blood vessel, HT: healthy tissue, TT: tumour tissue.

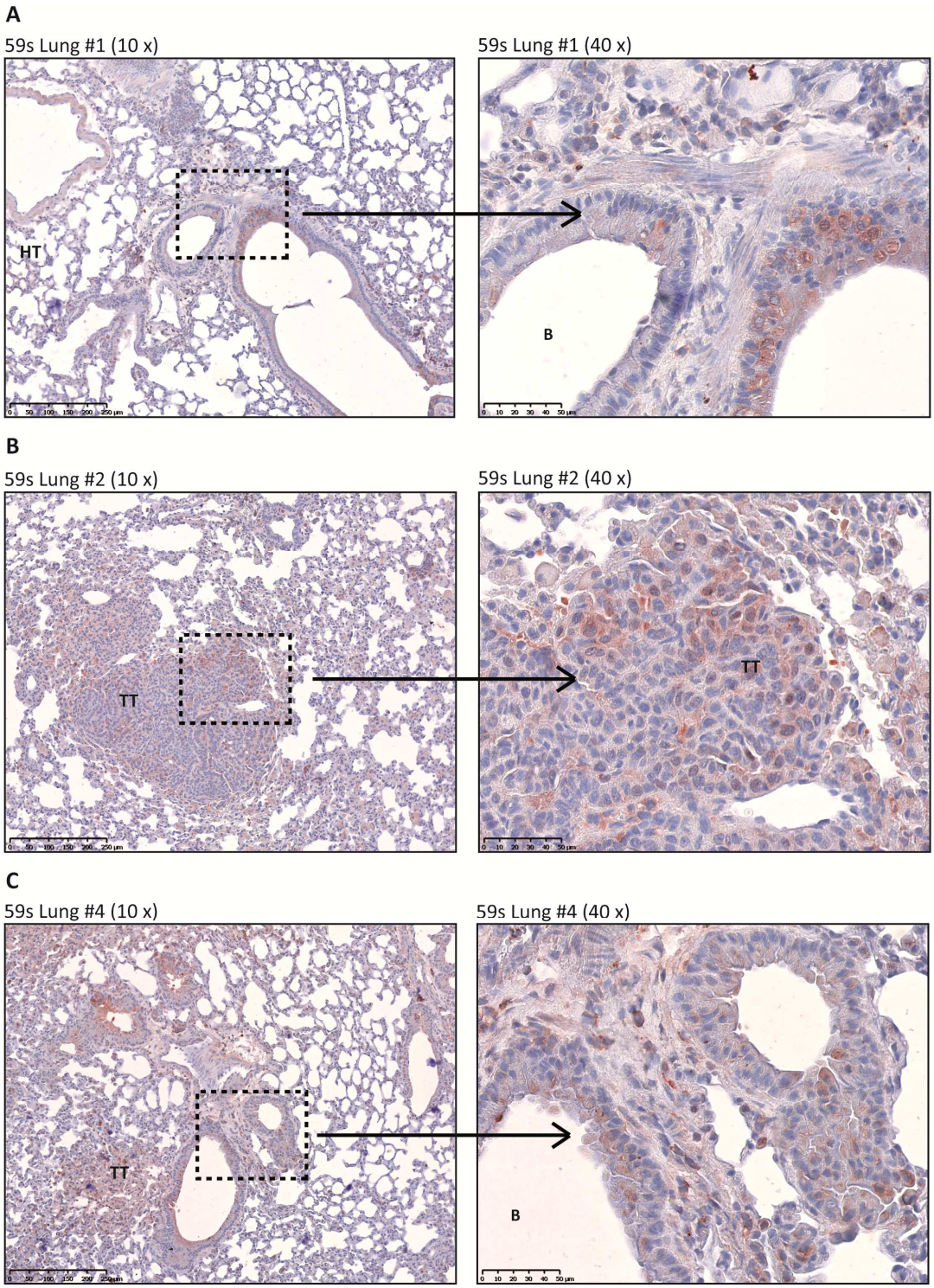

Figure 7: IHC stainings of Prmt6 in specific tumour tissues in the lung of Kras^{LA2} mice (PRMT6_2affi).

(**A** - **C**) Paraffin embedded lung tissue sections from Kras^{LA2} mice (59s Lung #1, #2 and #4) were stained with a PRMT6 antibody (PRMT6_2affi), which was diluted 1:100 (AEC, red) and counterstained with Hematoxylin (blue). A representative result from all Kras^{LA2} mice tissue sections is given using a 10 x magnification (left panel, maximal scale bar length: 250 µm) and 40 x magnification (right panel, maximal scale bar length: 50 µm). B: bronchiole, HT: healthy tissue, TT: tumour tissue.

inflammatory processes were still in process after intravenous injection of LLC1 cells into the tail of healthy C57BL/6 mice. As a result, lung tumours were not fully developed in LLC1 #3 compared to LLC1 #1 and #2 (personal communication, Rajkumar Savai).

In order to confirm the specificity of all previous observations made in lung tumour sections using PRMT6_2affi, IHC stainings of all sections (C57BL/6, LLC1 and $Kras^{LA2}$) were repeated with two additional PRMT6 antibodies, a second affinity-purified PRMT6 antibody (PRMT6_3affi) from the lab and a commercial PRMT6 antibody (PRMT6_bethyl). PRMT6_3affi is able to cross-react with murine Prmt6 identical to PRMT6_2affi (91.5% amino acid sequence identity). Equally, PRMT6_bethyl also cross-reacts with murine Prmt6 as demonstrated in Western blot analysis (Lorenzo et al., 2014; Neault et al., 2012). Therefore, one of the three analysed and very similar stained murine lung sections of the C57BL/6 (HealthyCon #1), LLC1 (LLC1 #1) and $Kras^{LA2}$ (59s Lung #1) mice were representatively selected and are depicted in Figure S1 and S2.

In general, PRMT6_3affi gave stronger signals in the IHC analysis than the stainings using PRMT6_2affi (AEC), while the Hematoxylin staining was less pronounced especially in the depicted HealthyCon #1 and LLC1 #1 (Figure 6 and S1). Nevertheless, the representative tissue section from the healthy C57BL/6 mouse (HealthyCon #1) showed that only a few cells in the alveolar structure are positively stained for Prmt6 (Figure S1A). These could possibly be macrophages. In contrast, the LLC1 #1 image demonstrated elevated Prmt6 levels in the nuclei as well as in the surrounding cytoplasms of lung tumour cells (Figure S1B). This result is in agreement with the stainings of LLC1 mouse sections using the PRMT6_2affi antibody (Figure 6), in which Prmt6 protein levels were elevated in a similar pattern. However, in case of the $Kras^{LA2}$ mouse, the staining of 59s Lung #1 with PRMT6_3affi differed a little bit from previous PRMT6 stainings of $Kras^{LA2}$ mice using PRMT6_2affi (Figure 7 and S1C). Here, the representative image of the $Kras^{LA2}$ mouse demonstrated increased Prmt6 levels in some cells, which also could possibly be macrophages embedded in the alveolar structure (Figure S1C) as in the case of the control staining (Figure S1A). Further

investigations are necessary to confirm this hypothesis, such as macrophage-specific stainings (Lloyd et al., 2008).

Finally, IHC-stainings with the PRMT6_bethyl antibody showed a similar staining pattern of the healthy C57BL/6 mouse (HealthyCon #1, Figure S2A) compared to the PRMT6_3affi antibody. Some stained cells are Prmt6-positive, which could possibly be macrophages. The representative LLC1 mouse section (LLC1 #1, Figure S2B) is also comparable with previous stained sections using PRMT6_2affi or PRMT6_3affi demonstrating increased Prmt6 levels in the nuclei and cytoplasms of lung tumour cells (Figure 6A, 6B, S1B). Similar to the PRMT6_3affi staining, the staining pattern of the Kras mouse (59s Lung #1, Figure S2C) differed a little bit compared to the previous PRMT6_2affi stainings of Kras (Figure 7).

Taken together, there are differences in the Prmt6 stainings of lung tumour sections from the different $Kras^{LA2}$ mice (Figure 7, S1C and S2C) using three different PRMT6 antibodies (PRMT6_2affi, PRMT6_3affi, PRMT6_bethyl). Nevertheless, Prmt6 protein levels seem to be increased in murine tumour cells and may be in some macrophages embedded in the alveolar structure of the $Kras^{LA2}$ and healthy C57BL/6 mice. Further stainings have to clarify these findings. In the case of the different Prmt6 stainings of the LLC1 mice, all sections demonstrated a quite similar staining pattern of healthy and lung tumour tissue areas, which confirmed that Prmt6 is overexpressed in the enlarged nuclei as well as in the surrounding cytoplasms of these tumour cells (Figure 6, S1B, S1C).

5.1.2 Prmt1 protein levels are elevated in murine lung tumour sections

In parallel to PRMT6, PRMT1 was also analysed in the cDNA microarray by Yoshimatsu and colleagues and was demonstrated to be increased in lung cancer tissues (Yoshimatsu et al., 2011). Furthermore, IHC stainings of PRMT1 showed that PRMT1 is overexpressed in human lung tumour sections (Elakoum et al., 2014). Therefore, IHC stainings of Prmt1 served as a positive control in this study. Hence, all murine tumour

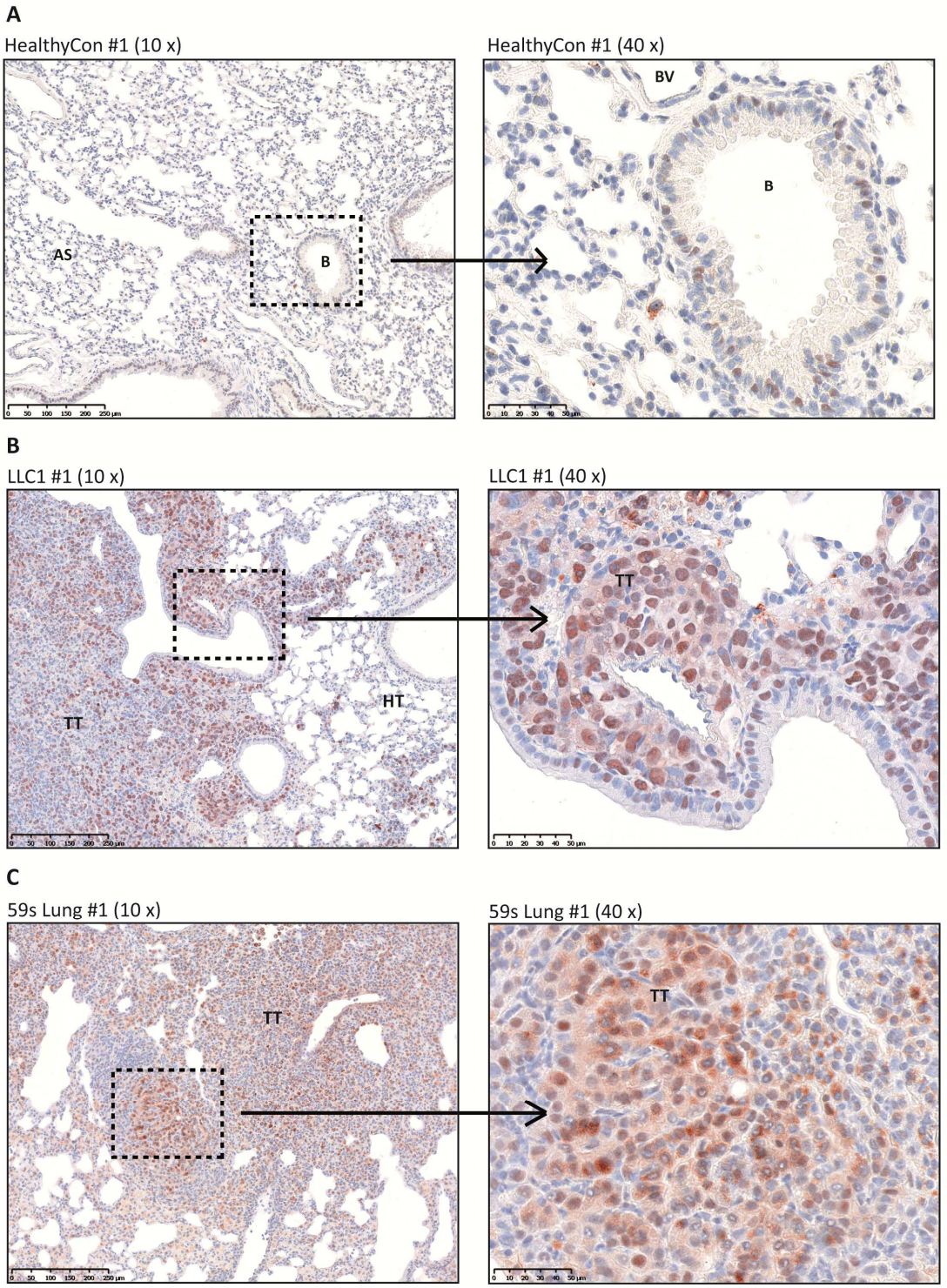

Figure 8: IHC stainings of Prmt1 in lung tumour sections of LLC1 and Kras^{LA2} mice (PRMT1_milli).

(**A** - **C**) A representative image of lung tissue sections from a (**A**) healthy C57BL/6 (HealthyCon #1), (**B**) LLC1 (LLC1 #1) and (**C**) Kras^{LA2} mouse (59s Lung #1) was photographed. A specific antibody directed against PRMT1 (PRMT1_milli, 1:1000) was used (AEC, red) and Hematoxylin served for counterstaining (blue). For each section a 10 x magnification (left panel, maximal scale bar length: 250 µm) and a 40 x magnification (right panel, maximal scale bar length: 50 µm) is shown. AS: alveolar sac, B: bronchiole, BV: blood vessel, HT: healthy tissue, TT: tumour tissue.

sections were stained for Prmt1 using a commercial (PRMT1_milli) and an affinity-purified PRMT1 antibody (PRMT1_affi) from the lab. Although raised against human PRMT1, both antibodies also cross-react with the murine Prmt1 (see manufacturer´s instructions and bachelor thesis, Anna Lena Merkel) (Sakamaki et al., 2011).

Similar to the PRMT6 stainings, all lung tumour sections of healthy C57BL/6, LLC1 and $Kras^{LA2}$ mice (three mice of each strain) were stained with a PRMT1_milli or a PRMT1_affi antibody. A representative result for all IHC stainings of each strain (HealthyCon #1, LLC1 #1, 59s Lung #1) is depicted in Figure 8 using PRMT1_milli. Although PRMT1_affi stained Prmt1 weaker in the lung tumour sections compared to PRMT1_milli, staining patterns of Prmt1 using this antibody were quite similar to the PRMT1_milli stainings in all sections (data not shown). However, the nuclei and surrounding cytoplasms of proliferating LLC1s (Figure 8B) and $Kras^{LA2}$ tumour cells (Figure 8C) were Prmt1-positive compared to tissue sections from healthy C57BL/6 mice (Figure 8A). A few bronchiolar cells were also positively stained for Prmt1 in the tumour sections as well as in the sections of healthy C57BL/6 mice.

In conclusion, Prmt1 protein levels were increased in lung tumour sections using the LLC1 and $Kras^{LA2}$ mouse models in comparison to healthy C57BL/6 mice. Although the expression pattern of Prmt1 was more prominent in the LLC1 and $Kras^{LA2}$ mice than in the Prmt6 stainings, both proteins were found to be overexpressed in murine lung cancer cells. This was particularly obvious in the tumour mass of LLC1 mice compared to tissue sections from healthy C57BL/6 mice, in which Prmt6 and Prmt1 levels were highly expressed in the enlarged nuclei and the surrounding cytoplasms of the tumour cells. These IHC results are in accordance with previous observations that gene expressions of *PRMT6* and *PRMT1* are increased in lung cancer (Yoshimatsu et al., 2011) and support the idea that both proteins might play a role in lung cancer.

5.1.3 PRMT6 is differently expressed in human and murine lung cancer cell lines

So far, PRMT6 expression was studied in two murine lung cancer models (LLC1 and Kras^{LA2}) compared to healthy tissue of C57BL/6 mice. Next, the analysis of PRMT6 was extended to several human NSCLC cell lines (H1299, H1650, A549 and H358), which are common lung cancer cell models. The NSCLC cell lines were compared to Beas2B, a transformed human bronchial epithelial cell line. Additionally, LLC1 cells were studied compared to MLE12 cells, a murine transformed lung epithelial cell line. Hence, RT-qPCR and Western blot analysis of PRMT6 were performed in these cell lines (Figure 9).

The transcript level of *PRMT6* was 3.5-fold higher in H358 and 1.2-fold higher in H1650 compared to Beas2B cells (Figure 9A). No *PRMT6* transcript was detected in A549 cells. The transcripts of *PRMT6* were 0.5 fold lower in H1299 than in Beas2B cells, similar to LLC1 compared to MLE12 cells. Western blot analysis revealed that PRMT6 protein levels in the different cell lines widely corresponded to their transcripts (Figure 9B). Here, PRMT6 was strongest expressed in H358, still highly expressed in H1650, and only moderately expressed in H1299 as well as Beas2B. Almost no PRMT6 protein was detected in A549 cells. In comparison to the human cell lines, Prmt6 expression was relatively low in the two murine cell lines LLC1 and MLE12. H3 was used to demonstrate equal loadings of protein samples whereas the housekeeping gene *RPS14/Rps14* was used for normalisation in the RT-qPCR analysis. A similar result was obtained using *RPLP0/Rplp0* as housekeeping gene (data not shown).

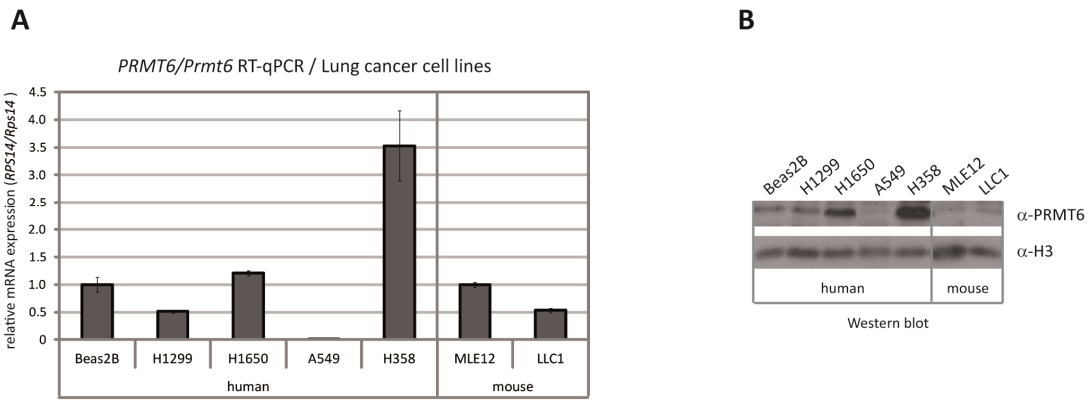

Figure 9: PRMT6 is differently expressed in human and murine lung cancer cell lines.

(**A**) Several NSCLC cell lines (Beas2B, H1299, H1650, A549 and H358) as well as murine cell lines (MLE12, LLC1) were analysed in the expression of *PRMT6* or *Prmt6* compared to Beas2B (human) or MLE12 cells (murine). The *PRMT6/Prmt6* primer pair was able to detect both transcript levels (human and murine). All values were normalised to *RPS14/Rps14* and were relative to their corresponding control (set to one). Error bars denote standard deviation of technical triplicates. Depicted is a representative result of three independent experiments.

(**B**) All human and murine cancer cell lines depicted in Figure (**A**) were analysed in the PRMT6 protein level (FT lysis, 20 µg of each sample) using the PRMT6 antibody (PRMT6_2affi). H3 was used as a loading control.

Taken together, the protein levels of PRMT6 correspond to their mRNA expression profile in the analysed human und murine lung cancer cell lines. However, they differ from cell line to cell line.

5.1.4 Depletion of *PRMT6* negatively affects clonogenic growth of NSCLC cell lines

The previously demonstrated data showed that PRMT6 was expressed to a different extent in several human as well as murine lung cancer cell lines. In order to investigate whether PRMT6 influences cell proliferation and survival of these transformed cells, a colony formation assay (CFA) was conducted in the two NSCLC cell lines H1299 and H358 (Figure 11 and 12). This CFA is a method to determine whether singly plated cells are still able to survive and to grow into colonies due to their unlimited division potential. Therefore, H1299 or H358 cells were seeded in very low density and colonies were detected with crystal violet after 10 and 14 days of siPRMT6 transfection. Additionally, it was tested whether the clonogenic growth was differently impaired in cells with a higher basal PRMT6 level (H358) than in a cell line with a moderate basal PRMT6 level (H1299).

In a first step, siRNA-experiments were performed to establish an efficient knockdown of *PRMT6* in both cell lines. This was analysed by RT-qPCR after 3 and 6 days (Figure 10A and 10C) and by Western blot after 6 days of siRNA transfection against *PRMT6* (Figure 10B and 10D). The RT-qPCR analysis demonstrated that the three specific siRNAs (siPRMT6_1, siPRMT6_4 or siPRMT6_5) depleted *PRMT6* with an efficiency of approximate 90% in comparison to the siControls (siNon, siScr) after three days of

PRMT6 knockdown in both cell lines (Figure 10A and 10C, left panel). After six days of knockdown the *PRMT6* depletion was partially lost in H1299 (70%), but still 90% present in H358 cells (right panel). The Western blots confirmed the almost complete depletion of *PRMT6* protein levels in H1299 and H358 cells after 6 days of siRNA-mediated transfection in the three specific siPRMT6 conditions (Figure 10B and 10D).

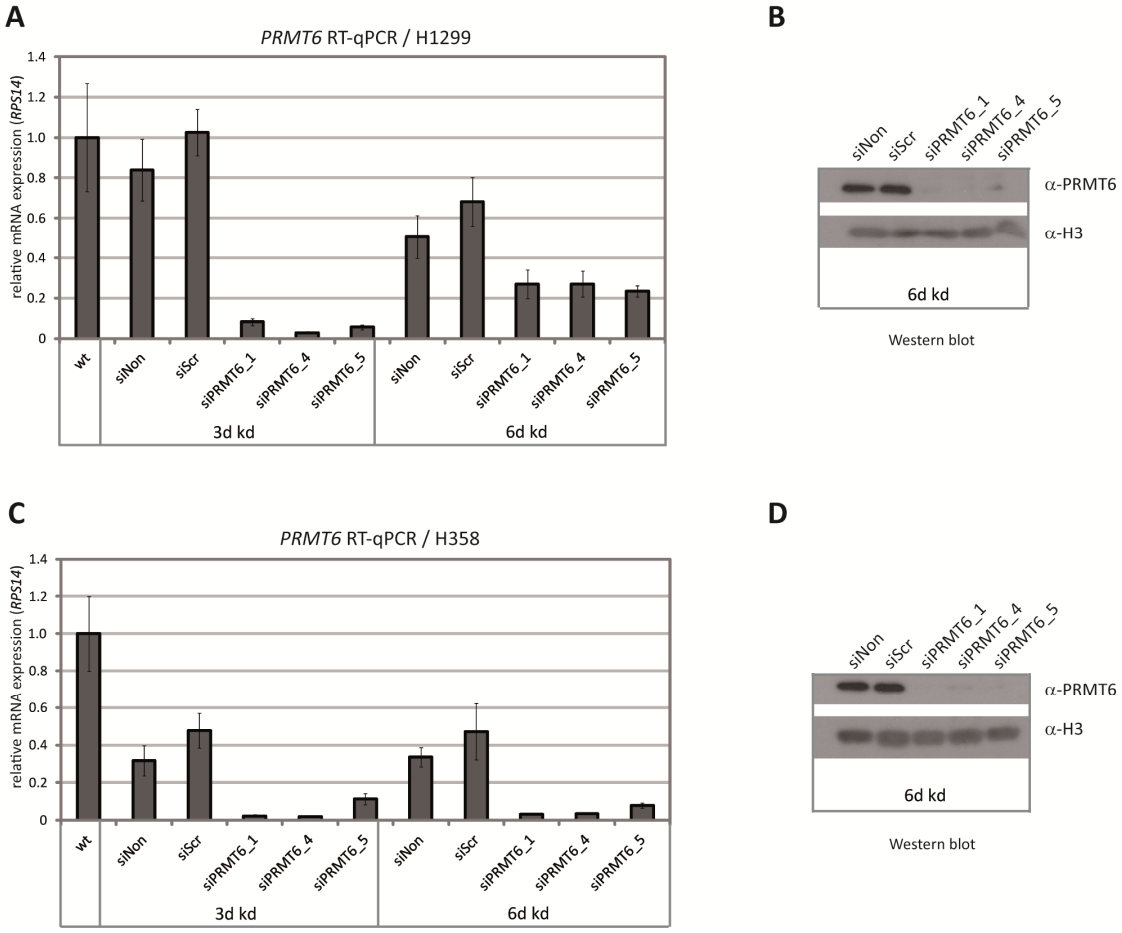

Figure 10: Establishment of an efficient *PRMT6* depletion in H1299 and H358 cells.

(**A** - **D**) H1299 or H358 cells were transfected with three alternative siRNAs directed against *PRMT6* (siPRMT6_1, siPRMT6_4 or siPRMT6_5) compared to the control transfections siNontargeting (siNon) or siScramble (siScr) using LipoRNAiMAX. Cells were harvested for RT-qPCR analysis after three and six days of siRNA-mediated depletion. Total RNA was prepared and examined for the transcript level of (**A** and **C**) *PRMT6*. *RPS14* served for normalisation and all values were relative to wild type cells (wt), which were set to one. Error bars denote standard deviation of technical triplicates. Similar results were obtained compared to the housekeeping gene *RPLP0* (data not shown).

(**B** and **D**) In parallel to (**A** and **C**), whole cell extracts of H1299 or H358 cells were harvested (FT lysis) and 20 µg protein of each sample was loaded on a SDS gel and analysed with a PRMT6-antibody. H3 detection served as corresponding loading control. The experiment was performed once.

Taken together, these data show that *PRMT6* depletion was successful in both analysed NSCLC cell lines.

In a second step, CFAs were performed in both cell lines, in which cells were initially plated in low density as decribed above. Representative dishes of the CFA in H1299 cells are depicted after 10 days of *PRMT6* knockdown in Figure 11A. The relative colony number was determined by counting colonies of *PRMT6*-depleted H1299 cells (Figure 11B). These *PRMT6*-depleted colonies (siPRMT6_1, siPRMT6_4 or siPRMT6_5) were 20 - 40% reduced compared to siNon or siScr after 10 and 14 days. Here, all values are relative to siNon (set to one). Another common method to measure the clonogenic ability of cells is the application "ColonyArea", an ImageJ plugin (Guzmán et al., 2014). This method was used for automatically generated quantification of the colony area (in %) of each dish after either 10 or 14 days. siRNA-mediated depletion of *PRMT6* caused either a reduction in colony area of at least 40% in all conditions after 10 days (dark grey bars) or 20% in case of siPRMT6_4 and siPRMT6_5 after 14 days (light grey bars) compared to siControls (Figure 11C). This effect was not detectable in H1299 cells with a *PRMT6* knockdown by siPRMT6_1. Further CFA images are depicted in Figure S3 (upper panel) of H1299 cell dishes 14 days after siPRMT6 transfection.

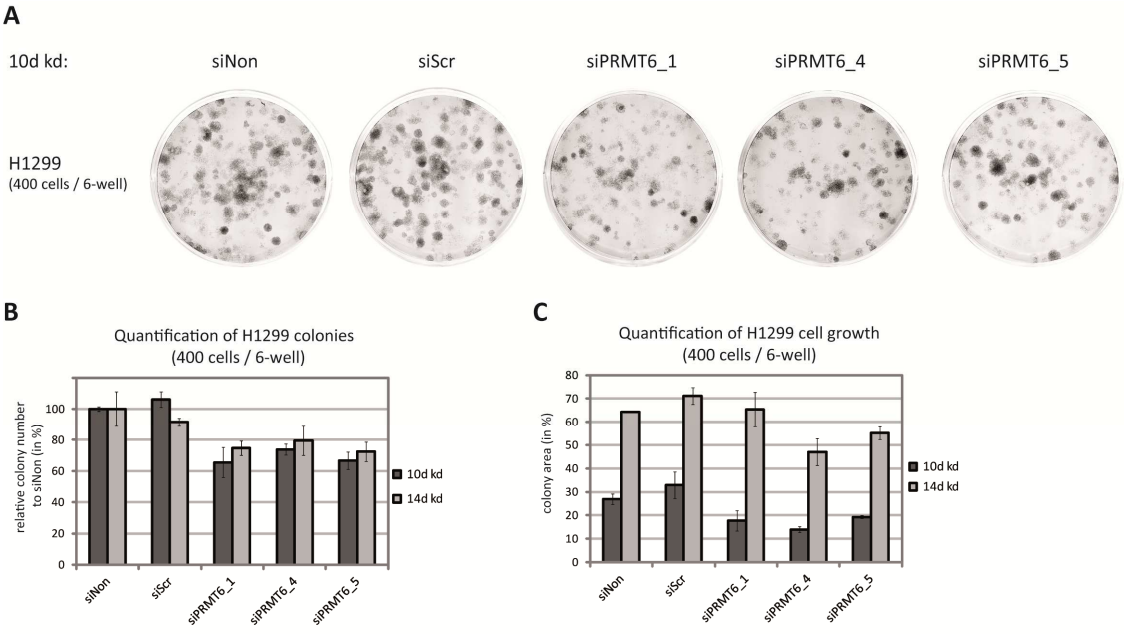

Figure 11: Depletion of *PRMT6* diminishes the clonogenic growth of H1299 cells.

(**A** - **C**) H1299 cells were treated with siRNAs directed against *PRMT6* (siPRMT6_1, siPRMT6_4 or siPRMT6_5) or Nontargeting (siNon) and Scramble (siScr) using LipoRNAiMAX as described in Figure 10. 48 hours post-transfection, 400 cells were replated in triplicates in a 6-well plate for a colony formation assay (CFA) and colonies were detected with crystal violet after 10 days of siRNA transfection. The experiment was performed once.

(**A**) Representative dishes of crystal violet-stained dishes were photographed after 10 days.

(**B** and **C**) The quantification of crystal violet-stained H1299 colonies was performed by (**B**) counting the colony number relative to siNon (in %) after 10 days (dark grey bars) and 14 days (light grey bars). Additionally, (**C**) the automatically generated quantification by "ColonyArea", an ImageJ plugin, was used to determine the colony area (in %) of each dish of either 10 days (dark grey bars) or 14 days (light grey bars). Depicted is a triple counting / scanning ± standard deviation.

In parallel, a CFA was performed in the NSCLC cell line H358, for which similar results were obtained as for H1299 cells. Selected images of the cell dishes are shown in Figure 12A after 10 days of siPRMT6 transfection. Two of three siPRMT6 conditions (siPRMT6_4, siPRMT6_5) exhibited a clear decrease in cell numbers. The quantification by counting the cell number was impossible because of the very small cell size and a too high cell number. Nevertheless, the cell growth quantification by "ColonyArea" was technically feasible and showed a similar result as judged by eye (Figure 12B). Depletion of *PRMT6* by siPRMT6_4 and siPRMT6_5 clearly showed a 75% reduced colony area compared to both siControls after 10 days (dark grey bars) and a 50% reduced colony area after 14 days (light grey bars). This effect was not detected in H358 cells depleted of *PRMT6* by siPRMT6_1. Additional images of the CFA in H358 cells after 14 days of siRNA-mediated depletion of *PRMT6* are executed in Figure S3 (lower panel).

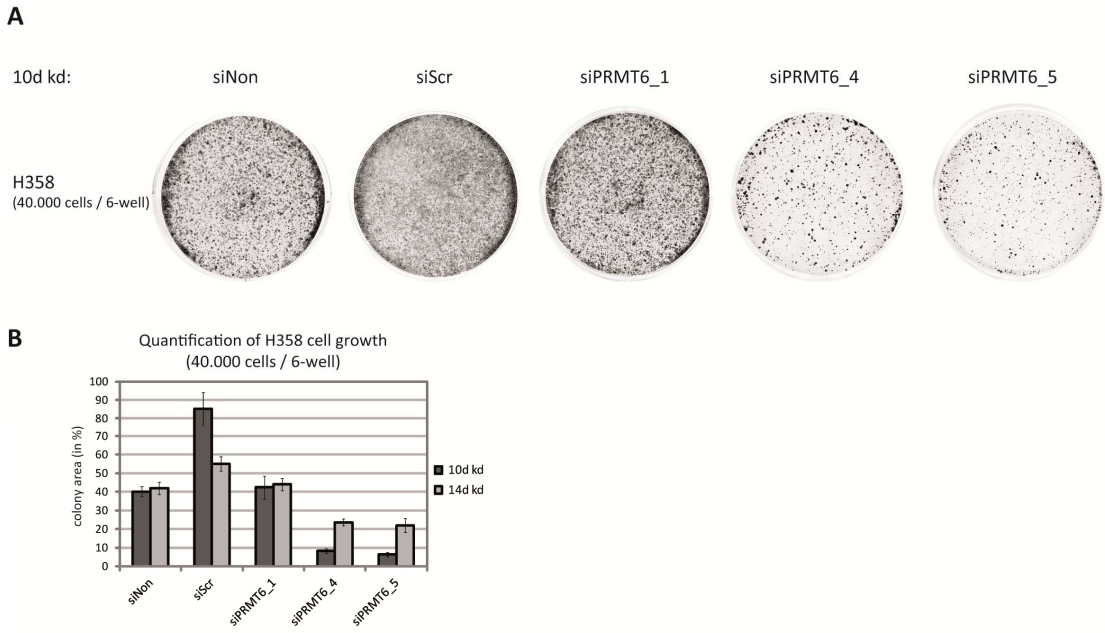

Figure 12: Depletion of *PRMT6* diminishes the clonogenic growth of H358 cells.

(**A** and **B**) H358 cells were treated with siRNAs directed against *PRMT6* (siPRMT6_1, siPRMT6_4 or siPRMT6_5) or Nontargeting (siNon) and Scramble (siScr) using LipoRNAiMAX as described in Figure 10. 48 hours post-transfection, 40.000 cells were replated in triplicates in a 6-well plate for a colony formation assay (CFA) and colonies were detected with crystal violet after 10 days of siRNA transfection. The experiment was performed once.

(**A**) Representative dishes of crystal violet-stained dishes were photographed after 10 days.

(**B**) The automatically generated quantification of crystal violet-stained H358 colonies was performed by "ColonyArea", an ImageJ plugin. The colony area (in %) of each dish was determined after 10 days (dark grey bars) and 14 days (light grey bars). Depicted is a triple counting / scanning ± standard deviation.

In summary, these results demonstrate that PRMT6 facilitates the clonogenic growth of NSCLC cell lines (H1299 and H358 cells). Two out of three used siRNAs directed against *PRMT*6 (siPRMT6_4 and siPRMT6_5) showed that *PRMT6* depletion causes a reduction in colony number compared to control siRNA transfected cells. Furthermore, these data suggest that defects in the ability to form colonies might be more prominent in *PRMT6*-depleted cells with previously high PRMT6 levels (H358) than in cells with previously moderate PRMT6 levels (H1299 cells). However, this CFA experiment was executed once in this study. Further experiments have to confirm these data.

5.2 PRMT6 positively regulates proliferation and blocks senescence

As explained above, *PRMT6* is deregulated in several types of human cancer, such as lung cancer (Yoshimatsu et al., 2011). On the one hand, this observation was confirmed by IHC stainings in several murine lung tumour tissues in this study (Figure 6, 7, S1 and S2). On the other hand, *PRMT6* depletion caused a reduced proliferation capability of tumour cells (CFA in H1299 and H358, Figure 11 and 12), which could probably lead to cell cycle arrest. Therefore, further investigations should confirm these data whether PRMT6 is also implicated in the proliferation and survival of the osteosarcoma cell line U2OS, which is another transformed cell line. In a first approach, the CFA was performed after establishment of an efficient *PRMT6* knockdown as it was previously the case for the NSCLC cell lines.

5.2.1 Depletion of *PRMT6* reduces the clonogenic growth of U2OS cells

An efficient depletion of *PRMT6* was achieved in U2OS cells using two alternative *PRMT6* siRNAs (siPRMT6_1, siPRMT6_2) in comparison to siControl (siLuci) (Figure 13). The Western blot showed a strong decrease of PRMT6 protein levels after three days of siPRMT6 transfection compared to siLuci (Figure 13A). CDK2 was used to demonstrate equal sample loadings. The RT-qPCR analysis demonstrated the diminished *PRMT6* transcript levels in the time interval of 0 to 14 days, which were slightly reduced over time and lost after 14 days (Figure 13B).

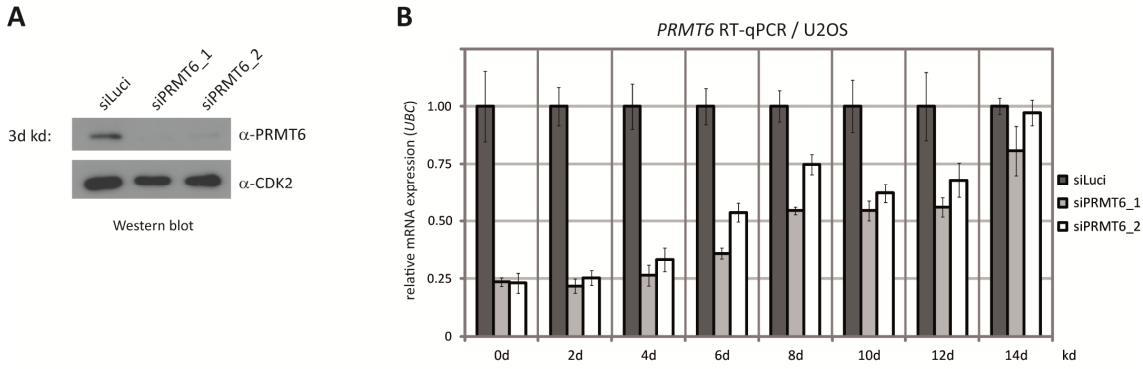

Figure 13: Establishment of an efficient *PRMT6* depletion in U2OS cells.

(**A** and **B**) U2OS cells were transfected with siRNA directed against *PRMT6* (siPRMT6_1 or siPRMT6_2) or Luciferase (siLuci) using LipoRNAiMAX. 48 hours post-transfection, 400 cells were replated in triplicates in a 6-well plate for Western blot or RT-qPCR analysis. A representative result of three independent experiments is shown.

(**A**) 72 hours after start of siRNA treatment cells were harvested (IPH lysis) and total protein (20 µg) of each sample was analysed using a PRMT6 antibody. CDK2 detection served as corresponding loading control.

(**B**) Every second day of *PRMT6* depletion (0 - 14 days knockdown), three dishes with siRNA transfected cells were harvested, pooled, total RNA was prepared and analysed by RT-qPCR. Transcript levels of *PRMT6*, normalised to *UBC* and relative to siLuci (set to one), were determined for siLuci (dark grey bars), siPRMT6_1 (light grey bars) and siPRMT6_2 (white bars). Error bars denote standard deviation of technical triplicates.

Then, a CFA was performed in order to test whether the clonogenic growth of U2OS cells was affected after depletion of *PRMT6*. Therefore, U2OS cells were seeded at a low cell density and forming colonies were detected after 10 and 14 days of siPRMT6 transfection by crystal violet staining. Images were taken and are depicted in Figure 14A. The quantification was performed either by triple counting of the colony number relative to siLuci (Figure 14B) or by automatical determination of the cell growth using "ColonyArea", an ImageJ plugin, after 10 and 14 days of *PRMT6* depletion (Figure 14C). In both cases, *PRMT6* depletion caused a reduction of U2OS colonies of about 60%.

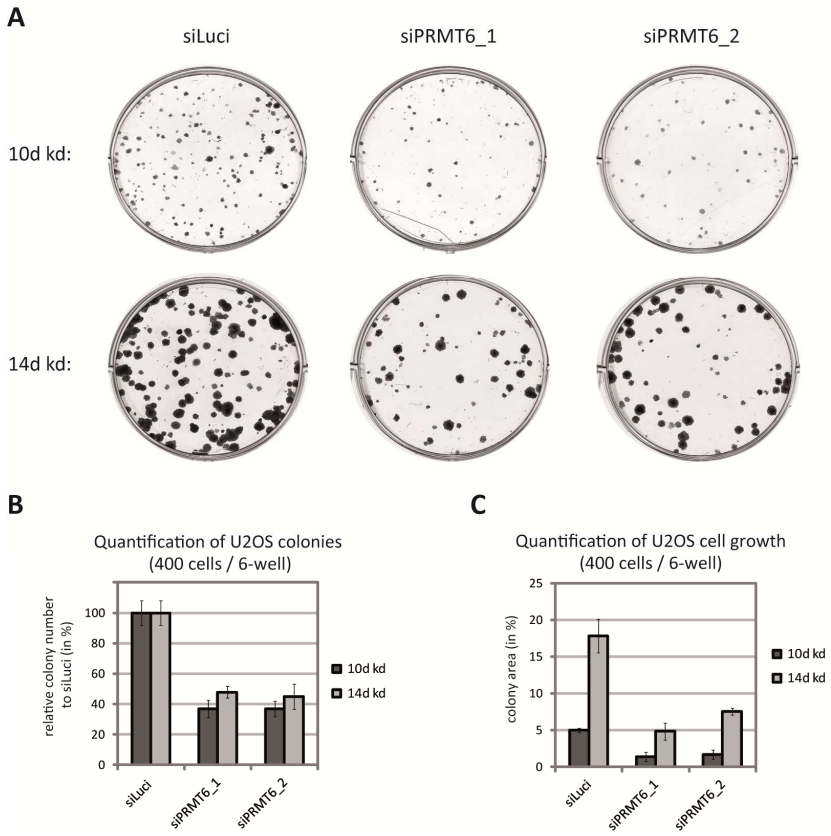

Figure 14: Depletion of *PRMT6* results in a reduced ability to form colonies of U2OS cells.

(**A** - **C**) In parallel to Western blot and RT-qPCR analysis shown in Figure 13, U2OS cells were transfected with siRNA directed against *PRMT6* (siPRMT6_1 or siPRMT6_2) or Luciferase (siLuci) using LipoRNAiMAX. 48 hours post-transfection, 400 cells were replated in triplicates in a 6-well plate for a colony formation assay (CFA) and colonies were detected with crystal violet either after 10 or 14 days of siRNA transfection. CFA were performed as biological triplicates and one representative result is shown.

(**A**) Representative dishes were photographed after 10 and 14 days.

(**B** and **C**) The evaluation of crystal violet-stained colonies was performed either by (**B**) counting relative to siLuci (in %) or U2OS cell growth was automatically quantified by (**C**) measuring the colony area (in %) using "ColonyArea", an ImageJ plugin. The result shown is the average of a triple counting / scanning ± standard deviation of 10 days (dark grey bars) and 14 days (light grey bars) of *PRMT6* knockdown.

In conclusion, *PRMT6*-depleted U2OS cells were also impaired in their clonogenic growth as demonstrated for H1299 and H358 cells.

5.2.2 Depletion of *PRMT6* positively influences *CDKN1A* gene expression in U2OS cells

Previous experiments have demonstrated that *PRMT6* depletion limits the proliferation capability of several transformed cell lines, including U2OS cells. Therefore, it is assumed that PRMT6 promotes proliferation of cancer cells, while other cell cycle regulatory pathways such as senescence might be prohibited by PRMT6. Cellular senescence is a protective mechanism against unlimited cell proliferation, which is a hallmark of cancer cells.

In order to answer the question whether key regulators of the cell cycle are involved in the PRMT6-mediated proliferation defects, several components of the TP53-cellular senescence pathway and further important cell cycle regulators were analysed in *PRMT6*-depleted U2OS cells. Beside the tumour suppressor gene TP53 and its target CDKN1A, the expression of the serine/threonine protein kinase CDK2 and the cyclin CCND1 were exemplary analysed. CDKN1A functions as a repressor by binding to CDK-cyclin complexes mostly via CDK2. In addition, CDKN1A is also able to block CDK4/6-CCND complex formation of the p16-INK4A-RB1 cascade. This prevents an efficient kinase activity of these complexes to phosphorylate RB1 (Malumbres and Barbacid, 2005). As a result, activation of E2F-target genes is prohibited in both pathways, which causes then a block in cell cycle progression. However, p16-INK4A itself could not be studied in U2OS cells due to the fact that it is silenced by deletion and DNA methylation (Miller et al., 1996; Park et al., 2002).

In addition, the two other CIP/KIP family members, CDKN1B and CDKN1C and the cyclin CCNA2 that is an important regulator of G1/S and G2/M transitions in the cell cycle and binds to CDK2 during S phase, were studied. The angiogenesis inhibitor *THBS1*, which was previously described as a repressed target gene of PRMT6, was thought to be used as a positive control in this experiment (Michaud-Levesque and Richard, 2009).

The experiment in U2OS cells was performed by using five independent siRNAs sequences targeting *PRMT6* (siPRMT6_1 - siPRMT6_5) in comparison to several controls (wt, Lipo, siNon, siScr). RT-qPCR analysis of *PRMT6* in *PRMT6*-depleted U2OS cells demonstrated an efficient *PRMT6* knockdown of 70 - 90 % (Figure 15A). Interestingly, *CDKN1A* gene expression was 1.8- to 4.8-fold increased in *PRMT6*-depleted cells compared to the controls (Figure 15B). These findings were confirmed by Western blot (Figure 15C). Here, PRMT6 depletion correlated with an increase in CDKN1A protein level whereas CDK2 was unaffected. Additionally, the two other CIP/KIP family members, CDKN1B and CDKN1C, the cyclins CCNA2 and CCND1, the tumour suppressor gene TP53 and THBS1 were analysed by RT-qPCRs as mentioned above.

As a result, *TP53* transcript levels were slightly reduced compared to the controls wild type (wt) and Lipo in U2OS cells depleted of *PRMT6* (Figure 15D). This effect was not detected in comparison to siNon or siScr. In case of siPRMT6_3, *TP53* trancript was even 2-fold increased compared to siNon or siScr. Therefore, no effect of PRMT6 on TP53 transcript levels was detected with regard to both controls (siNon, siScr). A similar result was detected for *CDKN1C* transcript level, the third member of the CIP/KIP family (Figure 15F). *CDKN1C* was not uniformly regulated compared to all controls in *PRMT6*-depleted U2OS cells. In case of *CDKN1B* and *CCNA2*, these two genes were slightly downregulated in U2OS cells depleted of *PRMT6* (Figure 15E, 15G). This effect was detected compared to wild type (wt) or Lipo transfection, whereas it was only weak compared to siNon or siScr in the RT-qPCR analysis. In contrast, *CCND1* transcript level was slighty increased in the *PRMT6* knockdown compared to all control conditions (Figure 15H). However, *THBS1* transcript level was not uniformly affected by the different siPRMT6 sequences (Figure 15I).

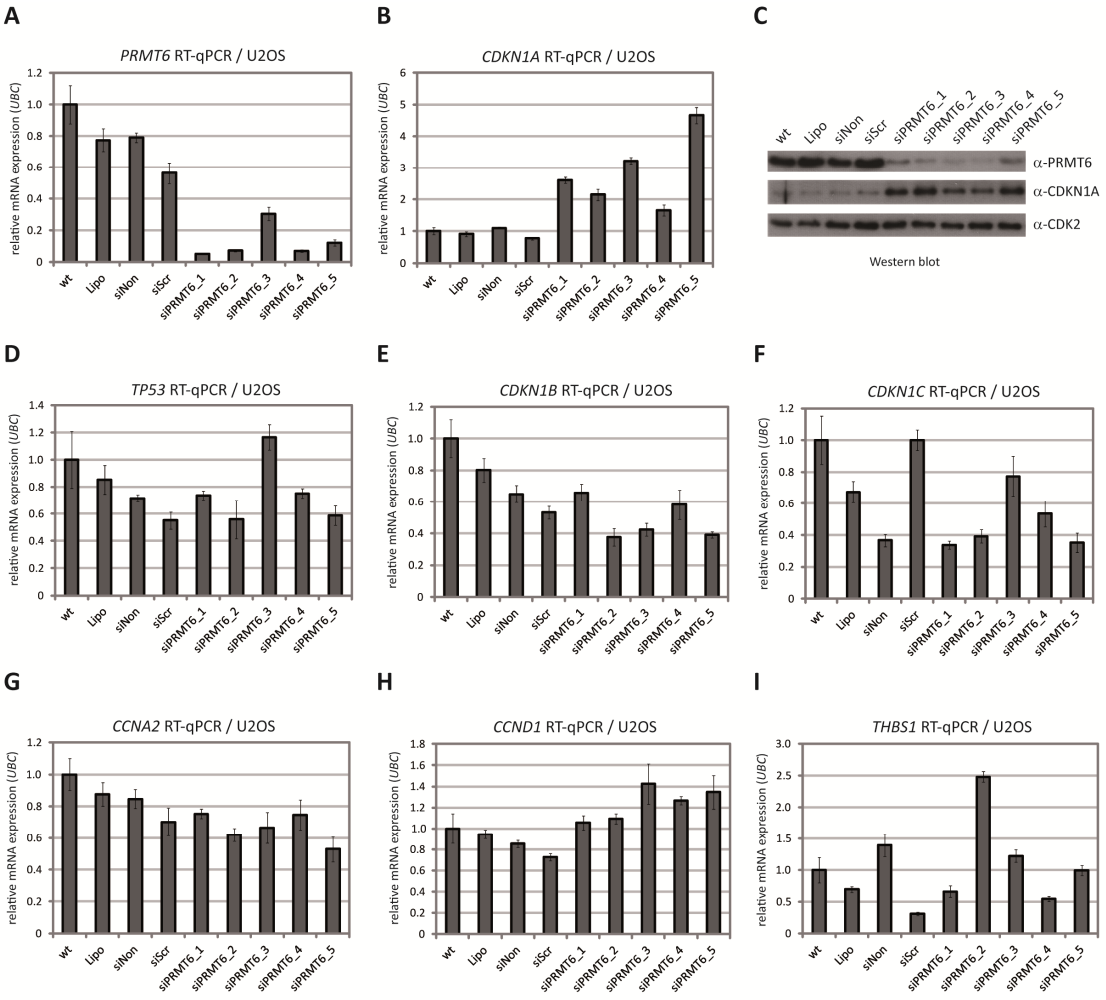

Figure 15: *PRMT6* depletion causes an increased *CDKN1A* gene expression in U2OS cells.

(**A** - **I**) U2OS cells were transfected with several alternative siRNAs targeting *PRMT6* (siPRMT6_1 - siPRMT6_5) or Nontargeting (siNon) and Scramble (siScr) using LipoRNAiMAX. Wild type cells (wt) and cells treated only with Lipofectamine RNAiMAX (Lipo) served as additional controls. After 72 hours cells were harvested either for RNA isolation or total protein analysis (IPH lysis). A representative result of three independent experiments is given.

(**A** and **B**) and (**D** - **I**) Transcript levels of (**A**) *PRMT6*, (**B**) *CDKN1A*, (**D**) *TP53*, (**E**) *CDKN1B* and (**F**) *CDKN1C* or (**G**) *CCNA2* and (**H**) *CCND1* as well as (**I**) *THBS1* were studied in RT-qPCR, in which *UBC* served for normalisation. All values were relative to wild type (wt) cells (set to one). Error bars denote standard deviation of technical triplicates.

(**C**) Each protein sample (30 µg) was loaded on a SDS gel and analysed by Western blot using antibodies directed against PRMT6, CDKN1A and CDK2, serving as loading control.

Taken together, *PRMT6* depletion was accompanied by a prominent effect on CDKN1A transcript and protein level in U2OS cells. For both analyses, an enhanced gene expression and protein synthesis of CDKN1A was detected. In case of all the other analysed genes no clear effect was found in *PRMT6*-depleted U2OS cells.

5.2.3 PRMT6 binds to the TSS of the *CDKN1A* gene locus in U2OS cells

PRMT6 was demonstrated to regulate *CDKN1A* gene expression in a negative manner. Therefore, it was assumed that PRMT6 directly regulate *CDKN1A* and binds to its gene locus. To test the hypothesis, chromatin immunoprecipitation (ChIP) analysis of PRMT6 at the *CDKN1A* gene locus was performed. Primer pairs were used spanning the *CDKN1A* gene locus from -6.8 kb to +8.6 kb using wild type U2OS cells (Figure 16). PRMT6 enrichment was analysed by ChIP-qPCR compared to IgG rabbit. Both, the graphical presentation of % input of chromatin (Figure 16A, left panel) and the fold IgG (right panel) showed similar results. PRMT6 binds at the *CDKN1A* gene locus with the strongest association at the transcriptional start site (TSS, 3- to 4-fold) in comparison to IgG rabbit control. As PRMT6 is the major methyltransferase of H3R2me2a (Guccione et al., 2007; Hyllus et al., 2007), I analysed whether this methylation mark correlated with PRMT6 at the *CDKN1A* gene locus (Figure 16B). Thus, ChIP analysis using an H3R2me2a antibody was conducted. H3R2me2a was specifically enriched 2- to 3-fold at the TSS compared to surrounding regions of the *CDKN1A* gene locus.

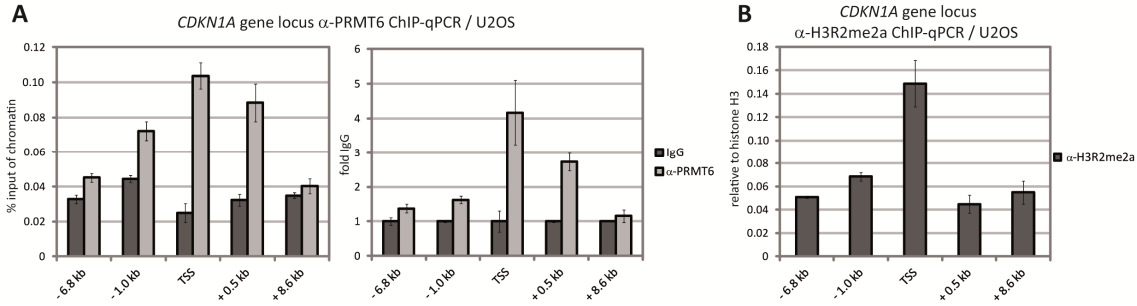

Figure 16: PRMT6 binding peaks at the TSS of the *CDKN1A* gene locus accompanied by an enhanced level of H3R2me2a in U2OS cells.

(**A** and **B**) U2OS cells were harvested 72 hours after seeding, chromatin was isolated and subjected to ChIP analysis using antibodies against (**A**) PRMT6 (light grey bars) and IgG rabbit as control (dark grey bars) or in (**B**) H3R2me2a relative to histone H3. Immunoprecipitated DNA was analysed in triplicates using primer pairs spanning the indicated regions of the *CDKN1A* gene locus. Mean values are expressed in (**A**) as % input of chromatin or fold IgG, which was equated to one. Error bars denote standard deviation of technical triplicates. A representative result of three independent experiments is given.

In conclusion, these data show that PRMT6 and H3R2me2a peak at the TSS of the *CDKN1A* gene locus in U2OS cells, whereby this H3R2me2a-associated repressive PRMT6 activity seems to be responsible for the pro-proliferative function of PRMT6.

5.2.4 PRMT6 is a negative regulator of senescence in TIG3-T cells

Given that PRMT6 positively affects clonogenic growth of U2OS cells and that PRMT6 regulates *CDKN1A*, which is a prominent gene implicated in cell cycle arrest, it was questioned whether PRMT6 also contributes to senescence, a permanent arrest in the non-transformed cell line TIG3-T. Even though these human diploid fibroblasts are immortalised by ectopic h*TERT* expression (catalytic subunit of the telomerase holoenzyme), they are still able to pass stress-induced senescence. This can be accomplished by senescence inducers such as non-telomeric DNA damage (Chen et al., 2001a) and in this case possibly by PRMT6.

Therefore, TIG3-T cells were infected with retroviral plasmids targeting PRMT6 (shPRMT6 sequences are identical to corresponding siRNAs) or Luciferase (shLuci) and were selected with Puromycin (1 µg/ml). Cells were analysed in a senescence-associated ß-galactosidase (SA-ß-gal) staining after seven days of shRNA-mediated infection (Figure 17). Figure 17A shows an efficient PRMT6 protein depletion in all analysed conditions. The number of SA-ß-gal-positive cells was increased using three independent shPRMT6 sequences compared to some SA-ß-gal positive cells in the shLuci or control condition (Figure 17B).

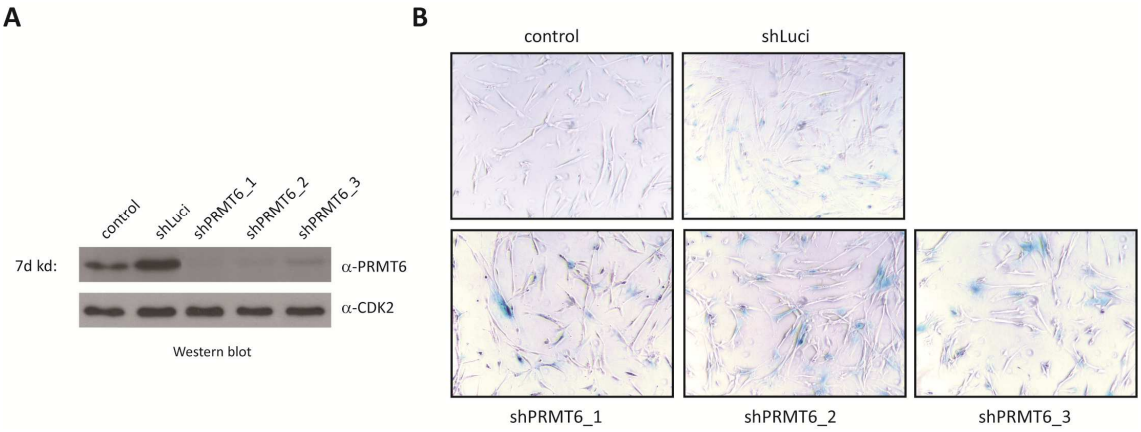

Figure 17: *PRMT6* depletion results in an enhanced senescent phenotype in TIG3-T cells.

(**A** and **B**) TIG3-T cells were infected with retroviral plasmids coding for three alternative shRNAs targeting *PRMT6* (shPRMT6_1, shPRMT6_2, shPRMT6_3) or shLuciferase (shLuci) and the empty plasmid (control) as an additional control. 48 hours post-infection, cells were selected with 1 µg/ml Puromycin for additional 72 hours. A representative result of three independent experiments is shown.

(**A**) Efficient PRMT6 knockdown was confirmed by Western blot analysis (FT lysis) after seven days of shRNA-mediated depletion of *PRMT6*. CDK2 detection served as corresponding loading control.

(**B**) After six days of shRNA-mediated depletion (day 0 corresponds to day 3 of selection) cells were replated and detected for SA-ß-gal activity at day 7.

Taken together, these results point towards a role of PRMT6 in promoting proliferation and blocking senescence in TIG3-T cells.

5.2.5 Depletion of *PRMT6* enhances *CDKN1A* and *p16-INK4A* gene expression in TIG3-T cells

To answer the question whether the permanent arrest in TIG3-T cells is caused by a similar influence of PRMT6 on the target gene *CDKN1A* as shown for the transformed cell line U2OS, siRNA-mediated experiments were performed in these non-transformed cells. Furthermore, the CDK inhibitor p16-INK4A gene locus, which is not mutated in these cells, could be studied according to a possible regulation by PRMT6.

In a first approach it was analysed whether *CDKN1A* and *p16-INK4A* gene expression were upregulated in *PRMT6*-depleted TIG3-T cells. Efficient knockdown of *PRMT6* (60 - 90%) using three alternative shRNAs (shPRMT6_1 - shPRMT6_3) in comparison to shLuci or control (empty plasmid) was demonstrated by RT-qPCR or Western blot analysis (Figure 18A, 18B). *CDKN1A* and *p16-INK4A* transcripts were 1.4- to 1.7-fold increased compared to control conditions after treatment of the cells with retroviral plasmids coding for shPRMT6_2 or shPRMT6_3 (Figure 18C, 18D). In contrast, *CDKN1A* and *p16-INK4A* transcripts were unaffected by shPRMT6_1. The analysis of CDKN1A and p16-INK4A protein levels showed an enhanced CDKN1A level by shPRMT6_1 and shPRMT6_2. The p16-INK4A protein level was increased in all shPRMT6 conditions in comparison to shLuci and control in TIG3-T cells (Figure 18E).

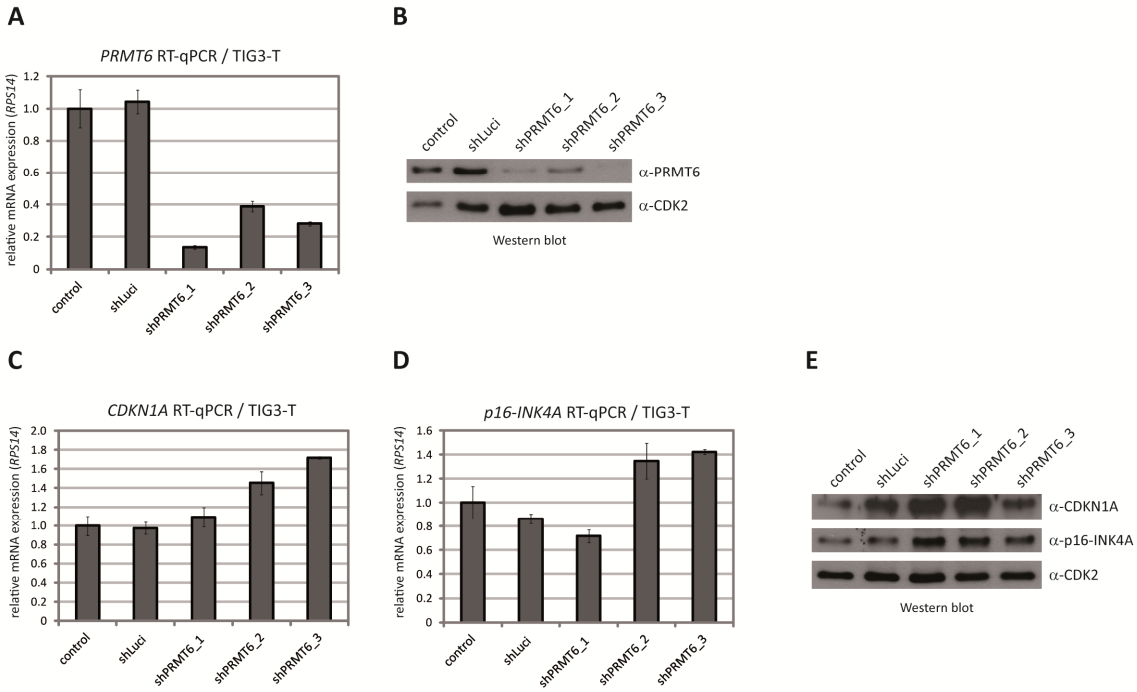

Figure 18: *PRMT6* depletion causes an increased *CDKN1A* and *p16-INK4A* gene expression in TIG3-T cells.

(**A** - **E**) TIG3-T cells were infected with retroviral plasmids coding for shPRMT6 (shPRMT6_1, shPRMT6_2 or shPRMT6_3) compared to shLuciferase (shLuci) or empty plasmid (control). After 48 hours cells were selected with 1 µg/ml Puromycin for the following 72 hours. After additional seven days of shRNA-mediated depletion of *PRMT6* (day 0 corresponds to three days after start of Puromycin selection) cells were harvested either for isolation of total RNA (**A**, **C** and **D**) or protein extracts using FT lysis (**B** and **E**). After the transcription of RNA into cDNA RT-qPCR analysis was performed using primers directed against (**A**) *PRMT6*, (**C**) *CDKN1A* and (**D**) *p16-INK4A* transcript levels normalised to *RPS14* and relative to control (empty plasmid), which was set to one. Error bars denote standard deviation of technical triplicates.

For Western blot analysis, 30 µg protein of each sample was loaded on a SDS gel for determination of (**B**) PRMT6, (**E**) CDKN1A, p16-INK4A and (**B** and **E**) CDK2 level, which was used to demonstrate equal sample loadings. Shown is a representative result of threee independent experiments.

In conclusion, two out of three specific shRNAs directed against *PRMT6* caused an increased gene expression and protein synthesis of CDKN1A in TIG3-T cells. Gene expression of *p16-INK4A* was also positively affected by two PRMT6-specific shRNAs, while its protein level was even affected through all three used retroviral plasmids coding for shPRMT6. Both cell cycle inhibitors are repressed by PRMT6 in non-transformed cells.

5.2.6 PRMT6 binds to the *CDKN1A* and *p16-INK4A* gene locus in TIG3-T cells

To elucidate whether PRMT6 directly regulates CDKN1A and p16-INK4A by binding to their gene loci in TIG3-T cells, ChIP analysis was performed using TIG3-T wild type cells. *CDKN1A* gene was studied by primer pairs spanning the locus from -6.8 kb to +8.6 kb (Figure 19). Here, calculation of % input of chromatin (Figure 19A, left panel) and fold IgG (right panel) was conducted. PRMT6 enrichment was detected by a PRMT6 antibody compared to IgG control. The *CDKN1A* gene locus was targeted by PRMT6 with a preferential binding of PRMT6 to the TSS up to 8-fold and with a small portion to the +0.5 kb transcribed region (4-fold) compared to surrounding chromatin areas and the IgG rabbit controls. The PRMT6 binding was accompanied by a 5-fold enhanced H3R2me2 level at the TSS compared to surrounding regions (Figure 19B). H3R2me2 level was detected by anti-H3R2me2a.

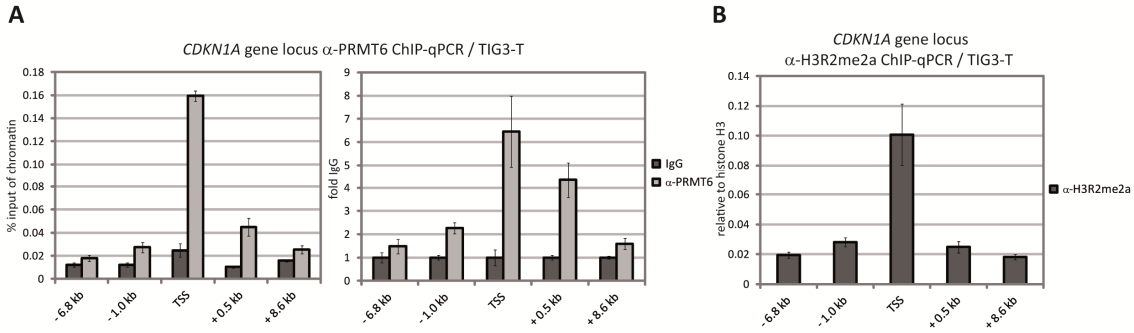

Figure 19: PRMT6 binding peaks at the TSS of the *CDKN1A* gene locus accompanied by an enhanced H3R2me2a level in TIG3-T cells.

(**A** and **B**) TIG3-T cells were harvested 72 hours after seeding and isolated chromatin was subjected to ChIP analysis using specific antibodies directed against (**A**) PRMT6 (light grey bars) with the corresponding IgG rabbit control (dark grey bars) or chromatin was examined with an antibody for (**B**) H3R2me2a in comparison to H3. Immunoprecipitated DNA was analysed in triplicates by qPCR with specific primers covering the area around the TSS of *CDKN1A* gene locus. Mean values are expressed in (**A**) as % input of chromatin or fold IgG, which was equated to one or in (**B**) mean values are relative to histone H3. Error bars denote standard deviation of technical triplicates. A representative result of three independent experiments is shown.

In case of the *p16-INK4A* gene locus, the result was less clear than for the *CDKN1A* gene locus. PRMT6 binding was detected at the 0.5 kb region upstream of the TSS (about 3-fold) compared to IgG after calculation of % input of chromatin (Figure 20A,

left panel). Using the fold IgG calculation, PRMT6 was even more distributed over the whole chromatin area as pictured in the graphic (right panel). The methylation mark H3R2me2a was not enriched at the *p16-INK4A* gene locus (Figure 20B).

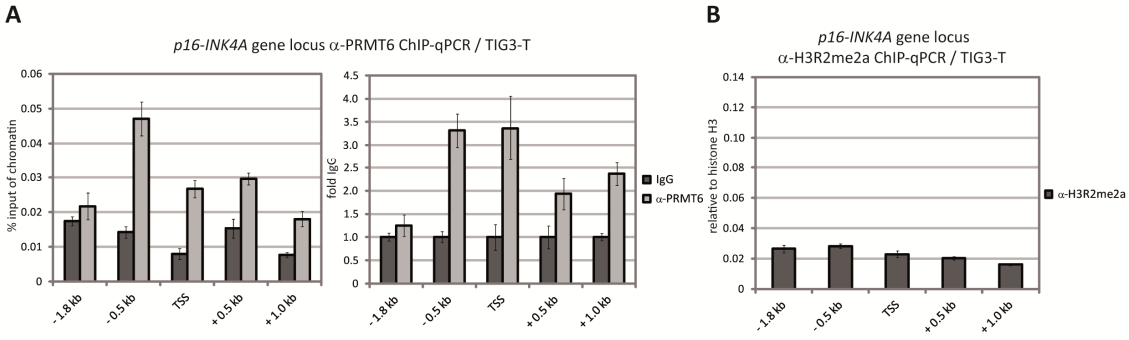

Figure 20: PRMT6 binds to the *p16-INK4A* gene locus in TIG3-T cells.

(**A** and **B**) TIG3-T cells were harvested 72 hours after seeding and isolated chromatin was subjected to ChIP analysis using specific antibodies directed against (**A**) PRMT6 (light grey bars) with the corresponding IgG rabbit control (dark grey bars) or chromatin was examined with an antibody for (**B**) H3R2me2a in comparison to H3. Immunoprecipitated DNA was analysed in triplicates by qPCR with specific primer pairs covering the area around the TSS of the *p16-INK4A* gene locus. Mean values are expressed in (**A**) as % input of chromatin or fold IgG, which was equated to one or in (**B**) mean values are relative to histone H3. Error bars denote standard deviation of technical triplicates. A representative result of three independent experiments is depicted.

In summary, the binding of PRMT6 overlapped with the presence of H3R2me2a at the TSS of the *CDKN1A* gene locus as demonstrated for U2OS cells. Similarly, PRMT6 also binds at the TSS of the *p16-INK4A* locus. However, H3R2 dimethylation was not detected above background level of the control regions suggesting that PRMT6 possesses no methyltransferase activity towards H3 at this locus and regulates p16-INK4A independently of its enzymatic activity. Nevertheless, *CDKN1A* and *p16-INK4A* are both transcriptional downstream targets of PRMT6 in TIG3-T cells that explain its function to regulate proliferation in a positive manner, while senescence is blocked by PRMT6.

5.2.7 Establishment of an efficient oncogene-induced senescence in TIG3 BRAF-ER cells

Premature cellular senescence can be triggered by different stress stimuli, such as oxidative stress, DNA or expression of oncogenes. In order to study PRMT6 and its relationship to CDKN1A in oncogene-induced senescence (OIS), the TIG3 BRAF-ER cell model was used (Figure 21). These fibroblasts possess a protein kinase domain of *Braf* fused to a mutant form of the hormone binding domain of the estrogen receptor (*ER*), referred as ligand binding domain (*LBD*) (Agger et al., 2009; Woods et al., 1997). LBD is responsive to 4-hydroxytamoxifen (4-OHT), but not to ß-estradiol.

Normally, *Braf* is constitutively expressed, but the protein remains inactive through chaperone binding at the LBD. Its activity can be rapidly induced by treatment of the cells with 4-OHT. A conformational change in Braf-LBD results in the dissociation of chaperones. Activation of the MAPK signaling cascade induces a G1-arrest in the cell cycle and cells undergo oncogene-induced senescence (OIS). The biomarker ß-galactosidase is enhanced expressed and detected by SA-ß-gal staining (chapter 4.1.7). Similar to the former cell model, TIG3-T cells, OIS cannot be bypassed by h*TERT* expression in oncogene overexpressing fibroblasts (Wei and Sedivy, 1999).

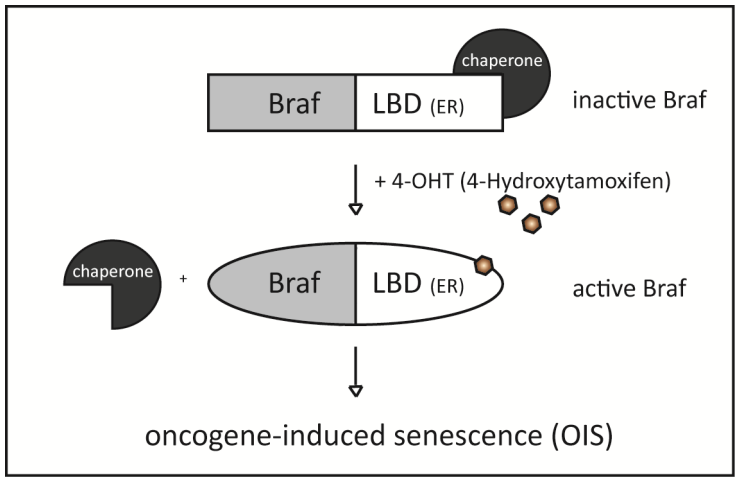

Figure 21: Schematic depiction of the oncogene-induced senescence (OIS) model (TIG3 BRAF-ER).

To examine whether senescence is inducible in these TIG3 BRAF-ER cells, they were treated with 4-OHT treatment (200 nM) over a time period of six days (Figure 22). In Figure 22A, representative images of a SA-ß-gal staining are shown. A 40% increase of SA-ß-gal-positive stained fibroblasts was detected after four and six days (Figure 22B). A decline in *EZH2* expression, a subunit of the H3K27 methyltransferase complex PRC2, is another indicator that TIG3 BRAF-ER cells undergo rapid OIS after oncogenic stress induction (Agger et al., 2009). *EZH2* was highly expressed in pre-senescent cells (day 0) and prevents cellular senescence. In TIG3 BRAF-ER cells, *EZH2* expression was rapidly decreased to 10 - 20% after two days of 4-OHT treatment (Figure 22C).

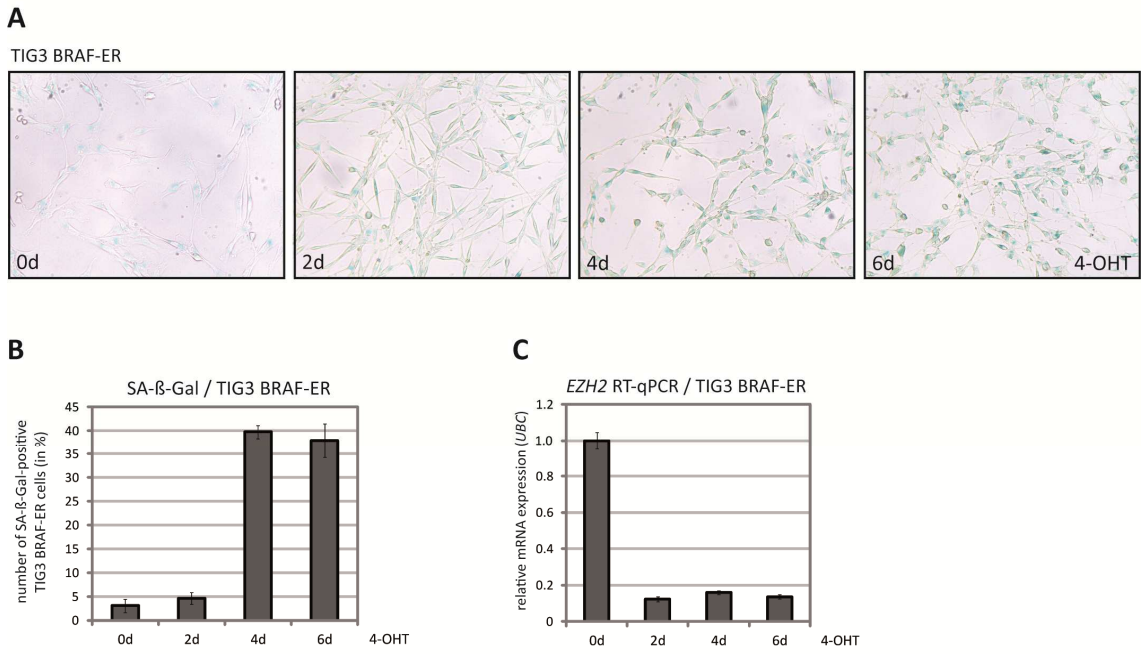

Figure 22: Establishment of an efficient OIS induction in TIG3 BRAF-ER cells.

(**A** and **B**) TIG3 BRAF-ER cells were treated with 200 nM 4-OHT and detected for SA-ß-gal activity at the indicated time points. Images were taken with a bright field microscope (**A**). The number of SA-ß-gal-positive TIG3 BRAF-ER cells was quantified by counting 300 cells in a triplicate. The average from the counting (in %) ± SD is shown in (**B**).

(**C**) TIG3 BRAF-ER cells were treated with 200 nM 4-OHT as in (**A**). At the indicated time points cells were harvested, total RNA was prepared and analysed by RT-qPCR for the transcript level of *EZH2*. *UBC* served for normalisation and values were relative to day 0 (set to one). Error bars denote standard deviation of technical triplicates. A representative result of several independent experiments is given.

5.2.8 Oncogene-induced senescence causes an enhanced *CDKN1A* and *p16-INK4A* expression unlike a reduced *PRMT6* expression in TIG3 BRAF-ER cells

The tumour suppressors' CDKN1A and p16-INK4A are key regulators in cellular senescence (Kuilman et al., 2010). Here, both genes were strongly upregulated in TIG3 BRAF-ER cells (Figure 23), in which a senescent phenotype was induced by 4-OHT treatment (Figure 22). *CDKN1A* gene expression was 6-fold (Figure 23A) and *p16-INK4A* gene expression was nearly 8-fold increased (Figure 23B) after eight days of 4-OHT treatment compared to day 0. To answer the question whether PRMT6 was implicated in this process of stress-induced senescence (OIS), RT-qPCR and Western blot analyses of PRMT6 were performed under these conditions (Figure 23C, 23D). Transcript levels of *PRMT6* were slightly increased at day 2 and 4 of 4-OHT treatment compared to day 0. Interestingly, PRMT6 expression was decreased after eight days of 4-OHT treatment (60% reduction) compared to day 0 (Figure 23C). Analysis of PRMT6 protein level demonstrated that PRMT6 was reduced even after 2 days of 4-OHT treatment (Figure 23D). This effect was maintained until day 8.

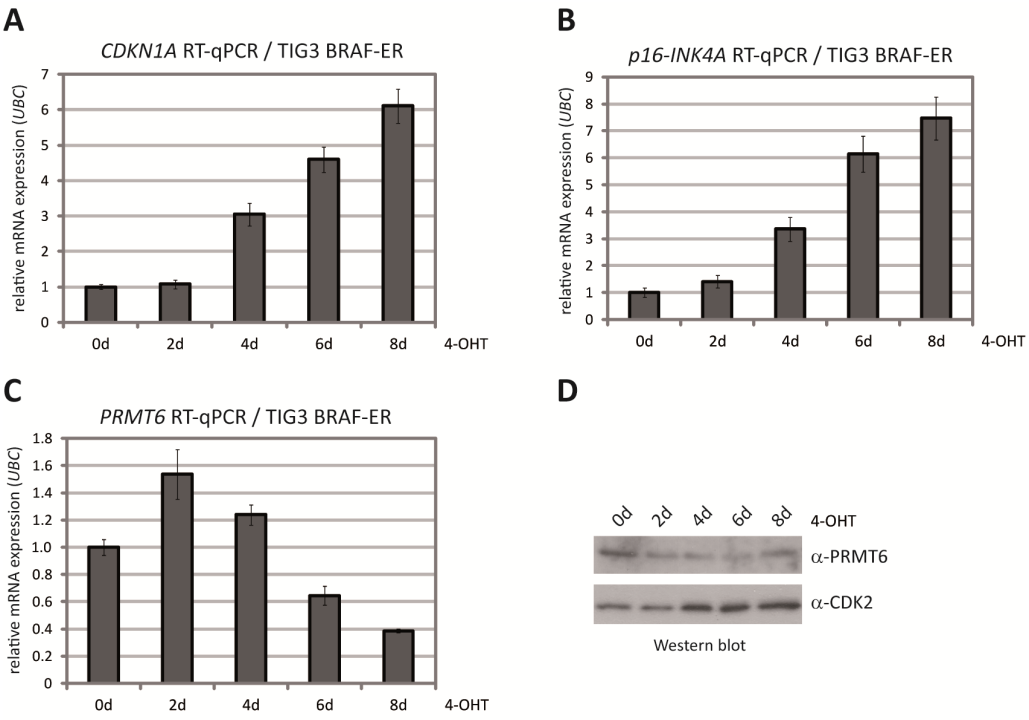

Figure 23: OIS induction causes increased *CDKN1A* as well as *p16-INK4A* gene expression accompanied by a reduced *PRMT6* gene expression in TIG3 BRAF-ER cells.

(**A** - **C**) TIG3 BRAF-ER cells were treated with 200 nM 4-OHT. At the indicated time points cells were harvested, total RNA was prepared and analysed by RT-qPCR for the transcript levels of (**A**) *CDKN1A*, (**B**) *p16-INK4A* and (**C**) *PRMT6*. *UBC* served for normalisation and values were relative to day 0 (set to one). Error bars denote standard deviation of technical triplicates.

(**D**) TIG3 BRAF-ER cells were treated with 200 nM 4-OHT as in (**A** - **C**). Whole cell extracts were harvested (IPH lysis) at the indicated time points and 20 µg protein of each sample was analysed by Western blot with an antibody directed against PRMT6 (right panel). CDK2 detection served as corresponding loading control. Experiments were performed as biological triplicates and one representative experiment is shown here.

In conclusion, the increase in *CDKN1A* and *p16-INK4A* gene expression correlated with a decrease in PRMT6 expression. For this reason, PRMT6 seems to play a distinct role in stress-induced senescence (OIS) in TIG BRAF-ER cells, in which a decrease in PRMT6 expression might cause a transcriptional induction of these two target genes.

5.2.9 Depletion of *CDKN1A* causes a delayed onset of OIS in TIG3 BRAF-ER cells

In order to examine whether OIS induction in these cells was dependent on *CDKN1A*, a siRNA-mediated depletion of *CDKN1A* was established in these cells. *CDKN1A* gene expression was strongly reduced using a pool of three *CDKN1A* siRNA-sequences (siCDKN1A) compared to the control siGFP in a time period of six days of 4-OHT treatment in TIG BRAF-ER cells (Figure 24A). *PRMT6* expression was unaffected within this time course compared to siGFP (Figure 24B). Evaluation of SA-ß-gal staining revealed that *CDKN1A*-depleted TIG3 BRAF-ER cells exhibited a delayed onset of OIS compared to the control transfection with siGFP (60% reduction) after six days of 4-OHT treatment (Figure 24C).

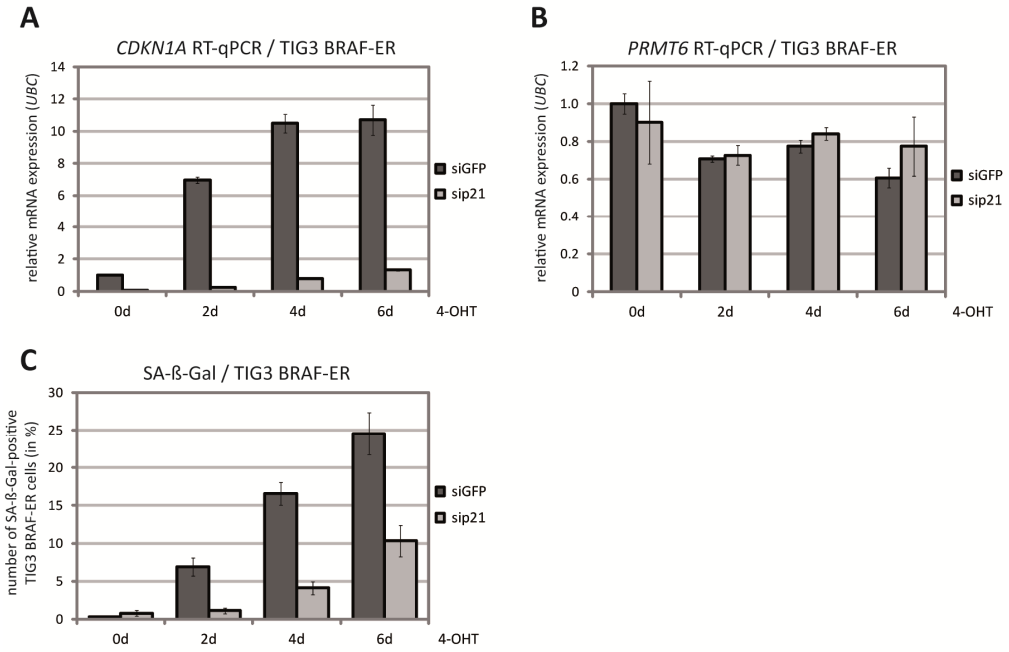

Figure 24: Depletion of *CDKN1A* results in a delayed onset of OIS in TIG3 BRAF-ER cells.

(**A** and **B**) TIG3 BRAF-ER cells were transfected with siCDKN1A (pool of three sequences) or siGFP as a control for 48 hours (PEI transfection), then treated with 200 nM 4-OHT. Cells were harvested and isolated RNA was examined for transcript levels of (**A**) *CDKN1A* and (**B**) *PRMT6* in the siGFP- (dark grey bars) or siCDKN1A-depleted cells (light grey bars). All values were normalised to *UBC* and day 0 of siGFP was set to one. Error bars denote standard deviation of technical triplicates.

(**C**) TIG3 BRAF-ER cells were treated with siRNA and 200 nM 4-OHT as described in (**A** and **B**) and detected for SA-ß-gal activity at the indicated time points. Day 0 was the time point of 48 hours after siRNA transfection. Quantification of the number of SA-ß-gal-positive TIG3 BRAF-ER cells either for siGFP- (dark grey bars) or siCDKN1A-depleted cells (light grey bars) was performed in counting a triplicate of each 300 cells per 6-well plate. Average (in %) ± standard deviation of a representative counting result of three independent experiments is shown.

A similar result was obtained using the sip21 pool in comparison to three alternative control siRNAs (siGFP, siNon, siScr) instead of only one control (siGFP), which confirms the available results in an independent larger experimental setup. Here, *CDKN1A* gene expression was also strongly reduced compared to the controls (Figure 25A). The corresponding SA-ß gal staining demonstrated a delayed onset of OIS in *CDKN1A*-depleted cells (Figure 25B) as described above (Figure 24C).

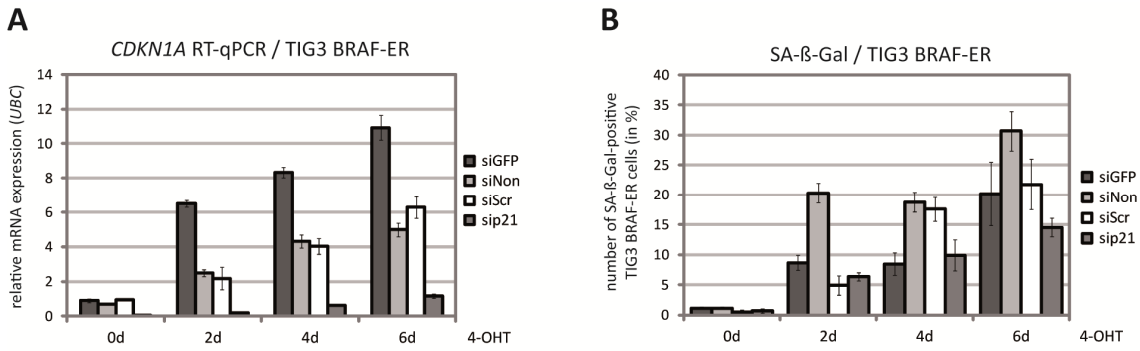

Figure 25: Depletion of *CDKN1A* results in a delayed onset of OIS using various siRNA controls in TIG3 BRAF-ER cells.

(**A** and **B**) TIG3 BRAF-ER cells were subjected to (**A**) RT-qPCR analysis and (**B**) SA-ß-gal staining using siRNAs (pool of three sequences) directed against the *CDKN1A* transcript level or GFP (siGFP), Nontargeting (siNon) and Scramble (siScr) as siRNAs controls (PEI transfection) and treatment with 200 nM 4-OHT. All values of the RT-qPCR were normalised to *UBC* and day 0 of siGFP set to one. Error bars denote standard deviation of technical triplicates. The experiment was performed as biological triplicates and one representative result is shown here.

In conclusion, knockdown of *CDKN1A* caused a delayed onset of OIS in TIG3 BRAF-ER cells demonstrated by several independent experiments. CDKN1A seems to be essential for Braf-induced senescence in these cells.

5.2.10 Overexpression of *PRMT6* causes a delayed onset of OIS in TIG3 BRAF-ER cells

In parallel to the *CDKN1A*-depleted cell analysis and its effect on the onset of OIS in TIG3 BRAF-ER cells (Figure 24, 25), I wanted to examine whether OIS is inhibited in a similar manner by overexpression of PRMT6. Therefore, *PRMT6* was overexpressed compared to a control transfection (pcDNA3.1) in the same cell line. Overexpression of *PRMT6* was efficient (up to 500 fold at day 3) as demonstrated by RT-qPCR when compared to control transfection (Figure 26A). Enhanced *PRMT6* expression resulted in a slight reduction of senescent cells (up to 25% at day 3) compared to a control transfection in TIG3 BRAF-ER cells (Figure 26B). Even after four days a delayed OIS was detected in *PRMT6* overexpressed cells.

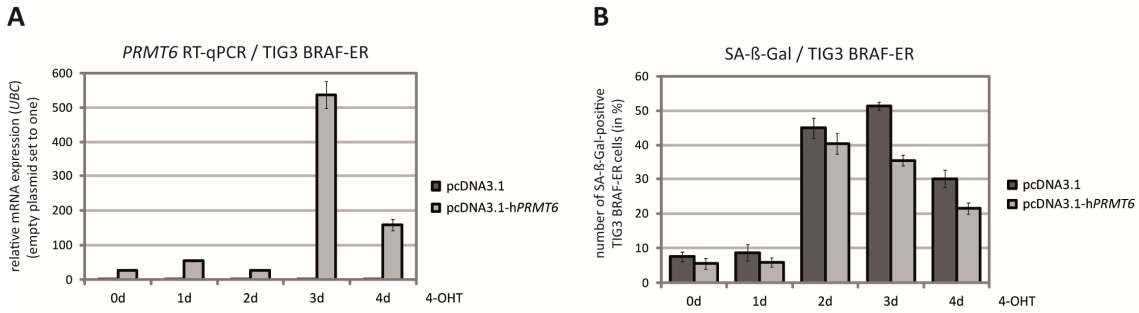

Figure 26: Overexpression of *PRMT6* leads to a reduced OIS level in TIG3 BRAF-ER cells.

(**A** and **B**) TIG3 BRAF-ER cells were transfected with pcDNA3.1 (empty plasmid) or pcDNA3.1-h*PRMT6* plasmids using FuGENE HD. 48 hours post-transfection, cells were treated with 200 nM 4-OHT for the indicated time period.

(**A**) Cells were harvested at the indicated time points, total RNA was prepared and analysed by RT-qPCR for the transcript levels of *PRMT6* comparing pcDNA3.1- (dark grey bars) with pcDNA3.1-h*PRMT6* overexpressing cells (light grey bars). All values were normalised to *UBC* and were relative to the corresponding empty plasmid, which was set to one at each time point (day 0, 1, 2, 3 and 4). Error bars denote standard deviation of technical triplicates.

(**B**) SA-ß-gal staining and counting of SA-ß-gal-positive TIG3 BRAF-ER cells either of pcDNA3.1- (dark grey bars) or pcDNA3.1-h*PRMT6* overexpressing cells (light grey bars) was performed at the indicated time points as in (**A**). Day 0 corresponds to two days after start of plasmid overexpression. Data show a representative result of the average of a triplicate counting (in %) ± standard deviation of three independent experiments.

Taken together, these data showed that PRMT6 is involved in Braf-induced senescence of TIG3 BRAF-ER cells. Moreover, they support the idea that OIS onset is dependent on PRMT6 because *PRMT6* overexpression caused a delayed onset of OIS similar to the effect demonstrated by depletion of *CDKN1A* in these cells. PRMT6 seems to regulate senescence in a negative manner through transcriptional repression of the two tumour suppressor genes CDKN1A and p16-INK4A.

5.3 Validation of novel interaction partners of PRMT6

The MS/MS analysis of MCF7 extracts overexpressing TAP-tagged PRMT6 revealed 43 putative interaction partners of PRMT6 implying various novel functions of PRMT6 in transcription, replication and cell cycle processes or DNA damage response (PhD thesis, Claudia Stein). To examine whether PRMT6 interacts with PCNA, DDB1 and DDB2, which are proteins of the DNA repair machinery (Essers et al., 2005; Iovine et al., 2011b), several co-immunoprecipitations (Co-IPs) were performed using MCF7 cell extracts in this study.

5.3.1 PRMT6 interacts with PCNA in MCF7 cells

MCF7 extracts overexpressing Flag-tagged PCNA were subjected to IP using four alternative crude sera directed against endogenous PRMT6 (CS PRMT6_1 - CS PRMT6_4) (Figure 27). In parallel, IPs with either IgG rabbit or two PRMT6 preimmune sera (PI PRMT6_1 and PI PRMT6_3) served as corresponding controls. Immunostaining of the IP reactions with a PCNA antibody revealed a weak interaction between PRMT6 and PCNA for all four crude sera. The heavy chain of the IgG antibody was located close to the 40 kDa PCNA band, which is detected as an unspecific band at the upper edge of the blot. The PCNA-antibody could not detect a signal within the control IPs (IgG rabbit, PI PRMT6_1 and PI PRMT6_3). The efficiency of the PRMT6 IP was approximately 10% compared to the input band (2%), which was detected in the corresponding PRMT6 antibody staining and judged by eye. The Co-IP analysis showed a weak, but significant interaction between PRMT6 and PCNA in this study.

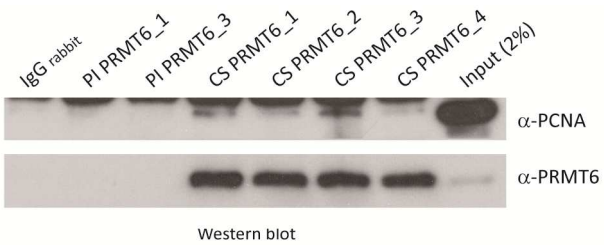

Figure 27: Endogenous PRMT6 interacts with overexpressed Flag-tagged PCNA in MCF7 cells.

MCF7 cells were seeded and after 24 hours transfected with a p3xFLAG10-Hs*PCNA* plasmid using PEI. 48 hours later, cells were harvested and a cell lysis was performed with IPH buffer (400 mM NaCl). Protein extracts were diluted to a final lysis buffer concentration of 200 mM NaCl. 1 mg extract of each sample was subjected to IP of overexpressed PCNA with endogenous PRMT6. Several PRMT6 crude sera (CS PRMT6_1 - PRMT6_4, each 5 µl) were used in IP in comparison to two PRMT6 preimmune sera (PI PRMT6_1, PI PRMT6_3, each 5 µl) or IgG rabbit (45 µg) as controls. The IPs and the input (2%) were detected with an anti-PCNA antibody after blotting. PRMT6 detection served as IP control. A representative result of three independent experiments is given.

5.3.2 PRMT6 interacts with DDB1 in MCF7 cells

The interaction between PRMT6 and DDB1 was also analysed by Co-IP studies (Figure 28). Therefore, PRMT6 was precipitated with each of the four alternative PRMT6 crude sera (CS PRMT6_1 - CS PRMT6_4) using whole cell extract from Flag-tagged DDB1 overexpressing MCF7 cells. The immunostaining of the PRMT6 IPs was performed with DDB1 antibody. A very weak DDB1-specific band appeared in the IgG rabbit control, whereas the DDB1 signal was clear above background in each of the PRMT6 crude sera IPs. An IP efficiency of more than 10% compared to the input was observed in the corresponding PRMT6 detection (42 kDa). PRMT6 clearly interacts with DDB1 at a height of 130 kDa.

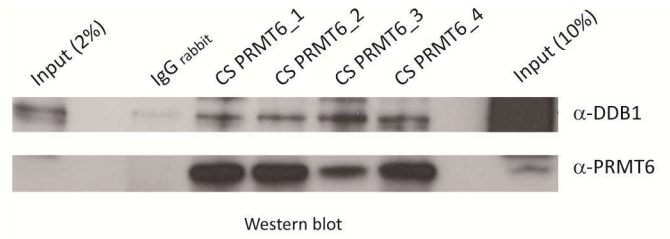

Figure 28: Endogenous PRMT6 interacts with overexpressed Flag-tagged DDB1 in MCF7 cells.

Overexpression of the pcDNA3-flag-*DDB1* plasmid in MCF7 cells (PEI transfection), cell lysis and all indicated IPs (each 1 mg protein extract) were performed as already described in Figure 27. All samples, together with the inputs (2% and 10%), were examined with antibodies directed against DDB1 and PRMT6 (IP control) in Western blot. The Western blot shows a representative result of three independent experiments.

5.3.3 PRMT6 also interacts with DDB2 in MCF7 cells

The protein DDB1 is often found in the UV-DDB complex together with DDB2, which binds to UV-damaged DNA sites (Iovine et al., 2011b; Scrima et al., 2008). Therefore, Co-IP analysis was extended to DDB2, although it was not found in the MS/MS analysis. Here, cell extracts of wild type MCF7 cells were analysed for the interaction between endogenous PRMT6 and endogenous DDB2 (Figure 29). An interaction between precipitated PRMT6 using the already described PRMT6 crude sera and DDB2 (45 kDa) was detected after immunostaining of the IPs with DDB2 antibody. No band appeared in the IgG rabbit control. The PRMT6 IP efficiency was again clearly over input (2%). As described above for PRMT6 and DDB1, PRMT6 also interacts with DDB2.

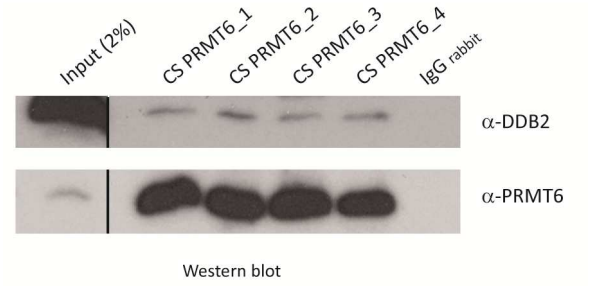

Figure 29: Endogenous PRMT6 interacts with endogenous DDB2 in MCF7 cells.

After 72 hours of seeding MCF7 cells were harvested, lysed in IPH buffer (400 mM NaCl) and equal amounts of protein extracts (each 1 mg) were incubated with the indicated PRMT6 crude sera (CS PRMT6_1 - PRMT6_4), preimmune sera (PI PRMT6_1, PI PRMT6_3) and IgG control, already described in Figure 27. DDB2 detection of all IPs and the input (2%) as well as the PRMT6 detection (IP control) is depicted. The scan was cut indicated by the black line, but all stainings depicted are from the same Western blot and exposure time. Shown is a representative result of three independent experiments.

In conclusion, the interaction between PRMT6 and two putative interaction partners found in the MS/MS analysis, PCNA and DDB1, was confirmed within this study. Additionally, PRMT6 interacts with DDB2, a component of the UV-DDB complex.

6 DISCUSSION

PRMTs possess manifold biological functions including the transcriptional activation and repression of genes, mRNA splicing, signal transduction and DNA damage repair (Bedford and Clarke, 2009). The deregulation of PRMTs and PRMT-related processes is also linked to the pathogenesis of various diseases such as human cancer (Baldwin et al., 2014; Cha and Jho, 2012; Yang and Bedford, 2013). Previously, it was reported that *PRMT6* is overexpressed in different types of human cancer compared to non-neoplastic tissues. Therefore, PRMT6 might be an attractive target for therapeutic strategies to efficiently treat cancer. Especially in the case of lung cancer, novel strategies are urgently required because lung cancer is the leading cause of cancer-related death in humans worldwide.

6.1 Prmt6 protein levels are increased in murine lung cancer

A cDNA microarray and several siRNA experiments gave an initial hint that PRMT6 expression is increased in lung cancer and that PRMT6 might positively affects the growth of lung cancer cells (Yoshimatsu et al., 2011). For this reason, PRMT6 levels were analysed in different lung tumours in the present work. Immunohistochemical (IHC) stainings of tissue sections from the two murine lung cancer models LLC1 and $Kras^{LA2}$ demonstrated that the expression of Prmt6 is increased in lung tumours compared to healthy tissue. In detail, Prmt6 protein levels were elevated in the enlarged nuclei and surrounding cytoplasms of tumour cells within the tumour mass of LLC1 mice (Figure 6A, 6B, S1B and S2B). A similar result was obtained for the $Kras^{LA2}$ model. Here, tumour cells as well as cells embedded in the alveolar and bronchiolar structure showed increased Prmt6 levels compared to healthy C57BL/6 mice, although there were some differences in the Prmt6 stainings of $Kras^{LA2}$ mice (Figure 7, S1C and S2C). These data confirm that Prmt6 protein levels are increased in murine lung cancer.

Beside PRMT6, PRMT1 was also described to be overexpressed in lung cancer tissues (Yoshimatsu et al., 2011). In 2014, another study performed IHC stainings of PRMT1 in

human lung tumour tissues and could demonstrate that PRMT1 expression is increased in these sections (Elakoum et al., 2014). Therefore, IHC stainings of Prmt1 in the murine sections served as a positive control within this study and showed that Prmt1 expression was indeed elevated in tumour cells from LLC1 and $Kras^{LA2}$ mice (Figure 8).

Previous immunofluorescence (IF) stainings demonstrated that PRMT6 is predominantly located in the nucleus of human HeLa and MCF7 cells (Frankel et al., 2002; Hyllus et al., 2007). As mentioned above, the analysis of Prmt6 in LLC1 and $Kras^{LA2}$ mice revealed that Prmt6 expression was also strongly increased in the nucleus of lung tumour cells compared to healthy tissue areas. Moreover, protein levels of Prmt6 were elevated in the cytoplasms of these cells. It is unlikely that the increased Prmt6 stainings in the cytoplasms of lung tumour cells are unspecific due to the fact that three alternative PRMT6 antibodies demonstrated a similar staining pattern of Prmt6 in LLC1 and $Kras^{LA2}$ lung cancer sections (Figure 6, 7, S1 and S2). It is possible that the nuclear expression of Prmt6 is so high that it is also detectable in the cytoplasm of these cells. Alternatively, PRMT6 might possess different physiological functions and therefore variability in its protein localisation in different cell compartments occurs, which might be dependent on the cell type and cell line. For example, several previous publications demonstrated that the subcellular localisation of PRMTs varies, e.g. PRMT1 ranges from predominantly nuclear to predominantly cytoplasmic dependent on the analysed cell line (Côté et al., 2003; Frankel et al., 2002; Herrmann et al., 2005; Tang et al., 1998). In addition, Goulet and colleagues revealed that PRMT1 N-terminal unique sequences affect the intracellular localisation of its different isoforms in HeLa cells (Goulet et al., 2007). An example for the regulation of the cellular localisation of PRMTs by PTMs is the S216 phosphorylation of PRMT4, which promotes a cytoplasmic localisation of this mainly nuclear protein (Feng et al., 2009). For these reasons, it can not be excluded that PRMT6 possesses as well different localisations in various cell lines or cell types.

Tumours are composed of proliferating tumour and stromal cells, including surrounding blood vessels, endothelial cells, inflammatory and immune cells as well as fibroblasts, which form the cellular environment of the tumour, also called as tumour

microenvironment (Hao et al., 2012). In order to test whether Prmt6-positive stained cells within the tumour mass of LLC1 and $Kras^{LA2}$ mice are those proliferating cells, specific double stainings of Prmt6 with Ki-67 could be envisaged using the lung cancer sections from this study. Moreover, Ki-67 is a nuclear proliferation marker, which was already used to demonstrated a reduced proliferation rate of two different NSCLC cell lines (A549, H1299) after depletion of *PRMT1* and *PRMT4* (Elakoum et al., 2014). Furthermore, PRMT5 is essential for the growth of lung cancer cells demonstrated by depletion of *PRMT5* in A549 cells (Gu et al., 2012). In comparison to these three PRMTs, the knockdown of *PRMT6* also negatively affected the clonogenic growth of the two analysed NSCLC cell line H1299 and H358, which was analysed by colony formation assay (CFA) (Figure 11, 12) in this study. This is a common method to determine whether singly plated transformed cells are still able to survive and to grow into colonies due to their unlimited division potential. Additionally, it seems that this inhibitory effect caused by the depletion of *PRMT6* might be more prominent in NSCLC cells with previously high PRMT6 levels (H358) (Figure 12, S3 lower panel) than in cells with previously moderate PRMT6 levels (H1299) (Figure 11, S3 upper panel). In conclusion, these data indicate that PRMT6 also possesses a function in the regulation of the proliferative capability of transformed cell lines similar to PRMT1, PRMT4 and PRMT5. These data are in line with a previous study demonstrating that PRMT6 promotes the estrogen-stimulated proliferation of breast cancer cells (Harrison et al., 2010).

Certain cells embedded in the alveolar structure of the lung tumour sections from $Kras^{LA2}$ mice as well as of sections from healthy C57BL/6 mice were positively stained for Prmt6 (Figure S1A, S1C, S2A). It is possible that these cells are alveolar macrophages. In general, macrophages are widely distributed innate immune cells that are also found in the lung (Hao et al., 2012). They can be subdivided into classically activated (M1) and alternatively activated (M2) macrophages. Interestingly, macrophages are the dominant leukocyte population in tumours, in which especially the M2 phenotype provides an immunosuppressive microenvironment for tumour growth (Quatromoni and Eruslanov, 2012). These tumour-associated macrophages

(TAMs) secrete many cytokines, chemokines and proteases, which promote angiogenesis, growth and metastasis of several tumours (Hao et al., 2012). In order to clarify whether these cells are macrophages, IHC or IF double stainings of Prmt6 with common macrophage-specific markers, such as F4/80, CD68 or CD11b, could be performed by using murine tissue sections (Lloyd et al., 2008; Ma et al., 2010; Quatromoni and Eruslanov, 2012). In addition, some cells of the $Kras^{LA2}$ and healthy C57BL/6 mice were also positively stained for Prmt6 in the epithelium of bronchioles (Figure 5A and 7A). It is possible that these cells are Clara cells, which are non-ciliated, secretory bronchiolar epithelial cells, and also function as stem/progenitor cells for repair in the bronchioles (Wang et al., 2012b). IHC double stainings of Prmt6 with the Clara cell marker CCSP (Clara cell secretory protein), which is a crucial secretory protein produced by Clara cells, could show whether Prmt6 is expressed in these cells. Interestingly, a study by O'Brien and colleagues demonstrated that PRMT4 is already linked to lung development because this type I PRMT is expressed in alveolar type II, endothelial and also in Clara epithelial cells, which was examined by CCSP staining (O'Brien et al., 2010). It would be interesting to analyse whether PRMT6 also plays a role in pulmonary epithelial cell proliferation and differentiation as shown for PRMT4.

As described above, Prmt6 levels were highly increased in lung tumour sections from murine LLC1 mice (Figure 6A, 6B, S1B and S2B) compared to healthy tissue areas in the same tissue sections. In contrast, protein levels of Prmt6 were relatively low in cultured LLC1 compared to MLE12 (murine transformed lung epithelial cells) and several other human NSCLC cell lines (Figure 9). So far, the identity of the detected Prmt6 levels in these LLC1-derived tissue sections is still unknown. It is possible that the elevated PRMT6 levels in LLC1 mice are caused by cells within the tumour microenvironment, such as immune cells (e.g. macrophages). However, it is difficult to answer this issue because it would be necessary to analyse the influence of this surrounding environment on the expression of Prmt6 in comparison to the elevated PRMT6 expression in the tumour cells.

In order to investigate whether the high PRMT6 protein level is essentiell for lung tumour formation in LLC1 mice, gene functional knockout of *Prmt6* could be achieved

using the novel CRISPR/Cas9 system (Fennell et al., 2014; Mali et al., 2013). Then, *Prmt6* proficient and *Prmt6* deficient LLC1 cells could be injected into the tail vein of healthy C57BL/6 mice and the comparison of these mice could help to analyse whether both mice develop similar or different tumour patterns in the lung after IHC staining of Prmt6. It would also be interesting to perform this knockout of *Prmt6* by CRISPR/Cas9 in cultured LLC1, to inject these cells into the flank of healthy C57BL/6 mice in comparison to untransfected LLC1 cells and to analyse whether the size of LLC1 tumours is impaired by depletion of *Prmt6* in such an allograft model. In this context, the group of Ernesto Guccione demonstrated that depletion of *PRMT6* in breast cancer cells, followed by orthopic injection into SCID (severe combined immunodeficiency) mice caused an inhibition of tumour formation compared to mice injected with control cells (Phalke et al., 2012). These data indicate that PRMT6 could also play an important role in lung cancer.

In parallel to the analysis of the importance of PRMT6 in LLC1 mice, it is possible to use *Prmt6* knockout mice from Stéphane Richard´s group for cross-breedings with $Kras^{LA2}$ mice from Tyler Jacks lab (Johnson et al., 2001; Neault et al., 2012). Here, it is likely that *Prmt6* knockout reduces *Kras*-driven tumourigenesis compared to *Prmt6* wild type $Kras^{LA2}$ mice in a time- and/or growth-dependent manner.

In this context, Gu and colleagues have already demonstrated that the depletion of *PRMT5* abolishes the growth of A549 lung tumour xenografts in mice and that PRMT5 is involved in FGFR (fibroblast growth factor receptor) signaling, a pathway needed for tumour growth (Gu et al., 2012). Another study showed that PRMT5 regulates the HIF-1 (hypoxia-inducible factor 1) signaling pathway (Lim et al., 2012). HIF-1 is a key player in the cellular adaption to hypoxia, which dominates in fast growing tumours. These data raise the question whether PRMT6 is also implicated in pathways necessary for efficient tumour growth, such as the FGFR or HIF-1 pathway. At least, this study has already demonstrated by performing CFAs in NSCLC cell lines that PRMT6 is important for the unimpeded growth of tumour cells as described above.

6.2 PRMT6 regulates cell proliferation and senescence by transcriptional repression of tumour suppressor genes

In parallel to the CFA in H1299 and H358 cells, siRNA-mediated depletion of *PRMT6* caused also proliferation defects in the transformed cell line U2OS demonstrated by another CFA (Figure 14). Moreover, non-transformed human diploid fibroblasts (TIG3-T) underwent stress-induced senescence due to a depletion of *PRMT6* mediated by infection with retroviral plasmids coding for alternative shRNAs against *PRMT6* (Figure 17). This was further supported by measuring population doublings and performing FACS analyses. It was demonstrated that depletion of *PRMT6* strongly impaired the proliferative capacity of TIG3-T cells and resulted in an accumulation of these cells in G1-phase, a typical hallmark of senescent cells (PhD thesis, Claudia Stein and Stein et al., 2012). These findings are in line with previous publications, which showed that PRMT6 positively affects estrogen-stimulated proliferation of breast cancer cells (Harrison et al., 2010) and positively impacts the growth of NSCLC cells (Yoshimatsu et al., 2011). Moreover, it was found that PRMT6 was downregulated in replicatively and oxidatively premature senescent cells compared to young cells similar to PRMT1, PRMT4 and PRMT5 (Lim et al., 2008).

In the search for possible responsible downstream target genes of PRMT6, the CDK inhibitor genes CDKN1A of the Cip/Kip family and p16-INK4A of the INK4 family were identified to be transcriptionally repressed and bound by PRMT6 (Figure 15, 16, 18, 19 and 20). Both genes are key regulators of cellular senescence which function via the TP53-CDKN1A-RB1 and p16-INK4A-RB1 cascade in inhibition of phosphorylation of RB1 (retinoblastoma 1) and E2F-target gene expression (Narita et al., 2003). This process presents a natural barrier to tumourigenesis by prohibition of unlimited cell proliferation (Prieur and Peeper, 2008; Serrano and Blasco, 2007), in which derepression of CDKN1A and p16-INK4A causes a growth arrest in G1-phase. Cellular senescence can be triggered by telomere shortening (replicative cellular senescence) or various types of other stress signals, such as DNA damage, oxidative stress or expression of oncogenes (premature cellular senescence). Beside the G1-arrest, senescent cells develop further typical senescence-associated features (Campisi and

d'Adda di Fagagna, 2007). They exhibit a flat, enlarged cell morphology accompanied by increased activity of ß-galactosidase (ß-gal) and changes in gene expression as in the case of the analysed human diploid fibroblasts. Especially the SA-ß-gal assay, which was performed in this study (Figure 17), is a common method to confirm that these cells are able to undergo replicative or premature senescence (Dimri et al., 1995; Lim et al., 2008).

In parallel to our findings (Figure 30A; Stein et al., 2012), Stéphane Richard´s group generated a *Prmt6* knockout mouse, which is viable, and demonstrated that isolated MEFs from these mice had also growth defects (G1-arrest) and underwent rapid cellular senescence (Figure 30D; Neault et al., 2012). Here, it was found that PRMT6 regulated *CDKN1A* in a TP53-dependent manner. Additionally, Marc Timmers´ laboratory showed that depletion of *PRMT6* promoted an accumulation of U2OS cells in G2-phase due to the fact that CDKN1A induces a growth arrest in G1- as well as G2-phase (Figure 30B; Kleinschmidt et al., 2012). In this context, Ernesto Guccione´s group demonstrated that *PRMT6* knockdown caused a diminished proliferation rate, a senescent phenotype (SA-ß-gal staining) and a reduced anchorage independent growth (soft agar assays) of breast cancer cells by a TP53-independent repression of *CDKN1A* (Figure 30C; Phalke et al., 2012). In conclusion, three further groups also revealed that PRMT6 possesses an important cell cycle regulatory function in repression of *CDKN1A* and induction of senescence using different cell systems and techniques for knockdown or knockout of *PRMT6*.

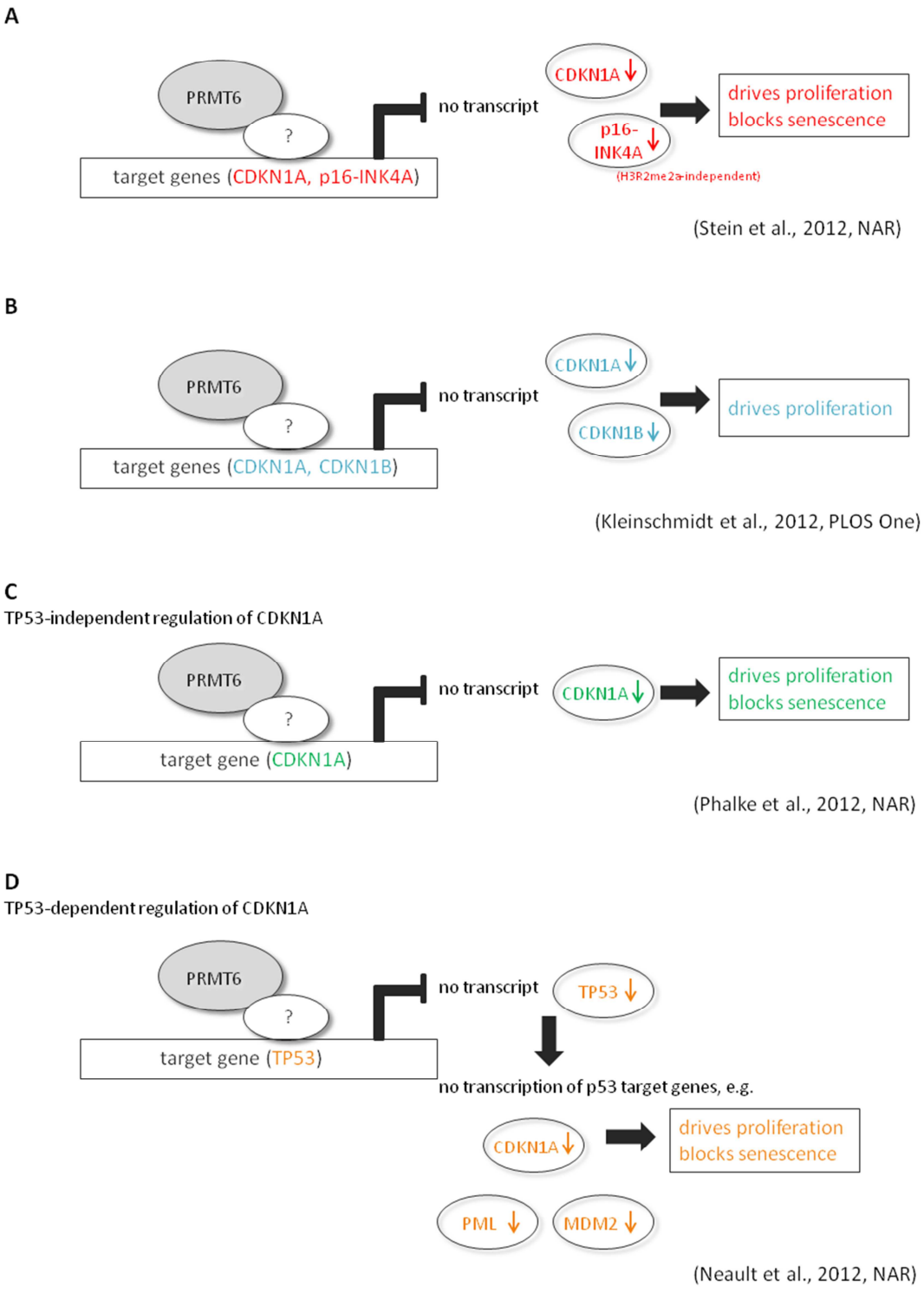

Figure 30: PRMT6 is a negative transcriptional regulator - Comparison of four publications.

CDKN1A was originally identified as a potential mediator of the tumour suppressor activity of the transcription factor TP53 (Dulić et al., 1994; el-Deiry et al., 1993; Slebos et al., 1994). From the literature it is known that CDKN1A expression can also be regulated independently of TP53. For example, the transcription factors SP1, SP3,

HOXA10 (homeobox protein Hox-A10), GAX (growth arrest-specific homeobox) or KLF6 (kruppel-like factor 6) control *CDKN1A* transcription and upregulate its transcription in response to various stimuli and anticancer agents (Abbas and Dutta, 2009). In this study, transcript level of TP53 was not significantly altered in *PRMT6*-depleted U2OS (Figure 15D) indicating that the regulation of *CDKN1A* expression by PRMT6 might be independent of TP53. A similar result was detected in the fibroblast cell line TIG3-T (PhD thesis, Claudia Stein). These results are in line with the data from Ernesto Guccione´s group, who has analysed the two breast cancer cell lines MCF7 (with wild type TP53) and MDA-MB-231 (triple negative and mutant TP53) and found that PRMT6 also regulates *CDKN1A* in a TP53-independent manner as mentioned above (Figure 30C; Phalke et al., 2012). Nevertheless, it is still possible that TP53 can recruit PRMT6 to its target gene CDKN1A in these analysed MCF7 cells similar to our analysed U2OS and TIG3-T cells without affecting its expression. In contrast to these data, Neault and colleagues demonstrated that the binding of PRMT6 and enrichment in H3R2me2a upstream of the Trp53 locus was diminished in Prmt6$^{-/-}$ MEFs indicating that PRMT6 is a regulator of TP53 (Figure 30D; Neault et al., 2012). Here, Prmt6$^{-/-}$ MEFs exhibited an elevated expression of *Trp53* as well as an increased expression of Trp53- target genes, such as *Cdkn1a* and *PML*. Moreover, deletion of the *Trp53* gene (*Trp53*$^{-/-}$) completely rescued the pre-senescent phenotype as shown in Prmt6$^{-/-}$ MEFs. These data indicate that PRMT6 regulates senescence in a TP53-dependent manner in these analysed mice compared to the results described in this thesis.

The expression of the two other Cip/Kip family members *CDKN1B* and *CDKN1C* was not significantly altered in *PRMT6*-depleted U2OS cells, indicating that PRMT6 does not regulate their expression (Figure 15E, 15F). The group of Marc Timmers revealed that *PRMT6* knockdown caused an upregulation of *CDKN1A* as well as *CDKN1B*, but not of *CDKN1C* in U2OS cells (Figure 30B; Kleinschmidt et al., 2012). However, the relatively mild effect on the CDKN1B transcript by depletion of *PRMT6* was not detectable in the present work (Figure 15E). The same applied to the two other genes of the INK4A/B tumour suppressor locus. Neither the transcript of p14 (p14-ARF), which represents the alternate open reading frame of the INK4A locus, nor the adjacent CDK inhibitor

gene p15 (p15-INK4B, CDKN2B) were affected in their transcript levels upon depletion of *PRMT6* in TIG3-T cells (PhD thesis, Claudia Stein and Stein et al., 2012). In addition, the exemplary analysed CCND1, which is a G1/S-specific cyclin, and CCNA2, which promotes both cell cycle G1/S- and G2/M-transitions and binds to CDK2 during S phase, were not specifically altered in their expression by PRMT6 (Figure 15C, 15G and 15H). Moreover, the transcript level of the angiogenesis inhibitor *THBS1* was not uniformly affected in U2OS cells upon *PRMT6* knockdown (Figure 15I), although it was identified as a transcriptional repressed target gene of PRMT6 and implied a role of PRMT6 in tumourigenesis (Michaud-Levesque and Richard, 2009). However, these data strengthen the hypothesis that PRMT6 predominantly targets the two tumour suppressor CDKN1A and p16-INK4A.

CDKN1A and p16-INK4A loci are bound by PRMT6 demonstrated by independent chromatin immunoprecipitation (ChIP) analyses in U2OS and TIG3-T cells (Figure 16, 19 and 20). In case of the CDKN1A gene locus, PRMT6 binding overlapped with dimethylated H3R2, which both peaked at the TSS of CDKN1A in comparison to surrounding regions of this locus (Figure 16 and 19). Similarly, Kleinschmidt and colleagues demonstrated that overexpression of PRMT6 resulted in an increase of the H3R2me2a level at the TSS of the CDKN1A gene locus (Kleinschmidt et al., 2012). Hence, it is likely that the histone methyltransferase activity of PRMT6 might be necessary for repression of the CDKN1A gene locus. Further experiments could confirm this hypothesis by using a catalytic inactive PRMT6 mutant in ChIP analysis.

In contrast to the CDKN1A locus, at the p16-INK4A gene locus PRMT6 binding was detected at the TSS as well as neighbouring regions, while H3R2me2a was not increased (Figure 20). This finding indicates that PRMT6 does not function as a histone arginine methyltransferase towards H3R2 to repress the p16-INK4A locus; rather it supports the idea that PRMT6 could here methylate different histone residues. It is conceivable that PRMT6 methylates H2AR29 or H3R42 and thereby fulfils its repressive function on the p16-INK4A locus (Casadio et al., 2013; Waldmann et al., 2011). Alternatively, it is possible that PRMT6 similar to other PRMTs binds to and methylates diverse nonhistone protein substrates such as transcriptional coregulators and thereby

regulates the derepression of the p16-INK4A locus (Lee and Stallcup, 2009). For example, it is known that PRMT1 influences gene expression independently of its ability to modify histone residues by functioning as a transcriptional coactivator of the transcription factor RUNX1. PRMT1 methylates RUNX1, which impedes the interaction between RUNX1 with the corepressor SIN3A and thereby leads to a transcriptional activation of RUNX1-target genes (Zhao et al., 2008). Another example is the methylation of the histone acetyltransferase and nuclear receptor coactivator SRC-3 (steroid receptor coactivator 3) by PRMT4, which causes a dissociation of CBP and PRMT4 from SRC-3 and then reduces the stability of SRC-3 (Feng et al., 2006; Naeem et al., 2007). These findings could also be applicable for PRMT6 to presumably indirectly regulate the expression of p16-INK4A by effector proteins. Here, PRMT6 could bind to those transcriptional coregulators, influence their stability (e.g. by degradation) and capability to interact with other proteins. However, these findings indicate that PRMT6 seems to act in a different manner at both loci.

Since PRMT6 does not possess a DNA binding domain and is not able to directly bind target genes it remains elusive by which factors PRMT6 is recruited to these gene loci to fulfil its repressive function there. In order to unravel this mechanism, the transcription factor MYC is a potential candidate, which could lead PRMT6 to the CDKN1A gene locus. MYC is known to be recruited to MIZ-1 binding sites at the CDKN1A gene promoter by the DNA-binding factor MIZ-1 together with the DNA methyltransferase DNMT3a resulting in transcriptional repression of CDKN1A (Brenner et al., 2005). Alternatively, it was also demonstrated that MYC interacts with the transcription factor SP1, which inhibits the transcriptional activity of SP1 and subsequently leads to a transcriptional repression of CDKN1A (Gartel and Shchors, 2003). In case of the p16-INK4A locus, the recruitment of PRMT6 by one or more Polycomb group proteins may also be possible and could be analysed in future experiments. In this context, previous studies in our group already demonstrated that PRMT6 interacts with several core components of PRC1 (polycomb repressive complex 1) or PRC2, such as CBX8 or EZH2 (PhD thesis, Claudia Stein and personal communication, René Reiner Nötzold). Furthermore, it was shown that the catalytic

activity of PRMT6 was enhanced in the presence of H3K27me3 (Hyllus et al., 2007). This epigenetic mark is catalysed by EZH2, which promotes the recruitment of the PRC1 complex to the p16-INK4A locus and thereby regulates the transcriptional expression of this locus in a repressive manner (Lanigan et al., 2011).

Interestingly, cellular senescence was not only induced by depletion of *PRMT6* in TIG3-T cells (Figure 17), but PRMT6 is also implicated in stress-induced senescence. Here, oncogene-induced senescence (OIS) was analysed in TIG3 BRAF-ER cells by activation of the oncogene Braf upon 4-OHT (4-hydroxytamoxifen) treatment (Figure 22) (Agger et al., 2009; Woods et al., 1997). As a result, OIS caused a reduction of PRMT6 on mRNA and protein level, while *CDKN1A* and *p16-INK4A* transcript levels were strongly increased (Figure 23). In order to unravel the relevance of CDKN1A in this OIS model, siRNA-mediated depletion of *CDKN1A* was performed followed by subsequent 4-OHT treatment (Figure 24A). In fact, depletion of *CDKN1A* impaired the onset of OIS as measured by SA-ß-gal staining (Figure 24C). Furthermore, PRMT6 seems to be important for the onset of OIS because overexpression of *PRMT6* has also led to a delayed OIS onset similar to CDKN1A (Figure 26). In this context, Phalke and colleagues showed that a double knockdown of *PRMT6* and *CDKN1A* rescued the detected *PRMT6* depletion phenotype as described above (Phalke et al., 2012). However, it is still unknown by which transcription factors PRMT6 gene is itself regulated in proliferation or cellular senescence and thereby causing an activation or repression of PRMT6 transcription. So far, only one study demonstrated that PRMT1 transcription is controlled by binding of c-Myc to a conserved site in the first intron of the PRMT1 gene. Thereby, PRMT1 transcription is upregulated, which plays an important role during thyroid hormone-dependent Xenopus metamorphosis (Fujimoto et al., 2012).

The present work showed that PRMT6 promotes cell proliferation and blocks cellular senescence in transformed as well as non-transformed cells by transcriptional repression of the CDK inhibitors CDKN1A and p16-INK4A. Moreover, PRMT6 seems to be overexpressed in lung cancer and seems to promote tumour growth as demonstrated by this study and Yoshimatsu et al. (2011). These findings support the

idea to develop epigenetic inhibitors targeting PRMT6, which could probably help in the treatment of lung cancer and perhaps also with other cancer types by reducing the proliferation rate of rapidly dividing tumours. Interestingly, inhibitor screening assays were already developed for PRMT1, in which for example allantodapsone was identified as a selective PRMT1 inhibitor (Hauser et al., 2012; Spannhoff et al., 2007).

6.3 Identification of novel cellular functions of PRMT6

A previous gel filtration analysis of nuclear extracts from several human cell lines in our group demonstrated that endogenous PRMT6 elutes within a molecular weight range of 150 - 440 kDa compared to its monomeric molecular weight of 42 kDa (PhD thesis, Claudia Stein). From the literature it is already known that type I PRMTs require dimerisation for their enzymatic activity (Weiss et al., 2000; Zhang and Cheng, 2003; Zhang et al., 2000). Furthermore, some of the PRMTs, such as PRMT1 and PRMT5, are part of higher molecular weight complexes (Friesen et al., 2001, 2002; Lin et al., 1996). PRMT1 interacts with BTG1 and TIS21, whereby the enzymatic activity of PRMT1 is positively modulated (Lin et al., 1996). PRMT5 associates with MEP50 (methylosome protein 50) and both are components of the methylosome, in which MEP50 promotes an enhanced enzymatic activity of PRMT5 (Friesen et al., 2002). However, homodimerisation of PRMT6 would not explain the presence of PRMT6 in these high molecular weight fractions with a molecular weight up to 440 kDa. Rather, it would suggest that PRMT6 also interacts with so far unidentified proteins, which possibly would link PRMT6 to novel cellular functions.

In order to uncover novel interaction partners and functions of PRMT6 a MS/MS analysis of purified TAP-tagged PRMT6 from MCF7 cells was performed in our group. As a result of this unbiased approach, 43 putative interaction partners of PRMT6 were identified. Among them were proteins involved in the regulation of transcription, proliferation, replication and DNA repair (PhD thesis, Claudia Stein). Especially the two identified candidates DDB1 and PCNA together with DDB2 and CUL4A were of interest because of their link in DNA damage repair. It is remarkable that DDB1 and PCNA, but

not DDB2 and CUL4A, were found in the MS/MS analysis. It is possible that the interaction between PRMT6 and these two proteins is rather weak in unstimulated MCF7 cells used in this study and hence they were not detected in our unbiased approach. For this reason it is likely that an interaction between PRMT6 and DDB2 or CUL4A may only be present within the DNA damage response for example caused by UV irradiation.

6.3.1 PRMT6 interacts with PCNA, DDB1 and DDB2

DDB1 is a multifunctional protein that was first identified as a subunit of the damaged DNA binding protein complex (UV-DDB). In that complex, DDB1 heterodimerises with DDB2, recognises UV-induced photolesions of the DNA and promotes the initial step of global genome NER (GG-NER) (Iovine et al., 2011b). DDB1 also plays a role in transcriptional regulation of UV-induced genes, such as FMOD (Bevilacqua et al., 2005; Iovine et al., 2009). Subsequently, DDB1 was found to function as an adaptor/linker protein between CUL4A and the DDB1-CUL4-associated factors (DCAF) in the CUL4A-RING ubiquitin E3-ligase complex (CRL4) (Iovine et al., 2011b). This DDB1-CUL4A complex targets different substrates for ubiquitylation followed by degradation through the ubiquitin-proteasome system (UPS). For example, CRL4-mediated ubiquitylation of DDB2 causes a rapidly degradation of DDB2 during the early steps of GG-NER after UV irradiation (Chen et al., 2001b; El-Mahdy et al., 2006; Nag et al., 2001; Sugasawa et al., 2005). Further known ubiquitylation targets are the replication licensing protein CDT1, the CDK inhibitor CDKN1A or the transcription factor E2F1. All these ubiquitylations are dependent on the interaction with the cofactor PCNA (Abbas et al., 2008; Nishitani et al., 2008; Senga et al., 2006; Shibutani et al., 2008). PCNA is required for the replication-dependent destruction of CDT1 or CDKN1A in S phase and thereby couples DNA replication with CUL4-DDB1-dependent proteolysis (Arias and Walter, 2006; Kim et al., 2008; Nishitani et al., 2008). Interestingly, PCNA is itself monoubiquitinated by CRL4, which is a relevant feature for PCNA-dependent DNA repair (Soria et al., 2006; Terai et al., 2010). Furthermore, the complex ubiquitylates core histones (H2A, H3 and H4). However, that does not lead to their degradation, but

rather weakens the interaction between histones and DNA and thereby facilitates the recruitment of repair proteins (e.g. XPC) to damaged DNA sites (Kapetanaki et al., 2006; Wang et al., 2006).

Interestingly, it was observed that CUL4A expression is increased in human breast cancer and a variety of further tumour cell lines, such as A549 cells (Chen et al., 1998; Hori et al., 1999). Additionally, a conditional CUL4A transgenic mouse model confirmed that CUL4A is oncogenic *in vivo*. Here, overexpression of CUL4A has led to an atypical epithelial cell growth demonstrated by IHC stainings of lung tissue sections of these mice (Yang et al., 2014). The analysis of the expression of several CUL4A-associated proteins revealed that for example the expression of *Cdkn1a* was decreased in these lung tumours. In this context, IHC analysis demonstrated that PCNA expression was increased in these lung tumours suggesting that PCNA could be involved in Cul4A-mediated *Cdkn1a* downregulation. Therefore, it would be interesting to analyse a link between CUL4A, PCNA, Cdkn1A, which is a target gene of PRMT6 in the human system, and PRMT6 itself in this specific murine lung tumour model.

Previous data demonstrated that PRMT6 is implicated in base excision repair (BER) as a positive regulator of DNA polymerase ß (Pol ß) (El-Andaloussi et al., 2006). Moreover, PRMT6 stimulates *CCND1* expression upon DNA damage, presumably by PRMT6-mediated dimethylation of H3R2 (Iberg et al., 2008). The identification of several DNA repair-related putative interaction partners of PRMT6 in the MS/MS analysis raised the question whether PRMT6 possesses further functions in DNA repair than hitherto assumed. Indeed, the conducted CoIPs/Western blots in this study strengthen this hypothesis due to the confirmed interactions of PRMT6 with PCNA, DDB1 and DDB2, respectively (Figure 27-29). Additionally, the interaction of PRMT6 with CUL4A was verified by former CoIP studies (bachelor thesis, Lisa Schubert).

Future experiments could clarify whether the interaction between PRMT6 and the CRL4 components is enhanced after UV damage. We will address the question whether PRMT6 accumulates at DNA specific damage sites after induction of local UV damage by using GFP-tagged PRMT6 overexpressing cells in cooperation with Adriaan

Houtsmuller (from the Erasmus MC in Rotterdam). In this context, γ-H2AX is also a molecular marker for cellular DNA double-strand breaks (DSBs) caused in telomere-initiated senescent cells (d'Adda di Fagagna et al., 2003). Therefore, phosphorylated histone H2AX (γ-H2AX) stainings could be used to study whether these factors co-localise at DNA damage foci together with PRMT6.

In addition, it has to be further investigated whether PRMT6 influences the activity or substrate specificity of the E3 ubiquitin ligase complex CRL4 either in DNA damage response or during replication. This can be achieved by comparing the ubiquitylations of *PRMT6* proficient versus *PRMT6* deficient cells. Possibly, PRMT6 is itself a substrate of CRL4. This hypothesis could be analysed in the already established OIS model of TIG3 BRAF-ER cells. A study from Kotake´s laboratory has created a novel link of DDB1-CUL4A to cellular senescence (Kotake et al., 2009). They demonstrated that these CRL4 components are, together with MLL1, required for oncogene-induced p16-INK4A activation. Previous results in this study have shown that PRMT6 transcript and protein level were decreased in TIG3 BRAF-ER cells after activation of the oncogene Braf by 4-OHT, while the expression of *p16-INK4A* transcript increased (Figure 23). It has to be analysed, whether at least the reduction of PRMT6 protein level is caused by DDB1-CUL4A ubiquitylation followed by degradation of PRMT6.

A previous study demonstrated that CRL4 also interacts and monoubiquitylates the transcription factor TP73, which is a structural and functional homolog of the tumour suppressor TP53. Thereby, it represses TP73-dependent transcription of target genes, such as *CDKN1A*, *GADD45* and *PUMA*, and apoptosis without affecting its protein stability (Malatesta et al., 2013). *DDB1* depletion as shown by Malatesta et al. has the same effect on CDKN1A expression as *PRMT6* depletion in this study (Figure 15, 18). Therefore, it would be interesting to analyse whether PRMT6 is linked to this DDB1-CUL4A-mediated ubiquitylation of TP73 and its subsequent repression of for example *CDKN1A* as a TP73-target gene.

In this study, IPs were performed by immunoprecipitation of PRMT6 from MCF7 cell extracts and subsequent immunostaining of the interaction partner. In order to

strengthen these data, further endogenous or inverse CoIPs of PRMT6 and the CRL4 components could be performed in the future to analyse if the specific interactor also immunoprecipitates PRMT6. In addition, further experiments have to clarify whether these novel interactors of PRMT6 are substrates of PRMT6 and whether they co-regulate the biological function of PRMT6 or vice versa. Therefore, *in vitro* methyltransferase assays and *in vivo* labelings could answer the question whether already confirmed interactors are substrates of PRMT6. It should be clarified whether these are direct or indirect interactions by performing GST pulldown assays with recombinant proteins expressed in bacteria. If these are direct interactions, the use of deletion mutants could help to map the interaction domains in PRMT6 and its interaction partners.

6.3.2 Validation of additional PRMT6 interaction partners

Previous studies in our group already confirmed the interaction between PRMT6 and several other putative interaction partners by semi-endogenous and endogenous Co-IPs in MCF7 cells found in our MS/MS analysis (bachelor thesis, Lisa Schubert). It was possible to verify the interaction between PRMT6 and the transcription factors ILF2 and ILF3. The heterodimeric complex of ILF2 and ILF3 was first described to be required for transcriptional regulation of the IL-2 (interleukin-2) gene during T-cell activation (Corthésy and Kao, 1994; Kao et al., 1994). Interestingly, ILF2 was identified as an asymmetrically dimethylated protein in a proteomic screen (Boisvert et al., 2003) and ILF3 as an interactor of PRMT1 in mammalian cells (Tang et al., 2000b). It would be interesting to analyse whether PRMT6 methylates ILF2 and/or ILF3, presumably in its RGG (arginine-glycine-glycine) motif at the C-terminus. Moreover, ILF3 possesses a double-stranded RNA binding motif (dsRBM) (Fierro-Monti and Mathews, 2000) and thereby controls the mRNA turnover of several genes, such as IL-2 or the PRMT6-target gene CDKN1A (Shi et al., 2005; Shim et al., 2002).

Furthermore, the interaction of PRMT6 with the histone-binding protein RBBP7 (RbAp46) has previously been confirmed in our group. Similarly, PRMT6 interacts with

its homolog RBBP4 (RbAp48). RbAp46/48 (retinoblastoma-associated protein 46/48) are components of several chromatin-related complexes, such as the NuRD (nucleosome remodeling and deacetylase), PRC2 or the Sin3 complex (Loyola and Almouzni, 2004; Philpott et al., 2000). PRMT6 does not possess a DNA binding domain and therefore RbAp46/48, as well as the already mentioned transcription factors ILF2 or ILF3, could recruit PRMT6 to further specific chromatin regions.

Further CoIP studies demonstrated that PRMT6 also associates with AURKB, which is a key regulator of mitosis and participates in microtubule-kinetochore attachment, spindle checkpoint and cytokinesis (Fu et al., 2007). Future studies could unravel whether AURKB is a substrate of PRMT6 and whether PRMT6 is implicated in the regulation of mitosis as another process in the cell cycle.

6.3.3 Further putative interaction partners and functions of PRMT6

Future experiments should be performed to validate the interaction between PRMT6 with further putative interaction partners to get a better insight of PRMT6 in the regulation of important cell signal pathways and its role in human cancer. For example, the nuclear RNA-binding protein TAF15, that is a component of a distinct population of TFIID and RNA polymerase II complexes (Jobert et al., 2009), was identified as a putative interaction partner of PRMT6 within our MS/MS analysis. TAF15 is already linked to arginine methylation and could be a further substrate of PRMT6. A previous study demonstrated that TAF15 is arginine methylated at several RGG repeats in its C-terminus by PRMT1 (Jobert et al., 2009). This methylation is important for subcellular localisation of TAF15 and thereby for the regulation of TAF15 target genes in a positive manner. Further experiments have to clarify whether PRMT6 also interacts with TAF15, whether it methylates TAF15 and whether methylation of TAF15 influences its function as demonstrated for PRMT1.

In addition, the metabolic proteins ATP5B (ATP synthase subunit beta, mitochondrial), K6PP (6-phosphofructokinase type C), PGAM5 (phosphoglycerate mutase family

member 5) and HK1 (hexokinase 1) were also identified in our unbiased MS/MS approach (PhD thesis, Claudia Stein). In this context, a previous MS/MS analysis from Han´s laboratory has demonstrated that PRMT6 associates with CRTC2 (CREB-regulated transcriptional coactivator 2) in 293T cells, which was then confirmed by CoIP studies. Here, PRMT6 is involved in the regulation of hepatic glucose metabolism in a CRTC2-dependent manner (Han et al., 2014). Therefore, the interaction between PRMT6 and the putative interaction candidates from our analysis has to be verified in the future. If that is the case, PRMT6 would be linked to further novel functions in metabolic processes.

Interestingly, Lo Sardo and colleagues performed a yeast two-hybrid (Y2H) assay using full length PRMT6 as bait with a similar aim to identify novel interaction partners and putative substrates of PRMT6 (Lo Sardo et al., 2013). However, the comparison of their screen results with our MS/MS data set revealed no overlap in putative interaction partners of PRMT6 possibly due to the fact that different cell systems and methods were used. Among their 36 new putative interaction partners of PRMT6, they could validate the interaction of PRMT6 with hnRNP Q (heterogeneous nuclear ribonucleoprotein Q) in a GST-pulldown experiment, but not in a co-affinity purification (co-AP) in HEK293T cells. In comparison, we also could identify several hnRNPs (HNRNPUL2, HNRNPM, HNRNPG, HNRNPH1, HNRNPC and HNRNPF) as putative interaction partners of PRMT6 implying a role of PRMT6 in mRNA processing mechanisms.

7 REFERENCES

Abbas, T., and Dutta, A. (2009). p21 in cancer: intricate networks and multiple activities. Nat. Rev. Cancer *9*, 400–414.

Abbas, T., Sivaprasad, U., Terai, K., Amador, V., Pagano, M., and Dutta, A. (2008). PCNA-dependent regulation of p21 ubiquitylation and degradation via the CRL4Cdt2 ubiquitin ligase complex. Genes Dev. *22*, 2496–2506.

Agger, K., Cloos, P.A.C., Rudkjaer, L., Williams, K., Andersen, G., Christensen, J., and Helin, K. (2009). The H3K27me3 demethylase JMJD3 contributes to the activation of the INK4A-ARF locus in response to oncogene- and stress-induced senescence. Genes Dev. *23*, 1171–1176.

Antonysamy, S., Bonday, Z., Campbell, R.M., Doyle, B., Druzina, Z., Gheyi, T., Han, B., Jungheim, L.N., Qian, Y., Rauch, C., et al. (2012). Crystal structure of the human PRMT5:MEP50 complex. Proc. Natl. Acad. Sci. U. S. A. *109*, 17960–17965.

Arias, E.E., and Walter, J.C. (2006). PCNA functions as a molecular platform to trigger Cdt1 destruction and prevent re-replication. Nat. Cell Biol. *8*, 84–90.

Baldwin, R.M., Morettin, A., and Côté, J. (2014). Role of PRMTs in cancer: Could minor isoforms be leaving a mark? World J. Biol. Chem. *5*, 115–129.

Bedford, M.T., and Clarke, S.G. (2009). Protein arginine methylation in mammals: who, what, and why. Mol. Cell *33*, 1–13.

Bedford, M.T., and Richard, S. (2005). Arginine methylation an emerging regulator of protein function. Mol. Cell *18*, 263–272.

Ben-Porath, I., and Weinberg, R.A. (2005). The signals and pathways activating cellular senescence. Int. J. Biochem. Cell Biol. *37*, 961–976.

Berthet, C., Guéhenneux, F., Revol, V., Samarut, C., Lukaszewicz, A., Dehay, C., Dumontet, C., Magaud, J.-P., and Rouault, J.-P. (2002). Interaction of PRMT1 with BTG/TOB proteins in cell signalling: molecular analysis and functional aspects. Genes Cells *7*, 29–39.

Bevilacqua, M.A., Iovine, B., Zambrano, N., D'Ambrosio, C., Scaloni, A., Russo, T., and Cimino, F. (2005). Fibromodulin gene transcription is induced by ultraviolet irradiation, and its regulation is impaired in senescent human fibroblasts. J. Biol. Chem. *280*, 31809–31817.

Bhaumik, S.R., Smith, E., and Shilatifard, A. (2007). Covalent modifications of histones during development and disease pathogenesis. Nat. Struct. Mol. Biol. *14*, 1008–1016.

Bodnar, A.G., Ouellette, M., Frolkis, M., Holt, S.E., Chiu, C.P., Morin, G.B., Harley, C.B., Shay, J.W., Lichtsteiner, S., and Wright, W.E. (1998). Extension of life-span by introduction of telomerase into normal human cells. Science *279*, 349–352.

Boffa, L.C., Karn, J., Vidali, G., and Allfrey, V.G. (1977). Distribution of NG, NG,-dimethylarginine in nuclear protein fractions. Biochem. Biophys. Res. Commun. *74*, 969–976.

Boisvert, F.-M., Côté, J., Boulanger, M.-C., and Richard, S. (2003). A proteomic analysis of arginine-methylated protein complexes. Mol. Cell. Proteomics *2*, 1319–1330.

Boisvert, F.-M., Chénard, C.A., and Richard, S. (2005). Protein interfaces in signaling regulated by arginine methylation. Sci. STKE *2005*, re2.

Boulanger, M.-C., Miranda, T.B., Clarke, S., Di Fruscio, M., Suter, B., Lasko, P., and Richard, S. (2004). Characterization of the Drosophila protein arginine methyltransferases DART1 and DART4. Biochem. J. *379*, 283–289.

Boulanger, M.-C., Liang, C., Russell, R.S., Lin, R., Bedford, M.T., Wainberg, M.A., and Richard, S. (2005). Methylation of Tat by PRMT6 regulates human immunodeficiency virus type 1 gene expression. J. Virol. *79*, 124–131.

Bracken, A.P., Kleine-Kohlbrecher, D., Dietrich, N., Pasini, D., Gargiulo, G., Beekman, C., Theilgaard-Mönch, K., Minucci, S., Porse, B.T., Marine, J.-C., et al. (2007). The Polycomb group proteins bind throughout the INK4A-ARF locus and are disassociated in senescent cells. Genes Dev. *21*, 525–530.

Bradford, M.M. (1976). A rapid and sensitive method for the quantitation of microgram quantities of protein utilizing the principle of protein-dye binding. Anal. Biochem. *72*, 248–254.

Brenner, C., Deplus, R., Didelot, C., Loriot, A., Viré, E., De Smet, C., Gutierrez, A., Danovi, D., Bernard, D., Boon, T., et al. (2005). Myc represses transcription through recruitment of DNA methyltransferase corepressor. EMBO J. *24*, 336–346.

Brugarolas, J., Chandrasekaran, C., Gordon, J.I., Beach, D., Jacks, T., and Hannon, G.J. (1995). Radiation-induced cell cycle arrest compromised by p21 deficiency. Nature *377*, 552–557.

Brummelkamp, T.R., Bernards, R., and Agami, R. (2002). Stable suppression of tumorigenicity by virus-mediated RNA interference. Cancer Cell *2*, 243–247.

Campisi, J., and d'Adda di Fagagna, F. (2007). Cellular senescence: when bad things happen to good cells. Nat. Rev. Mol. Cell Biol. *8*, 729–740.

Cao, R., and Zhang, Y. (2004). The functions of E(Z)/EZH2-mediated methylation of lysine 27 in histone H3. Curr. Opin. Genet. Dev. *14*, 155–164.

Cao, R., Wang, L., Wang, H., Xia, L., Erdjument-Bromage, H., Tempst, P., Jones, R.S., and Zhang, Y. (2002). Role of histone H3 lysine 27 methylation in Polycomb-group silencing. Science *298*, 1039–1043.

Cardozo, T., and Pagano, M. (2004). The SCF ubiquitin ligase: insights into a molecular machine. Nat. Rev. Mol. Cell Biol. *5*, 739–751.

Casadio, F., Lu, X., Pollock, S.B., LeRoy, G., Garcia, B.A., Muir, T.W., Roeder, R.G., and Allis, C.D. (2013). H3R42me2a is a histone modification with positive transcriptional effects. Proc. Natl. Acad. Sci. U. S. A. *110*, 14894–14899.

Cha, B., and Jho, E.-H. (2012). Protein arginine methyltransferases (PRMTs) as therapeutic targets. Expert Opin. Ther. Targets *16*, 651–664.

Chang, B., Chen, Y., Zhao, Y., and Bruick, R.K. (2007). JMJD6 is a histone arginine demethylase. Science *318*, 444–447.

Chen, L.C., Manjeshwar, S., Lu, Y., Moore, D., Ljung, B.M., Kuo, W.L., Dairkee, S.H., Wernick, M., Collins, C., and Smith, H.S. (1998). The human homologue for the Caenorhabditis elegans cul-4 gene is amplified and overexpressed in primary breast cancers. Cancer Res. *58*, 3677–3683.

Chen, Q.M., Prowse, K.R., Tu, V.C., Purdom, S., and Linskens, M.H. (2001a). Uncoupling the senescent phenotype from telomere shortening in hydrogen peroxide-treated fibroblasts. Exp. Cell Res. *265*, 294–303.

Chen, X., Zhang, Y., Douglas, L., and Zhou, P. (2001b). UV-damaged DNA-binding proteins are targets of CUL-4A-mediated ubiquitination and degradation. J. Biol. Chem. *276*, 48175–48182.

Cheng, X., and Roberts, R.J. (2001). AdoMet-dependent methylation, DNA methyltransferases and base flipping. Nucleic Acids Res. *29*, 3784–3795.

Cheng, Y., Frazier, M., Lu, F., Cao, X., and Redinbo, M.R. (2011). Crystal structure of the plant epigenetic protein arginine methyltransferase 10. J. Mol. Biol. *414*, 106–122.

Cook, J.R., Lee, J.-H., Yang, Z.-H., Krause, C.D., Herth, N., Hoffmann, R., and Pestka, S. (2006). FBXO11/PRMT9, a new protein arginine methyltransferase, symmetrically dimethylates arginine residues. Biochem. Biophys. Res. Commun. *342*, 472–481.

Corthésy, B., and Kao, P.N. (1994). Purification by DNA affinity chromatography of two polypeptides that contact the NF-AT DNA binding site in the interleukin 2 promoter. J. Biol. Chem. *269*, 20682–20690.

Côté, J., Boisvert, F.-M., Boulanger, M.-C., Bedford, M.T., and Richard, S. (2003). Sam68 RNA binding protein is an in vivo substrate for protein arginine N-methyltransferase 1. Mol. Biol. Cell *14*, 274–287.

Couture, J.-F., Collazo, E., and Trievel, R.C. (2006). Molecular recognition of histone H3 by the WD40 protein WDR5. Nat. Struct. Mol. Biol. *13*, 698–703.

Cura, V., Troffer-Charlier, N., Wurtz, J.M., Bonnefond, L., and Cavarelli, J. (2014). Structural insight into arginine methylation by the mouse protein arginine methyltransferase 7: a zinc finger freezes the mimic of the dimeric state into a single active site. Acta Crystallogr. D. Biol. Crystallogr. *70*, 2401–2412.

Cuthbert, G.L., Daujat, S., Snowden, A.W., Erdjument-Bromage, H., Hagiwara, T., Yamada, M., Schneider, R., Gregory, P.D., Tempst, P., Bannister, A.J., et al. (2004). Histone deimination antagonizes arginine methylation. Cell *118*, 545–553.

d'Adda di Fagagna, F., Reaper, P.M., Clay-Farrace, L., Fiegler, H., Carr, P., Von Zglinicki, T., Saretzki, G., Carter, N.P., and Jackson, S.P. (2003). A DNA damage checkpoint response in telomere-initiated senescence. Nature *426*, 194–198.

Denman, R.B. (2005). PAD: the smoking gun behind arginine methylation signaling? Bioessays *27*, 242–246.

Dhalluin, C., Carlson, J.E., Zeng, L., He, C., Aggarwal, A.K., and Zhou, M.M. (1999). Structure and ligand of a histone acetyltransferase bromodomain. Nature *399*, 491–496.

Dietrich, N., Bracken, A.P., Trinh, E., Schjerling, C.K., Koseki, H., Rappsilber, J., Helin, K., and Hansen, K.H. (2007). Bypass of senescence by the polycomb group protein CBX8 through direct binding to the INK4A-ARF locus. EMBO J. *26*, 1637–1648.

Dimri, G.P., Lee, X., Basile, G., Acosta, M., Scott, G., Roskelley, C., Medrano, E.E., Linskens, M., Rubelj, I., and Pereira-Smith, O. (1995). A biomarker that identifies senescent human cells in culture and in aging skin in vivo. Proc. Natl. Acad. Sci. U. S. A. *92*, 9363–9367.

Dulić, V., Kaufmann, W.K., Wilson, S.J., Tlsty, T.D., Lees, E., Harper, J.W., Elledge, S.J., and Reed, S.I. (1994). p53-dependent inhibition of cyclin-dependent kinase activities in human fibroblasts during radiation-induced G1 arrest. Cell *76*, 1013–1023.

Elakoum, R., Gauchotte, G., Oussalah, A., Wissler, M.-P., Clément-Duchêne, C., Vignaud, J.-M., Guéant, J.-L., and Namour, F. (2014). CARM1 and PRMT1 are dysregulated in lung cancer without hierarchical features. Biochimie *97*, 210–218.

El-Andaloussi, N., Valovka, T., Toueille, M., Steinacher, R., Focke, F., Gehrig, P., Covic, M., Hassa, P.O., Schär, P., Hübscher, U., et al. (2006). Arginine methylation regulates DNA polymerase beta. Mol. Cell *22*, 51–62.

el-Deiry, W.S., Tokino, T., Velculescu, V.E., Levy, D.B., Parsons, R., Trent, J.M., Lin, D., Mercer, W.E., Kinzler, K.W., and Vogelstein, B. (1993). WAF1, a potential mediator of p53 tumor suppression. Cell *75*, 817–825.

El-Mahdy, M.A., Zhu, Q., Wang, Q., Wani, G., Praetorius-Ibba, M., and Wani, A.A. (2006). Cullin 4A-mediated proteolysis of DDB2 protein at DNA damage sites regulates in vivo lesion recognition by XPC. J. Biol. Chem. *281*, 13404–13411.

Essers, J., Theil, A.F., Baldeyron, C., van Cappellen, W.A., Houtsmuller, A.B., Kanaar, R., and Vermeulen, W. (2005). Nuclear dynamics of PCNA in DNA replication and repair. Mol. Cell. Biol. *25*, 9350–9359.

Feng, Q., Yi, P., Wong, J., and O'Malley, B.W. (2006). Signaling within a coactivator complex: methylation of SRC-3/AIB1 is a molecular switch for complex disassembly. Mol. Cell. Biol. *26*, 7846–7857.

Feng, Q., He, B., Jung, S.-Y., Song, Y., Qin, J., Tsai, S.Y., Tsai, M.-J., and O'Malley, B.W. (2009). Biochemical control of CARM1 enzymatic activity by phosphorylation. J. Biol. Chem. *284*, 36167–36174.

Feng, Y., Maity, R., Whitelegge, J.P., Hadjikyriacou, A., Li, Z., Zurita-Lopez, C., Al-Hadid, Q., Clark, A.T., Bedford, M.T., Masson, J.-Y., et al. (2013). Mammalian Protein Arginine Methyltransferase 7 (PRMT7) Specifically Targets RXR Sites in Lysine- and Arginine-rich Regions. J. Biol. Chem. *288*, 37010–37025.

Fennell, M., Xiang, Q., Hwang, A., Chen, C., Huang, C.-H., Chen, C.-C., Pelossof, R., and Garippa, R.J. (2014). Impact of RNA-Guided Technologies for Target Identification and Deconvolution. J. Biomol. Screen.

Fierro-Monti, I., and Mathews, M.B. (2000). Proteins binding to duplexed RNA: one motif, multiple functions. Trends Biochem. Sci. *25*, 241–246.

Finch, J.T., and Klug, A. (1976). Solenoidal model for superstructure in chromatin. Proc. Natl. Acad. Sci. U. S. A. *73*, 1897–1901.

Fisk, J.C., Zurita-Lopez, C., Sayegh, J., Tomasello, D.L., Clarke, S.G., and Read, L.K. (2010). TbPRMT6 is a type I protein arginine methyltransferase that contributes to cytokinesis in Trypanosoma brucei. Eukaryot. Cell *9*, 866–877.

Frankel, A., and Clarke, S. (2000). PRMT3 is a distinct member of the protein arginine N-methyltransferase family. Conferral of substrate specificity by a zinc-finger domain. J. Biol. Chem. *275*, 32974–32982.

Frankel, A., Yadav, N., Lee, J., Branscombe, T.L., Clarke, S., and Bedford, M.T. (2002). The novel human protein arginine N-methyltransferase PRMT6 is a nuclear enzyme displaying unique substrate specificity. J. Biol. Chem. *277*, 3537–3543.

Friesen, W.J., Paushkin, S., Wyce, A., Massenet, S., Pesiridis, G.S., Van Duyne, G., Rappsilber, J., Mann, M., and Dreyfuss, G. (2001). The methylosome, a 20S complex containing JBP1 and pICln, produces dimethylarginine-modified Sm proteins. Mol. Cell. Biol. *21*, 8289–8300.

Friesen, W.J., Wyce, A., Paushkin, S., Abel, L., Rappsilber, J., Mann, M., and Dreyfuss, G. (2002). A novel WD repeat protein component of the methylosome binds Sm proteins. J. Biol. Chem. *277*, 8243–8247.

Fu, J., Bian, M., Jiang, Q., and Zhang, C. (2007). Roles of Aurora kinases in mitosis and tumorigenesis. Mol. Cancer Res. *5*, 1–10.

Fujimoto, K., Matsuura, K., Hu-Wang, E., Lu, R., and Shi, Y.-B. (2012). Thyroid hormone activates protein arginine methyltransferase 1 expression by directly inducing c-Myc transcription during Xenopus intestinal stem cell development. J. Biol. Chem. *287*, 10039–10050.

Gartel, A.L., and Shchors, K. (2003). Mechanisms of c-myc-mediated transcriptional repression of growth arrest genes. Exp. Cell Res. *283*, 17–21.

Goulet, I., Gauvin, G., Boisvenue, S., and Côté, J. (2007). Alternative splicing yields protein arginine methyltransferase 1 isoforms with distinct activity, substrate specificity, and subcellular localization. J. Biol. Chem. *282*, 33009–33021.

Grignani, F., Kinsella, T., Mencarelli, A., Valtieri, M., Riganelli, D., Lanfrancone, L., Peschle, C., Nolan, G.P., and Pelicci, P.G. (1998). High-efficiency gene transfer and selection of human hematopoietic progenitor cells with a hybrid EBV/retroviral vector expressing the green fluorescence protein. Cancer Res. *58*, 14–19.

Gu, Z., Gao, S., Zhang, F., Wang, Z., Ma, W., Davis, R.E., and Wang, Z. (2012). Protein arginine methyltransferase 5 is essential for growth of lung cancer cells. Biochem. J. *446*, 235–241.

Guccione, E., Martinato, F., Finocchiaro, G., Luzi, L., Tizzoni, L., Dall' Olio, V., Zardo, G., Nervi, C., Bernard, L., and Amati, B. (2006). Myc-binding-site recognition in the human genome is determined by chromatin context. Nat. Cell Biol. *8*, 764–770.

Guccione, E., Bassi, C., Casadio, F., Martinato, F., Cesaroni, M., Schuchlautz, H., Lüscher, B., and Amati, B. (2007). Methylation of histone H3R2 by PRMT6 and H3K4 by an MLL complex are mutually exclusive. Nature *449*, 933–937.

Guzmán, C., Bagga, M., Kaur, A., Westermarck, J., and Abankwa, D. (2014). ColonyArea: An ImageJ Plugin to Automatically Quantify Colony Formation in Clonogenic Assays. PLoS One *9*, e92444.

Hahn, P., Wegener, I., Burrells, A., Böse, J., Wolf, A., Erck, C., Butler, D., Schofield, C.J., Böttger, A., and Lengeling, A. (2010). Analysis of Jmjd6 cellular localization and testing for its involvement in histone demethylation. PLoS One *5*, e13769.

Han, H.-S., Jung, C.-Y., Yoon, Y.-S., Choi, S., Choi, D., Kang, G., Park, K.-G., Kim, S.-T., and Koo, S.-H. (2014). Arginine Methylation of CRTC2 Is Critical in the Transcriptional Control of Hepatic Glucose Metabolism. Sci. Signal. *7*, ra19.

Han, Z., Guo, L., Wang, H., Shen, Y., Deng, X.W., and Chai, J. (2006). Structural basis for the specific recognition of methylated histone H3 lysine 4 by the WD-40 protein WDR5. Mol. Cell *22*, 137–144.

Hao, N.-B., Lü, M.-H., Fan, Y.-H., Cao, Y.-L., Zhang, Z.-R., and Yang, S.-M. (2012). Macrophages in tumor microenvironments and the progression of tumors. Clin. Dev. Immunol. *2012*, 948098.

Harrison, M.J., Tang, Y.H., and Dowhan, D.H. (2010). Protein arginine methyltransferase 6 regulates multiple aspects of gene expression. Nucleic Acids Res. *38*, 2201–2216.

Harshman, S.W., Young, N.L., Parthun, M.R., and Freitas, M.A. (2013). H1 histones: current perspectives and challenges. Nucleic Acids Res. *41*, 9593–9609.

Hasegawa, M., Toma-Fukai, S., Kim, J.-D., Fukamizu, A., and Shimizu, T. (2014). Protein arginine methyltransferase 7 has a novel homodimer-like structure formed by tandem repeats. FEBS Lett. *588*, 1942–1948.

Hauser, A.-T., Bissinger, E.-M., Metzger, E., Repenning, A., Bauer, U.-M., Mai, A., Schüle, R., and Jung, M. (2012). Screening assays for epigenetic targets using native histones as substrates. J. Biomol. Screen. *17*, 18–26.

Hayflick, L. (1965). The limited in vitro lifetime of human diploid cell strains. Exp. Cell Res. *37*, 614–636.

Hayflick, L., and Moorhead, P.S. (1961). The serial cultivation of human diploid cell strains. Exp. Cell Res. *25*, 585–621.

Henneke, I., Greschus, S., Savai, R., Korfei, M., Markart, P., Mahavadi, P., Schermuly, R.T., Wygrecka, M., Stürzebecher, J., Seeger, W., et al. (2010). Inhibition of urokinase activity reduces primary tumor growth and metastasis formation in a murine lung carcinoma model. Am. J. Respir. Crit. Care Med. *181*, 611–619.

Herglotz, J., Kuvardina, O.N., Kolodziej, S., Kumar, A., Hussong, H., Grez, M., and Lausen, J. (2013). Histone arginine methylation keeps RUNX1 target genes in an intermediate state. Oncogene *32*, 2565–2575.

Herrmann, F., Lee, J., Bedford, M.T., and Fackelmayer, F.O. (2005). Dynamics of human protein arginine methyltransferase 1(PRMT1) in vivo. J. Biol. Chem. *280*, 38005–38010.

Higashimoto, K., Kuhn, P., Desai, D., Cheng, X., and Xu, W. (2007). Phosphorylation-mediated inactivation of coactivator-associated arginine methyltransferase 1. Proc. Natl. Acad. Sci. U. S. A. *104*, 12318–12323.

Ho, M.-C., Wilczek, C., Bonanno, J.B., Xing, L., Seznec, J., Matsui, T., Carter, L.G., Onikubo, T., Kumar, P.R., Chan, M.K., et al. (2013). Structure of the arginine methyltransferase PRMT5-MEP50 reveals a mechanism for substrate specificity. PLoS One *8*, e57008.

Holbert, M.A., and Marmorstein, R. (2005). Structure and activity of enzymes that remove histone modifications. Curr. Opin. Struct. Biol. *15*, 673–680.

Hong, X., Zang, J., White, J., Wang, C., Pan, C.-H., Zhao, R., Murphy, R.C., Dai, S., Henson, P., Kappler, J.W., et al. (2010). Interaction of JMJD6 with single-stranded RNA. Proc. Natl. Acad. Sci. U. S. A. *107*, 14568–14572.

Hori, T., Osaka, F., Chiba, T., Miyamoto, C., Okabayashi, K., Shimbara, N., Kato, S., and Tanaka, K. (1999). Covalent modification of all members of human cullin family proteins by NEDD8. Oncogene *18*, 6829–6834.

Hughes, C.M., Rozenblatt-Rosen, O., Milne, T.A., Copeland, T.D., Levine, S.S., Lee, J.C., Hayes, D.N., Shanmugam, K.S., Bhattacharjee, A., Biondi, C.A., et al. (2004). Menin associates with a trithorax family histone methyltransferase complex and with the hoxc8 locus. Mol. Cell *13*, 587–597.

Hyllus, D., Stein, C., Schnabel, K., Schiltz, E., Imhof, A., Dou, Y., Hsieh, J., and Bauer, U.-M. (2007). PRMT6-mediated methylation of R2 in histone H3 antagonizes H3 K4 trimethylation. Genes Dev. *21*, 3369–3380.

Iberg, A.N., Espejo, A., Cheng, D., Kim, D., Michaud-Levesque, J., Richard, S., and Bedford, M.T. (2008). Arginine methylation of the histone H3 tail impedes effector binding. J. Biol. Chem. *283*, 3006–3010.

Imhof, A., and Becker, P.B. (2001). Modifications of the histone N-terminal domains. Evidence for an "epigenetic code"? Mol. Biotechnol. *17*, 1–13.

Invernizzi, C.F., Xie, B., Richard, S., and Wainberg, M.A. (2006). PRMT6 diminishes HIV-1 Rev binding to and export of viral RNA. Retrovirology *3*, 93.

Invernizzi, C.F., Xie, B., Frankel, F.A., Feldhammer, M., Roy, B.B., Richard, S., and Wainberg, M.A. (2007). Arginine methylation of the HIV-1 nucleocapsid protein results in its diminished function. AIDS *21*, 795–805.

Iovine, B., Nino, M., Irace, C., Bevilacqua, M.A., and Monfrecola, G. (2009). Ultraviolet B and A irradiation induces fibromodulin expression in human fibroblasts in vitro. Biochimie *91*, 364–372.

Iovine, B., Iannella, M.L., and Bevilacqua, M.A. (2011a). Damage-specific DNA binding protein 1 (DDB1) is involved in ubiquitin-mediated proteolysis of p27Kip1 in response to UV irradiation. Biochimie *93*, 867–875.

Iovine, B., Iannella, M.L., and Bevilacqua, M.A. (2011b). Damage-specific DNA binding protein 1 (DDB1): a protein with a wide range of functions. Int. J. Biochem. Cell Biol. *43*, 1664–1667.

Jackson, S., and Xiong, Y. (2009). CRL4s: the CUL4-RING E3 ubiquitin ligases. Trends Biochem. Sci. *34*, 562–570.

Jacobs, J.J., Kieboom, K., Marino, S., DePinho, R.A., and van Lohuizen, M. (1999). The oncogene and Polycomb-group gene bmi-1 regulates cell proliferation and senescence through the ink4a locus. Nature *397*, 164–168.

James, T.C., and Elgin, S.C. (1986). Identification of a nonhistone chromosomal protein associated with heterochromatin in Drosophila melanogaster and its gene. Mol. Cell. Biol. *6*, 3862–3872.

Jenuwein, T., and Allis, C.D. (2001). Translating the histone code. Science *293*, 1074–1080.

Jobert, L., Argentini, M., and Tora, L. (2009). PRMT1 mediated methylation of TAF15 is required for its positive gene regulatory function. Exp. Cell Res. *315*, 1273–1286.

Johnson, L., Mercer, K., Greenbaum, D., Bronson, R.T., Crowley, D., Tuveson, D.A., and Jacks, T. (2001). Somatic activation of the K-ras oncogene causes early onset lung cancer in mice. Nature *410*, 1111–1116.

Kao, P.N., Chen, L., Brock, G., Ng, J., Kenny, J., Smith, A.J., and Corthésy, B. (1994). Cloning and expression of cyclosporin A- and FK506-sensitive nuclear factor of activated T-cells: NF45 and NF90. J. Biol. Chem. *269*, 20691–20699.

Kapetanaki, M.G., Guerrero-Santoro, J., Bisi, D.C., Hsieh, C.L., Rapić-Otrin, V., and Levine, A.S. (2006). The DDB1-CUL4ADDB2 ubiquitin ligase is deficient in xeroderma pigmentosum group E and targets histone H2A at UV-damaged DNA sites. Proc. Natl. Acad. Sci. U. S. A. *103*, 2588–2593.

Kim, C., Lim, Y., Yoo, B.C., Won, N.H., Kim, S., and Kim, G. (2010). Regulation of post-translational protein arginine methylation during HeLa cell cycle. Biochim. Biophys. Acta *1800*, 977–985.

Kim, Y., Starostina, N.G., and Kipreos, E.T. (2008). The CRL4Cdt2 ubiquitin ligase targets the degradation of p21Cip1 to control replication licensing. Genes Dev. *22*, 2507–2519.

Kleinschmidt, M.A., de Graaf, P., van Teeffelen, H.A.A.M., and Timmers, H.T.M. (2012). Cell cycle regulation by the PRMT6 arginine methyltransferase through repression of cyclin-dependent kinase inhibitors. PLoS One *7*, e41446.

Kodama, J., Hashimoto, I., Seki, N., Hongo, A., Yoshinouchi, M., Okuda, H., and Kudo, T. (2001). Thrombospondin-1 and -2 messenger RNA expression in invasive cervical cancer: correlation with angiogenesis and prognosis. Clin. Cancer Res. *7*, 2826–2831.

Kotake, Y., Zeng, Y., and Xiong, Y. (2009). DDB1-CUL4 and MLL1 mediate oncogene-induced p16INK4a activation. Cancer Res. *69*, 1809–1814.

Kousaka, A., Mori, Y., Koyama, Y., Taneda, T., Miyata, S., and Tohyama, M. (2009). The distribution and characterization of endogenous protein arginine N-methyltransferase 8 in mouse CNS. Neuroscience *163*, 1146–1157.

Kouzarides, T. (2007). Chromatin modifications and their function. Cell *128*, 693–705.

Kuhn, P., Chumanov, R., Wang, Y., Ge, Y., Burgess, R.R., and Xu, W. (2011). Automethylation of CARM1 allows coupling of transcription and mRNA splicing. Nucleic Acids Res. *39*, 2717–2726.

Kuilman, T., Michaloglou, C., Mooi, W.J., and Peeper, D.S. (2010). The essence of senescence. Genes Dev. *24*, 2463–2479.

Kzhyshkowska, J., Schütt, H., Liss, M., Kremmer, E., Stauber, R., Wolf, H., and Dobner, T. (2001). Heterogeneous nuclear ribonucleoprotein E1B-AP5 is methylated in its Arg-Gly-Gly (RGG) box and interacts with human arginine methyltransferase HRMT1L1. Biochem. J. *358*, 305–314.

Lacroix, M., El Messaoudi, S., Rodier, G., Le Cam, A., Sardet, C., and Fabbrizio, E. (2008). The histone-binding protein COPR5 is required for nuclear functions of the protein arginine methyltransferase PRMT5. EMBO Rep. *9*, 452–458.

Lakowski, T.M., and Frankel, A. (2008). A kinetic study of human protein arginine N-methyltransferase 6 reveals a distributive mechanism. J. Biol. Chem. *283*, 10015–10025.

Lamond, A.I., and Earnshaw, W.C. (1998). Structure and function in the nucleus. Science *280*, 547–553.

Lanigan, F., Geraghty, J.G., and Bracken, A.P. (2011). Transcriptional regulation of cellular senescence. Oncogene *30*, 2901–2911.

Lee, J., and Zhou, P. (2007). DCAFs, the missing link of the CUL4-DDB1 ubiquitin ligase. Mol. Cell *26*, 775–780.

Lee, Y.-H., and Stallcup, M.R. (2009). Minireview: protein arginine methylation of nonhistone proteins in transcriptional regulation. Mol. Endocrinol. *23*, 425–433.

Lee, D.Y., Teyssier, C., Strahl, B.D., and Stallcup, M.R. (2005a). Role of protein methylation in regulation of transcription. Endocr. Rev. *26*, 147–170.

Lee, J., Sayegh, J., Daniel, J., Clarke, S., and Bedford, M.T. (2005b). PRMT8, a new membrane-bound tissue-specific member of the protein arginine methyltransferase family. J. Biol. Chem. *280*, 32890–32896.

Li, B., Carey, M., and Workman, J.L. (2007). The role of chromatin during transcription. Cell *128*, 707–719.

Lim, J.-H., Choi, Y.-J., Cho, C.-H., and Park, J.-W. (2012). Protein arginine methyltransferase 5 is an essential component of the hypoxia-inducible factor 1 signaling pathway.

Lim, Y., Lee, E., Lee, J., Oh, S., and Kim, S. (2008). Down-regulation of asymmetric arginine methylation during replicative and H2O2-induced premature senescence in WI-38 human diploid fibroblasts. J. Biochem. *144*, 523–529.

Lin, W.J., Gary, J.D., Yang, M.C., Clarke, S., and Herschman, H.R. (1996). The mammalian immediate-early TIS21 protein and the leukemia-associated BTG1 protein interact with a protein-arginine N-methyltransferase. J. Biol. Chem. *271*, 15034–15044.

Liu, Q., and Dreyfuss, G. (1995). In vivo and in vitro arginine methylation of RNA-binding proteins. Mol. Cell. Biol. *15*, 2800–2808.

Lloyd, C.M., Phillips, A.R.J., Cooper, G.J.S., and Dunbar, P.R. (2008). Three-colour fluorescence immunohistochemistry reveals the diversity of cells staining for macrophage markers in murine spleen and liver. J. Immunol. Methods *334*, 70–81.

Lorenzo, A. Di, Yang, Y., Macaluso, M., and Bedford, M.T. (2014). A gain-of-function mouse model identifies PRMT6 as a NF-κB coactivator. Nucleic Acids Res.

Di Lorenzo, A., and Bedford, M.T. (2011). Histone arginine methylation. FEBS Lett. *585*, 2024–2031.

Loyola, A., and Almouzni, G. (2004). Histone chaperones, a supporting role in the limelight. Biochim. Biophys. Acta *1677*, 3–11.

Luger, K., Mäder, A.W., Richmond, R.K., Sargent, D.F., and Richmond, T.J. (1997). Crystal structure of the nucleosome core particle at 2.8 A resolution. Nature *389*, 251–260.

Ma, J., Liu, L., Che, G., Yu, N., Dai, F., and You, Z. (2010). The M1 form of tumor-associated macrophages in non-small cell lung cancer is positively associated with survival time. BMC Cancer *10*, 112.

Malatesta, M., Peschiaroli, A., Memmi, E.M., Zhang, J., Antonov, A., Green, D.R., Barlev, N.A., Garabadgiu, A. V, Zhou, P., Melino, G., et al. (2013). The Cul4A-DDB1 E3 ubiquitin ligase complex represses p73 transcriptional activity. Oncogene *32*, 4721–4726.

Mali, P., Esvelt, K.M., and Church, G.M. (2013). Cas9 as a versatile tool for engineering biology. Nat. Methods *10*, 957–963.

Malumbres, M., and Barbacid, M. (2005). Mammalian cyclin-dependent kinases. Trends Biochem. Sci. *30*, 630–641.

Mantri, M., Krojer, T., Bagg, E.A., Webby, C.A., Butler, D.S., Kochan, G., Kavanagh, K.L., Oppermann, U., McDonough, M.A., and Schofield, C.J. (2010). Crystal Structure of the 2-Oxoglutarate- and Fe(II)-Dependent Lysyl Hydroxylase JMJD6. J. Mol. Biol.

Mariño-Ramírez, L., Kann, M.G., Shoemaker, B.A., and Landsman, D. (2005). Histone structure and nucleosome stability. Expert Rev. Proteomics *2*, 719–729.

Maurer-Stroh, S., Dickens, N.J., Hughes-Davies, L., Kouzarides, T., Eisenhaber, F., and Ponting, C.P. (2003). The Tudor domain "Royal Family": Tudor, plant Agenet, Chromo, PWWP and MBT domains. Trends Biochem. Sci. *28*, 69–74.

Michaloglou, C., Vredeveld, L.C.W., Soengas, M.S., Denoyelle, C., Kuilman, T., van der Horst, C.M.A.M., Majoor, D.M., Shay, J.W., Mooi, W.J., and Peeper, D.S. (2005). BRAFE600-associated senescence-like cell cycle arrest of human naevi. Nature *436*, 720–724.

Michaud-Levesque, J., and Richard, S. (2009). Thrombospondin-1 is a transcriptional repression target of PRMT6. J. Biol. Chem. *284*, 21338–21346.

Migliori, V., Müller, J., Phalke, S., Low, D., Bezzi, M., Mok, W.C., Sahu, S.K., Gunaratne, J., Capasso, P., Bassi, C., et al. (2012). Symmetric dimethylation of H3R2 is a newly identified histone mark that supports euchromatin maintenance. Nat. Struct. Mol. Biol. *19*, 136–144.

Miller, C.W., Aslo, A., Campbell, M.J., Kawamata, N., Lampkin, B.C., and Koeffler, H.P. (1996). Alterations of the p15, p16,and p18 genes in osteosarcoma. Cancer Genet. Cytogenet. *86*, 136–142.

Milne, T.A., Briggs, S.D., Brock, H.W., Martin, M.E., Gibbs, D., Allis, C.D., and Hess, J.L. (2002). MLL targets SET domain methyltransferase activity to Hox gene promoters. Mol. Cell *10*, 1107–1117.

Miranda, T.B., Miranda, M., Frankel, A., and Clarke, S. (2004). PRMT7 is a member of the protein arginine methyltransferase family with a distinct substrate specificity. J. Biol. Chem. *279*, 22902–22907.

Miranda, T.B., Webb, K.J., Edberg, D.D., Reeves, R., and Clarke, S. (2005). Protein arginine methyltransferase 6 specifically methylates the nonhistone chromatin protein HMGA1a. Biochem. Biophys. Res. Commun. *336*, 831–835.

Mirsadraee, S., Oswal, D., Alizadeh, Y., Caulo, A., and van Beek, E. (2012). The 7th lung cancer TNM classification and staging system: Review of the changes and implications. World J. Radiol. *4*, 128–134.

Mise, N., Savai, R., Yu, H., Schwarz, J., Kaminski, N., and Eickelberg, O. (2012). Zyxin is a transforming growth factor-β (TGF-β)/Smad3 target gene that regulates lung cancer cell motility via integrin α5β1. J. Biol. Chem. *287*, 31393–31405.

Motegi, A., Sood, R., Moinova, H., Markowitz, S.D., Liu, P.P., and Myung, K. (2006). Human SHPRH suppresses genomic instability through proliferating cell nuclear antigen polyubiquitination. J. Cell Biol. *175*, 703–708.

Muramatsu, D., Singh, P.B., Kimura, H., Tachibana, M., and Shinkai, Y. (2013). Pericentric heterochromatin generated by HP1 protein interaction-defective histone methyltransferase Suv39h1. J. Biol. Chem. *288*, 25285–25296.

Naeem, H., Cheng, D., Zhao, Q., Underhill, C., Tini, M., Bedford, M.T., and Torchia, J. (2007). The activity and stability of the transcriptional coactivator p/CIP/SRC-3 are regulated by CARM1-dependent methylation. Mol. Cell. Biol. *27*, 120–134.

Nag, A., Bondar, T., Shiv, S., and Raychaudhuri, P. (2001). The xeroderma pigmentosum group E gene product DDB2 is a specific target of cullin 4A in mammalian cells. Mol. Cell. Biol. *21*, 6738–6747.

Najbauer, J., Johnson, B.A., Young, A.L., and Aswad, D.W. (1993). Peptides with sequences similar to glycine, arginine-rich motifs in proteins interacting with RNA are efficiently recognized by methyltransferase(s) modifying arginine in numerous proteins. J. Biol. Chem. *268*, 10501–10509.

Narita, M., Nũnez, S., Heard, E., Narita, M., Lin, A.W., Hearn, S.A., Spector, D.L., Hannon, G.J., and Lowe, S.W. (2003). Rb-mediated heterochromatin formation and silencing of E2F target genes during cellular senescence. Cell *113*, 703–716.

Neault, M., Mallette, F.A., Vogel, G., Michaud-Levesque, J., and Richard, S. (2012). Ablation of PRMT6 reveals a role as a negative transcriptional regulator of the p53 tumor suppressor. Nucleic Acids Res. *40*, 9513–9521.

Nishitani, H., Shiomi, Y., Iida, H., Michishita, M., Takami, T., and Tsurimoto, T. (2008). CDK inhibitor p21 is degraded by a proliferating cell nuclear antigen-coupled Cul4-DDB1Cdt2 pathway during S phase and after UV irradiation. J. Biol. Chem. *283*, 29045–29052.

O'Brien, K.B., Alberich-Jordà, M., Yadav, N., Kocher, O., Diruscio, A., Ebralidze, A., Levantini, E., Sng, N.J.L., Bhasin, M., Caron, T., et al. (2010). CARM1 is required for proper control of proliferation and differentiation of pulmonary epithelial cells. Development *137*, 2147–2156.

Paik, W.K., and Kim, S. (1967). Enzymatic methylation of protein fractions from calf thymus nuclei. Biochem. Biophys. Res. Commun. *29*, 14–20.

Paik, W.K., and Kim, S. (1968). Protein methylase I. Purification and properties of the enzyme. J. Biol. Chem. *243*, 2108–2114.

Pak, M.L., Lakowski, T.M., Thomas, D., Vhuiyan, M.I., Hüsecken, K., and Frankel, A. (2011). A protein arginine N-methyltransferase 1 (PRMT1) and 2 heteromeric interaction increases PRMT1 enzymatic activity. Biochemistry *50*, 8226–8240.

Pal, S., and Sif, S. (2007). Interplay between chromatin remodelers and protein arginine methyltransferases. J. Cell. Physiol. *213*, 306–315.

Pal, S., Vishwanath, S.N., Erdjument-Bromage, H., Tempst, P., and Sif, S. (2004). Human SWI/SNF-associated PRMT5 methylates histone H3 arginine 8 and negatively regulates expression of ST7 and NM23 tumor suppressor genes. Mol. Cell. Biol. *24*, 9630–9645.

Park, Y.-B., Park, M.J., Kimura, K., Shimizu, K., Lee, S.H., and Yokota, J. (2002). Alterations in the INK4a/ARF locus and their effects on the growth of human osteosarcoma cell lines. Cancer Genet. Cytogenet. *133*, 105–111.

Parrinello, S., Samper, E., Krtolica, A., Goldstein, J., Melov, S., and Campisi, J. (2003). Oxygen sensitivity severely limits the replicative lifespan of murine fibroblasts. Nat. Cell Biol. *5*, 741–747.

Passeri, D., Marcucci, A., Rizzo, G., Billi, M., Panigada, M., Leonardi, L., Tirone, F., and Grignani, F. (2006). Btg2 enhances retinoic acid-induced differentiation by modulating histone H4 methylation and acetylation. Mol. Cell. Biol. *26*, 5023–5032.

Phalke, S., Mzoughi, S., Bezzi, M., Jennifer, N., Mok, W.C., Low, D.H.P., Thike, A.A., Kuznetsov, V.A., Tan, P.H., Voorhoeve, P.M., et al. (2012). p53-Independent regulation of p21Waf1/Cip1 expression and senescence by PRMT6. Nucleic Acids Res. *40*, 9534–9542.

Philpott, A., Krude, T., and Laskey, R.A. (2000). Nuclear chaperones. Semin. Cell Dev. Biol. *11*, 7–14.

Poon, R.T., Chung, K.K., Cheung, S.T., Lau, C.P., Tong, S.W., Leung, K.L., Yu, W.C., Tuszynski, G.P., and Fan, S.T. (2004). Clinical significance of thrombospondin 1 expression in hepatocellular carcinoma. Clin. Cancer Res. *10*, 4150–4157.

Prieur, A., and Peeper, D.S. (2008). Cellular senescence in vivo: a barrier to tumorigenesis. Curr. Opin. Cell Biol. *20*, 150–155.

Quatromoni, J.G., and Eruslanov, E. (2012). Tumor-associated macrophages: function, phenotype, and link to prognosis in human lung cancer. Am. J. Transl. Res. *4*, 376–389.

Ramalingam, S.S., Owonikoko, T.K., and Khuri, F.R. (2011). Lung cancer: New biological insights and recent therapeutic advances. CA. Cancer J. Clin. *61*, 91–112.

Rathert, P., Dhayalan, A., Murakami, M., Zhang, X., Tamas, R., Jurkowska, R., Komatsu, Y., Shinkai, Y., Cheng, X., and Jeltsch, A. (2008). Protein lysine methyltransferase G9a acts on non-histone targets. Nat. Chem. Biol. *4*, 344–346.

Robin-Lespinasse, Y., Sentis, S., Kolytcheff, C., Rostan, M.-C., Corbo, L., and Le Romancer, M. (2007). hCAF1, a new regulator of PRMT1-dependent arginine methylation. J. Cell Sci. *120*, 638–647.

Rothbart, S.B., and Strahl, B.D. (2014). Interpreting the language of histone and DNA modifications. Biochim. Biophys. Acta *1839*, 627–643.

Ruthenburg, A.J., Wang, W., Graybosch, D.M., Li, H., Allis, C.D., Patel, D.J., and Verdine, G.L. (2006). Histone H3 recognition and presentation by the WDR5 module of the MLL1 complex. Nat. Struct. Mol. Biol. *13*, 704–712.

Sakamaki, J., Daitoku, H., Ueno, K., Hagiwara, A., Yamagata, K., and Fukamizu, A. (2011). Arginine methylation of BCL-2 antagonist of cell death (BAD) counteracts its phosphorylation and inactivation by Akt. Proc. Natl. Acad. Sci. U. S. A. *108*, 6085–6090.

Lo Sardo, A., Altamura, S., Pegoraro, S., Maurizio, E., Sgarra, R., and Manfioletti, G. (2013). Identification and characterization of new molecular partners for the protein arginine methyltransferase 6 (PRMT6). PLoS One *8*, e53750.

Sayegh, J., Webb, K., Cheng, D., Bedford, M.T., and Clarke, S.G. (2007). Regulation of protein arginine methyltransferase 8 (PRMT8) activity by its N-terminal domain. J. Biol. Chem. *282*, 36444–36453.

Schuetz, A., Allali-Hassani, A., Martín, F., Loppnau, P., Vedadi, M., Bochkarev, A., Plotnikov, A.N., Arrowsmith, C.H., and Min, J. (2006). Structural basis for molecular recognition and presentation of histone H3 by WDR5. EMBO J. *25*, 4245–4252.

Scrima, A., Konícková, R., Czyzewski, B.K., Kawasaki, Y., Jeffrey, P.D., Groisman, R., Nakatani, Y., Iwai, S., Pavletich, N.P., and Thomä, N.H. (2008). Structural basis of UV DNA-damage recognition by the DDB1-DDB2 complex. Cell *135*, 1213–1223.

Seet, B.T., Dikic, I., Zhou, M.-M., and Pawson, T. (2006). Reading protein modifications with interaction domains. Nat. Rev. Mol. Cell Biol. *7*, 473–483.

Senga, T., Sivaprasad, U., Zhu, W., Park, J.H., Arias, E.E., Walter, J.C., and Dutta, A. (2006). PCNA is a cofactor for Cdt1 degradation by CUL4/DDB1-mediated N-terminal ubiquitination. J. Biol. Chem. *281*, 6246–6252.

Serrano, M., and Blasco, M.A. (2007). Cancer and ageing: convergent and divergent mechanisms. Nat. Rev. Mol. Cell Biol. *8*, 715–722.

Serrano, M., Hannon, G.J., and Beach, D. (1993). A new regulatory motif in cell-cycle control causing specific inhibition of cyclin D/CDK4. Nature *366*, 704–707.

Sgarra, R., Lee, J., Tessari, M.A., Altamura, S., Spolaore, B., Giancotti, V., Bedford, M.T., and Manfioletti, G. (2006). The AT-hook of the chromatin architectural transcription factor high mobility group A1a is arginine-methylated by protein arginine methyltransferase 6. J. Biol. Chem. *281*, 3764–3772.

Shi, L., Zhao, G., Qiu, D., Godfrey, W.R., Vogel, H., Rando, T.A., Hu, H., and Kao, P.N. (2005). NF90 regulates cell cycle exit and terminal myogenic differentiation by direct binding to the 3'-untranslated region of MyoD and p21WAF1/CIP1 mRNAs. J. Biol. Chem. *280*, 18981–18989.

Shibutani, S.T., de la Cruz, A.F.A., Tran, V., Turbyfill, W.J., Reis, T., Edgar, B.A., and Duronio, R.J. (2008). Intrinsic negative cell cycle regulation provided by PIP box- and Cul4Cdt2-mediated destruction of E2f1 during S phase. Dev. Cell *15*, 890–900.

Shim, J., Lim, H., R Yates, J., and Karin, M. (2002). Nuclear export of NF90 is required for interleukin-2 mRNA stabilization. Mol. Cell *10*, 1331–1344.

Singhroy, D.N., Mesplède, T., Sabbah, A., Quashie, P.K., Falgueyret, J.-P., and Wainberg, M.A. (2013). Automethylation of protein arginine methyltransferase 6 (PRMT6) regulates its stability and its anti-HIV-1 activity. Retrovirology *10*, 73.

Slebos, R.J., Lee, M.H., Plunkett, B.S., Kessis, T.D., Williams, B.O., Jacks, T., Hedrick, L., Kastan, M.B., and Cho, K.R. (1994). p53-dependent G1 arrest involves pRB-related proteins and is disrupted by the human papillomavirus 16 E7 oncoprotein. Proc. Natl. Acad. Sci. U. S. A. *91*, 5320–5324.

Soria, G., Podhajcer, O., Prives, C., and Gottifredi, V. (2006). P21Cip1/WAF1 downregulation is required for efficient PCNA ubiquitination after UV irradiation. Oncogene *25*, 2829–2838.

Spannhoff, A., Heinke, R., Bauer, I., Trojer, P., Metzger, E., Gust, R., Schüle, R., Brosch, G., Sippl, W., and Jung, M. (2007). Target-based approach to inhibitors of histone arginine methyltransferases. J. Med. Chem. *50*, 2319–2325.

Stein, C., Riedl, S., Rüthnick, D., Nötzold, R.R., and Bauer, U.-M. (2012). The arginine methyltransferase PRMT6 regulates cell proliferation and senescence through transcriptional repression of tumor suppressor genes. Nucleic Acids Res. *40*, 9522–9533.

Storer, M., Mas, A., Robert-Moreno, A., Pecoraro, M., Ortells, M.C., Di Giacomo, V., Yosef, R., Pilpel, N., Krizhanovsky, V., Sharpe, J., et al. (2013). Senescence Is a Developmental Mechanism that Contributes to Embryonic Growth and Patterning. Cell *155*, 1119–1130.

Strahl, B.D., and Allis, C.D. (2000). The language of covalent histone modifications. Nature *403*, 41–45.

Sugasawa, K., Okuda, Y., Saijo, M., Nishi, R., Matsuda, N., Chu, G., Mori, T., Iwai, S., Tanaka, K., Tanaka, K., et al. (2005). UV-induced ubiquitylation of XPC protein mediated by UV-DDB-ubiquitin ligase complex. Cell *121*, 387–400.

Sun, L., Wang, M., Lv, Z., Yang, N., Liu, Y., Bao, S., Gong, W., and Xu, R.-M. (2011). Structural insights into protein arginine symmetric dimethylation by PRMT5. Proc. Natl. Acad. Sci. U. S. A. *108*, 20538–20543.

Sun, Y., Chung, H.H., Woo, A.R.E., and Lin, V.C.-L. (2014). Protein arginine methyltransferase 6 enhances ligand-dependent and -independent activity of estrogen receptor α via distinct mechanisms. Biochim. Biophys. Acta *1843*, 2067–2078.

Takai, H., Smogorzewska, A., and de Lange, T. (2003). DNA damage foci at dysfunctional telomeres. Curr. Biol. *13*, 1549–1556.

Tang, J., Gary, J.D., Clarke, S., and Herschman, H.R. (1998). PRMT 3, a type I protein arginine N-methyltransferase that differs from PRMT1 in its oligomerization, subcellular localization, substrate specificity, and regulation. J. Biol. Chem. *273*, 16935–16945.

Tang, J., Frankel, A., Cook, R.J., Kim, S., Paik, W.K., Williams, K.R., Clarke, S., and Herschman, H.R. (2000a). PRMT1 is the predominant type I protein arginine methyltransferase in mammalian cells. J. Biol. Chem. *275*, 7723–7730.

Tang, J., Kao, P.N., and Herschman, H.R. (2000b). Protein-arginine methyltransferase I, the predominant protein-arginine methyltransferase in cells, interacts with and is regulated by interleukin enhancer-binding factor 3. J. Biol. Chem. *275*, 19866–19876.

Terai, K., Abbas, T., Jazaeri, A.A., and Dutta, A. (2010). CRL4(Cdt2) E3 ubiquitin ligase monoubiquitinates PCNA to promote translesion DNA synthesis. Mol. Cell *37*, 143–149.

Teyssier, C., Chen, D., and Stallcup, M.R. (2002). Requirement for multiple domains of the protein arginine methyltransferase CARM1 in its transcriptional coactivator function. J. Biol. Chem. *277*, 46066–46072.

Thoma, F., Koller, T., and Klug, A. (1979). Involvement of histone H1 in the organization of the nucleosome and of the salt-dependent superstructures of chromatin. J. Cell Biol. *83*, 403–427.

Thomas, D., Lakowski, T.M., Pak, M.L., Kim, J.J., and Frankel, A. (2010). Förster resonance energy transfer measurements of cofactor-dependent effects on protein arginine N-methyltransferase homodimerization. Protein Sci. *19*, 2141–2151.

Toussaint, O., Remacle, J., Dierick, J.-F., Pascal, T., Frippiat, C., Zdanov, S., Magalhaes, J.P., Royer, V., and Chainiaux, F. (2002). From the Hayflick mosaic to the mosaics of ageing. Role of stress-induced premature senescence in human ageing. Int. J. Biochem. Cell Biol. *34*, 1415–1429.

Troffer-Charlier, N., Cura, V., Hassenboehler, P., Moras, D., and Cavarelli, J. (2007). Functional insights from structures of coactivator-associated arginine methyltransferase 1 domains. EMBO J. *26*, 4391–4401.

Tropberger, P., and Schneider, R. (2010). Going global: novel histone modifications in the globular domain of H3. Epigenetics *5*, 112–117.

Vieira, F.Q., Costa-Pinheiro, P., Ramalho-Carvalho, J., Pereira, A., Menezes, F.D., Antunes, L., Carneiro, I., Oliveira, J., Henrique, R., and Jerónimo, C. (2014). Deregulated expression of selected histone methylases and demethylases in prostate carcinoma. Endocr. Relat. Cancer *21*, 51–61.

Waldmann, T., Izzo, A., Kamieniarz, K., Richter, F., Vogler, C., Sarg, B., Lindner, H., Young, N.L., Mittler, G., Garcia, B.A., et al. (2011). Methylation of H2AR29 is a novel repressive PRMT6 target. Epigenetics Chromatin *4*, 11.

Wang, Y.-C., and Li, C. (2012). Evolutionarily conserved protein arginine methyltransferases in non-mammalian animal systems. FEBS J. *279*, 932–945.

Wang, C., Zhu, Y., Chen, J., Li, X., Peng, J., Chen, J., Zou, Y., Zhang, Z., Jin, H., Yang, P., et al. (2014). Crystal Structure of Arginine Methyltransferase 6 from Trypanosoma brucei. PLoS One *9*, e87267.

Wang, H., Zhai, L., Xu, J., Joo, H.-Y., Jackson, S., Erdjument-Bromage, H., Tempst, P., Xiong, Y., and Zhang, Y. (2006). Histone H3 and H4 ubiquitylation by the CUL4-DDB-ROC1 ubiquitin ligase facilitates cellular response to DNA damage. Mol. Cell *22*, 383–394.

Wang, X., Huang, Y., Zhao, J., Zhang, Y., Lu, J., and Huang, B. (2012a). Suppression of PRMT6-mediated arginine methylation of p16 protein potentiates its ability to arrest A549 cell proliferation. Int. J. Biochem. Cell Biol. *44*, 2333–2341.

Wang, X.-Y., Keefe, K.M., Jensen-Taubman, S.M., Yang, D., Yan, K., and Linnoila, R.I. (2012b). Novel method for isolation of murine clara cell secretory protein-expressing cells with traces of stemness. PLoS One *7*, e43008.

Wang, Y., Wysocka, J., Sayegh, J., Lee, Y.-H., Perlin, J.R., Leonelli, L., Sonbuchner, L.S., McDonald, C.H., Cook, R.G., Dou, Y., et al. (2004). Human PAD4 regulates histone arginine methylation levels via demethylimination. Science *306*, 279–283.

Webby, C.J., Wolf, A., Gromak, N., Dreger, M., Kramer, H., Kessler, B., Nielsen, M.L., Schmitz, C., Butler, D.S., Yates, J.R., et al. (2009). Jmjd6 catalyses lysyl-hydroxylation of U2AF65, a protein associated with RNA splicing. Science *325*, 90–93.

Wei, S., and Sedivy, J.M. (1999). Expression of catalytically active telomerase does not prevent premature senescence caused by overexpression of oncogenic Ha-Ras in normal human fibroblasts. Cancer Res. *59*, 1539–1543.

Weiss, V.H., McBride, A.E., Soriano, M.A., Filman, D.J., Silver, P.A., and Hogle, J.M. (2000). The structure and oligomerization of the yeast arginine methyltransferase, Hmt1. Nat. Struct. Biol. *7*, 1165–1171.

Woods, D., Parry, D., Cherwinski, H., Bosch, E., Lees, E., and McMahon, M. (1997). Raf-induced proliferation or cell cycle arrest is determined by the level of Raf activity with arrest mediated by p21Cip1. Mol. Cell. Biol. *17*, 5598–5611.

Xie, B., Invernizzi, C.F., Richard, S., and Wainberg, M.A. (2007). Arginine methylation of the human immunodeficiency virus type 1 Tat protein by PRMT6 negatively affects Tat Interactions with both cyclin T1 and the Tat transactivation region. J. Virol. *81*, 4226–4234.

Xu, W., Cho, H., Kadam, S., Banayo, E.M., Anderson, S., Yates, J.R., Emerson, B.M., and Evans, R.M. (2004). A methylation-mediator complex in hormone signaling. Genes Dev. *18*, 144–156.

Yadav, N., Lee, J., Kim, J., Shen, J., Hu, M.C.-T., Aldaz, C.M., and Bedford, M.T. (2003). Specific protein methylation defects and gene expression perturbations in coactivator-associated arginine methyltransferase 1-deficient mice. Proc. Natl. Acad. Sci. U. S. A. *100*, 6464–6468.

Yang, Y., and Bedford, M.T. (2013). Protein arginine methyltransferases and cancer. Nat. Rev. Cancer *13*, 37–50.

Yang, Y.-L., Hung, M.-S., Wang, Y., Ni, J., Mao, J.-H., Hsieh, D., Au, A., Kumar, A., Quigley, D., Fang, L.T., et al. (2014). Lung tumourigenesis in a conditional Cul4A transgenic mouse model. J. Pathol. *233*, 113–123.

Yoshimatsu, M., Toyokawa, G., Hayami, S., Unoki, M., Tsunoda, T., Field, H.I., Kelly, J.D., Neal, D.E., Maehara, Y., Ponder, B.A.J., et al. (2011). Dysregulation of PRMT1 and PRMT6, Type I arginine methyltransferases, is involved in various types of human cancers. Int. J. Cancer *128*, 562–573.

Yu, Z., Chen, T., Hébert, J., Li, E., and Richard, S. (2009). A mouse PRMT1 null allele defines an essential role for arginine methylation in genome maintenance and cell proliferation. Mol. Cell. Biol. *29*, 2982–2996.

Yue, W.W., Hassler, M., Roe, S.M., Thompson-Vale, V., and Pearl, L.H. (2007). Insights into histone code syntax from structural and biochemical studies of CARM1 methyltransferase. EMBO J. *26*, 4402–4412.

Zakrzewicz, D., Zakrzewicz, A., Preissner, K.T., Markart, P., and Wygrecka, M. (2012). Protein Arginine Methyltransferases (PRMTs): Promising Targets for the Treatment of Pulmonary Disorders. Int. J. Mol. Sci. *13*, 12383–12400.

Zhang, X., and Cheng, X. (2003). Structure of the predominant protein arginine methyltransferase PRMT1 and analysis of its binding to substrate peptides. Structure *11*, 509–520.

Zhang, X., Zhou, L., and Cheng, X. (2000). Crystal structure of the conserved core of protein arginine methyltransferase PRMT3. EMBO J. *19*, 3509–3519.

Zhao, X., Jankovic, V., Gural, A., Huang, G., Pardanani, A., Menendez, S., Zhang, J., Dunne, R., Xiao, A., Erdjument-Bromage, H., et al. (2008). Methylation of RUNX1 by PRMT1 abrogates SIN3A binding and potentiates its transcriptional activity. Genes Dev. *22*, 640–653.

Zobel-Thropp, P., Gary, J.D., and Clarke, S. (1998). delta-N-methylarginine is a novel posttranslational modification of arginine residues in yeast proteins. J. Biol. Chem. *273*, 29283–29286.

Zou, Y., Webb, K., Perna, A.D., Zhang, Q., Clarke, S., and Wang, Y. (2007). A mass spectrometric study on the in vitro methylation of HMGA1a and HMGA1b proteins by PRMTs: methylation specificity, the effect of binding to AT-rich duplex DNA, and the effect of C-terminal phosphorylation. Biochemistry *46*, 7896–7906.

Zurita-Lopez, C.I., Sandberg, T., Kelly, R., and Clarke, S.G. (2012). Human Protein Arginine Methyltransferase 7 (PRMT7) Is a Type III Enzyme Forming -NG-Monomethylated Arginine Residues. J. Biol. Chem. *287*, 7859–7870.

8 APPENDIX

8.1 Supplementary figures

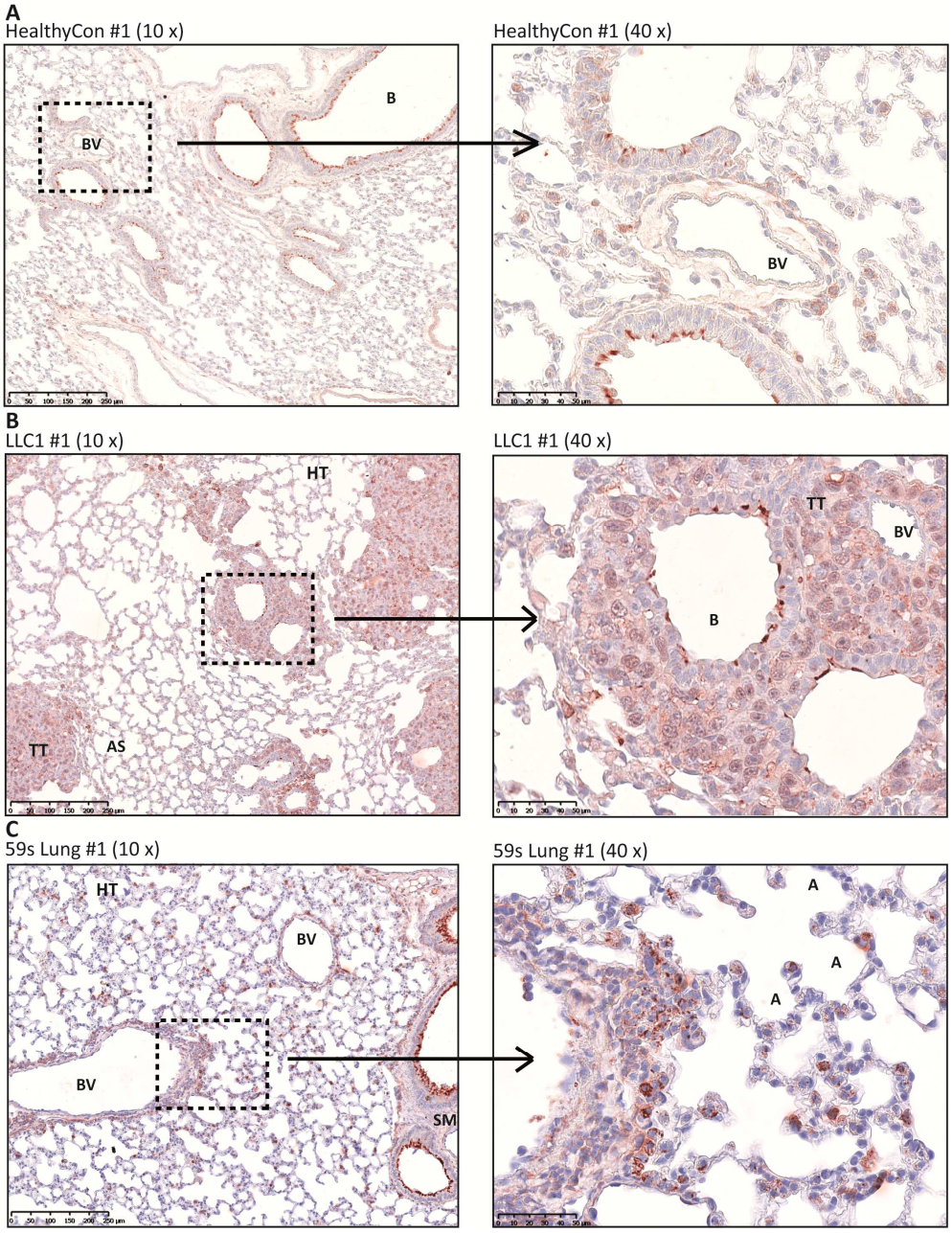

Figure S1: IHC stainings of Prmt6 in lung sections from C57BL/6, LLC1 and Kras^{LA2} mice (PRMT6_3affi).

(**A - C**) A representative image of a lung tissue section from a (**A**) healthy C57BL/6 (HealthyCon #1), (**B**) LLC1 (LLC #1) and (**C**) Kras^{LA2} mouse (59s Lung #1) was photographed using an affinity-purified PRMT6 antibody (PRMT6_3affi, 1:50; AEC, red) and Hematoxylin for counterstaining (blue). For each section a 10 x magnification (left panel, maximal scale bar length: 250 µm) and a 40 x magnification (right panel, maximal scale bar length: 50 µm) is shown. A: alveolus, AS: alveolar sac, B: bronchiole, BV: blood vessel, HT: healthy tissue, SM: smooth muscle, TT: tumour tissue.

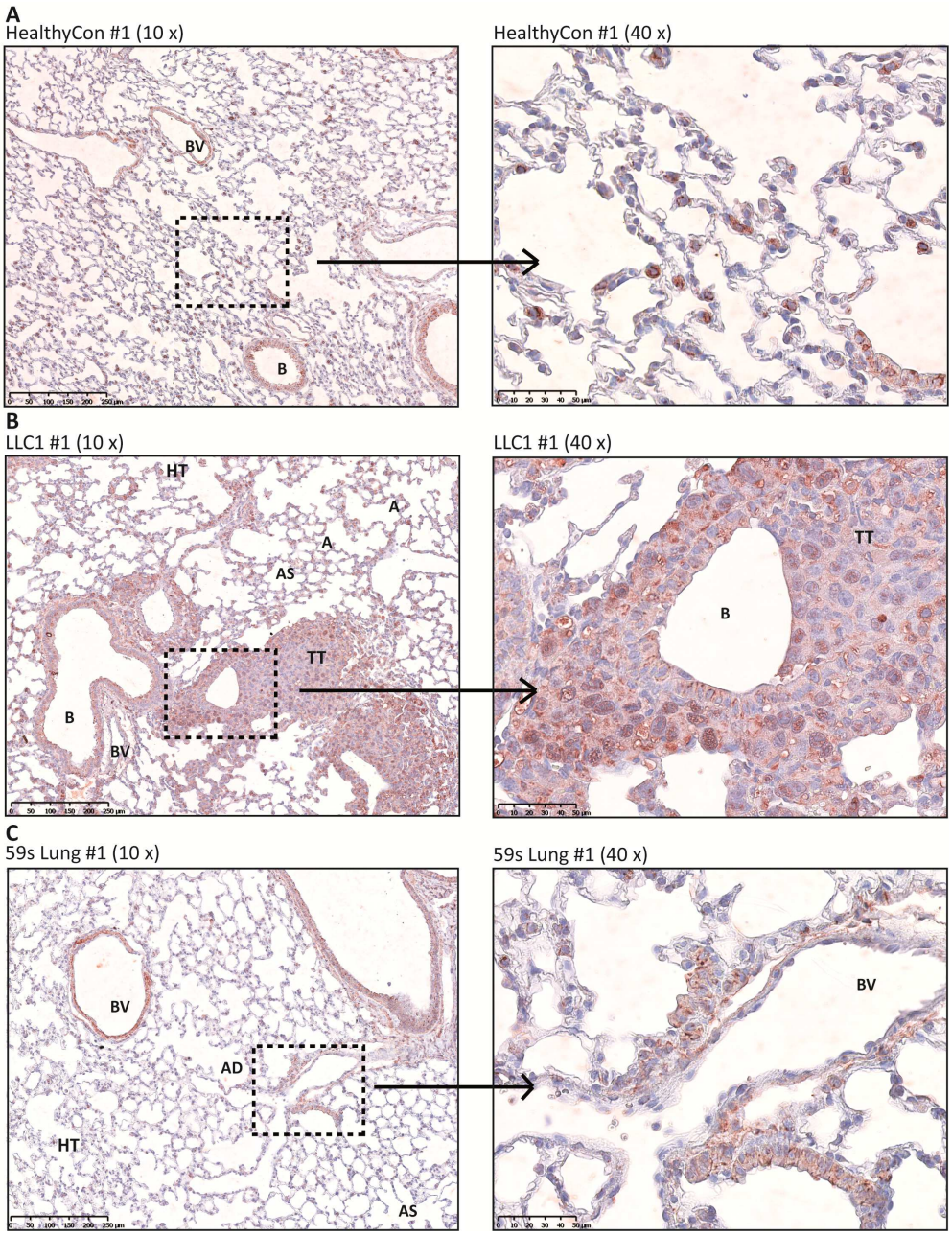

Figure S2: IHC stainings of Prmt6 in murine C57BL/6, LLC1 and Kras^{LA2} lung specimen (PRMT6_bethyl).

(**A - C**) A representative image of a lung tissue section from a (**A**) healthy C57BL/6 (HealthyCon #1), (**B**) LLC1 (LLC #1) and (**C**) Kras^{LA2} mouse (59s Lung #1) is shown. Stainings were performed using a commercial PRMT6 antibody from Bethyl Laboratories (PRMT6_bethyl, 1:100; AEC, red) with Hematoxylin for counterstaining. Each staining is depicted in a 10 x magnification (left panel, maximal scale bar length: 250 µm) and a 40 x magnification (right panel, maximal scale bar length: 50 µm). A: alveolus, AD: alveolar duct, AS: alveolar sac, B: bronchiole, BV: blood vessel, HT: healthy tissue, TT: tumour tissue.

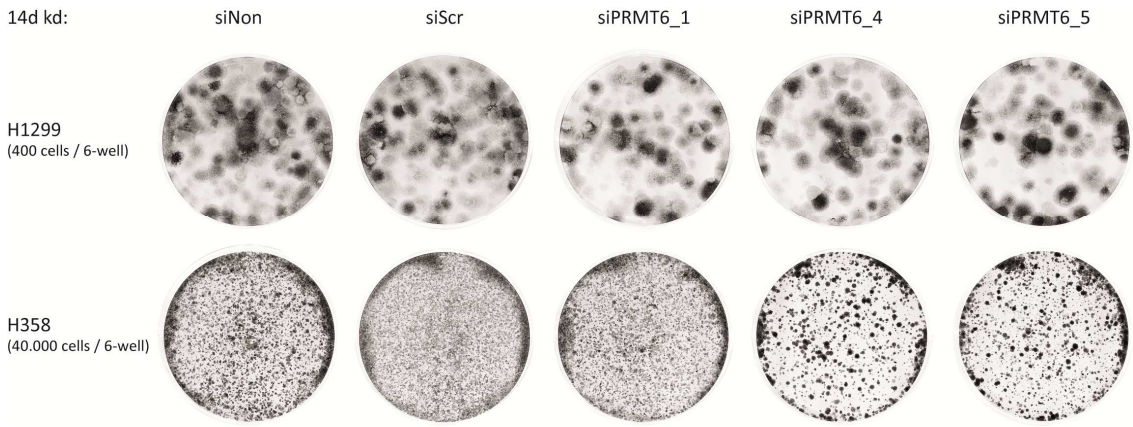

Figure S3: Clonogenic growth of H358 (high PRMT6 level) and of H1299 cells (moderate PRMT6 level) is affected after 14 days of *PRMT6* depletion.

H1299 or H358 cells were transfected with three alternative siRNAs directed against *PRMT6* (siPRMT6_1, siPRMT6_4 or siPRMT6_5) compared to the control transfections siNontargeting (siNon) or siScramble (siScr) using LipoRNAiMAX. 48 hours post-transfection either 400 cells (H1299) or 40.000 cells (H358) were replated in triplicates in a 6-well plate for a colony formation assay (CFA). Colonies were stained with crystal violet after 14 days of siRNA transfection. Representative dishes of crystal violet-stained dishes were photographed of H1299 (upper panel) and H358 (lower panel) at the indicated time point. The experiment was performed once.

8.2 List of abbreviations and acronyms

Amino acids are abbreviated with the common single letter code. The nucleotides Adenine, Cytosine, Guanine and Thymine are abbreviated with A, C, G and T, respectively. Post-translational modifications of histones are referred to with the abbreviation of the corresponding histone (H1, H3, H4, H2A or H2B), the amino acid residue in the single letter code including its position within the amino acid sequence and the modification state, which could be either symmetrically or asymmetrically methylated, in case of the methylation by protein arginine methyltransferases (e.g. me2a, me2s, me3, ac). Therefore, histone modifications are abbreviated for instance as H3R2me2a or H2AR29me2.

α	anti
4-OHT	4-hydroxytamoxifen
ac	acetyl/acetylated
ADMA	ω-N^G,N^G-asymmetric dimethylarginine
AdoHcy	S-adenosylhomocysteine
AdoMet	S-adenosyl-L-methionine
APS	ammonium persulfate
ASH2	absent, small, or homeotic discs 2
ATM	ataxia telangiectasia mutated
ATR	ataxia telangiectasia and Rad3-related
AURKB	aurora kinase B
BBC3 (PUMA)	BCL2 binding component 3
BER	base excision repair
bp	base pair
BRAF-ER	fusion protein of the LBD of ER with the kinase B-rapidly accelerated fibrosarcoma (constitutively expressed)
BRCA1	breast cancer 1, early onset
BSA	bovine serum albumine
BTG1	B-cell translocation gene 1
BTG2	BTG family, member 2
C-	carboxy-/carboxyl-
C57BL/6	common inbred strain of laboratory mouse
CARM1	coactivator-associated arginine methyltransferase 1
CCNA2	cyclin A2

CCND1	cyclin D1
CCNE1	cyclin E1
CDK	cyclin-dependent kinase
CDKN1A	cyclin-dependent kinase inhibitor 1A (p21, Cip1)
CDKN1B	cyclin-dependent kinase inhibitor 1B (p27, Kip1)
CDKN1C	cyclin-dependent kinase inhibitor 1C (p57, Kip2)
CDKN2A	cyclin-dependent kinase inhibitor 2A
cDNA	complementary DNA
CDT1	chromatin licensing and DNA replication factor 1
ChIP	chromatin immunoprecipitation
ChIP-qPCR	chromatin immunoprecipitation-quantitiative PCR
CHK2	checkpoint kinase 2
chromo	chromatin organisation modifier
chromodomain	chromatin organisation modifier domain
CORP5	cooperator of PRMT5
CRL4	CUL4A-RING ubiquitin E3-ligase complex
CRTC2	CREB-regulated transcriptional coactivator 2
Ct	threshold cycle
CUL4A	cullin 4A
DART	*Drosophila* arginine methyltransferase
DDB1	damage-specific DNA binding protein 1, 127kDa
DDB2	damage-specific DNA binding protein 2, 48kDa
ddH_2O	bidistilled water
DHX9	DEAH (Asp-Glu-Ala-His) box helicase 9
DMEM	Dulbecco´s modified Eagle´s medium
DMF	dimethylformamide
DMSO	dimethyl sulfoxide
DNA	deoxyribonucleic acid
dsDNA	double-stranded DNA
DTT	dithiotreithol
E. coli	*Escherichia coli*
E2F1	E2F transcription factor 1
ECL	enhanced chemiluminescence
EDTA	ethylenediaminetetraacetic acid
ER	estrogen receptor
ESC	embryonic stem cell
EZH2	enhancer of zeste 2 polycomb repressive complex 2 subunit

FACS	fluorescence-activated cell sorting
FCS	fetal calf serum
FGFR	fibroblast growth factor receptor
FMOD	fibromodulin
FT	freeze and thaw
fwd	forward
g	gravity
g	gram
G0-phase	gap phase 0
G1-phase	gap phase 1
GADD45	growth arrest and DNA-damage
GAR	glycine-arginine-rich
GFP	green fluorescent protein
GG-NER	global genome nucleotide excision repair
GR	glucocorticoid receptor
GST	glutathione-S-transferase
hCAF1	CCR4-associated factor 1
HEPES	4-(2-hydroxyethyl)piperazine-1-ethanesulfonic acid
HIF-1	hypoxia-inducible factor 1
His	histidine
HIV	human immunodeficiency virus
HMGA	high mobility group A
HMT1	hnRNP methyltransferase 1
hnRNP	heterogeneous nuclear ribonucleoprotein
HOX	Homeobox
HP1	heterochromatin protein 1
HRP	horseradish peroxidase
HSL7	histone synthetic lethal 7
IgG	immunoglobulin G
ILF2	interleukin enhancer binding factor 2
ILF3	interleukin enhancer binding factor 3, 90kDa
IP	immunoprecipitation
JBP1	Janus kinase-binding protein 1
JMJD6	Jumonji domain-containing 6 protein
kb	kilobase
kd	knockdown
kDa	kilo dalton

LB	lysogeny broth
LBD	ligand binding domain
M	molar
MAPK	mitogen-activated protein kinase
MDM2	mouse double minute 2 homolog (alias proto-oncogene, E3 ubiquitin protein ligase)
me	methyl/methylated
MEF	mouse embryonic fibroblast
MEP50	methylosome protein 50
miRNA	micro-ribonucleic acid
MLL	mixed-lineage leukemia
MMA	ω-N^G-monomethylarginine
mRNA	messenger ribonucleic acid
MS	mass spectrometry
MYC	v-myc avian myelocytomatosis viral oncogene homolog
N-	amino-
NC	nucleocapsid
NCBI	National Center for Biotechnology Information
ncRNA	non-coding RNA
NR	nuclear receptor
NSCLC	non-small cell lung cancer
NUMAC	nucleosomal methylation activator complex
OIS	oncogene-induced senescence
ON	over night
ORF	open reading frame
PADI4	peptidylarginine deiminase 4
PBS	phosphate buffered saline
PCNA	proliferating cell nuclear antigen
PCR	polymerase chain reaction
PDK1	pyruvate dehydrogenase kinase, isozyme 1
PEI	polyethylenimine
PHD	plant homeodomain
PMSF	phenylmethanesulfonyl fluoride
Pol	polymerase
PR	progesterone receptor
PRC2	Polycomb repressive complex 2
PRMT	protein arginine methyltransferase

PS	penicillin/streptomycin
PTM	post-translational modification
PVDF	polyvinylidene difluoride
qPCR	quantitative PCR
RB1	retinoblastoma 1
RBBP4 (RbAp48)	retinoblastoma binding protein 4
RBBP5	retinoblastoma binding protein 5
RBBP7 (RbAp46)	retinoblastoma binding protein 7
rev	reverse
Rev	regulator of viral protein expression
RHA	ATP-dependent RNA helicase A
Rmt1	type I protein arginine N-methyltransferase Rmt1
RNA	ribonucleic acid
RNAi	RNA interference
ROS	reactive oxygen species
ROX	6-carboxyl-X-rhodamine
RPLP0	ribosomal protein, large, P0
rpm	revolutions per minute
RPS14	ribosomal protein S14
RT	room temperature
RT-qPCR	real-time quantitative PCR
RUNX1	runt-related transcription factor 1
SAHF	senescence-associated heterochromatin foci
SA-ß-gal	senescence-associated ß-galactosidase
SCLC	small cell lung cancer
SDF	senescence-associated DNA damage foci
SDMA	ω-N^{G},$N^{'G}$-symmetric dimethylarginine
SDS	sodium dodecyl sulfate
SDS-PAGE	sodium dodecyl sulfate polyacrylamide gel electrophoresis
SH3	Src homology 3
SHR	steroid hormone receptor
shRNA	short hairpin RNA
SIN3A	SIN3 transcription regulator family member A
siRNA	small interfering RNA
Skb1	Shk1 kinase-binding protein 1
Skp1	S-phase-kinase-associated protein-1
SMARCA2 (BRM)	SWI/SNF related, matrix associated, actin dependent regulator of

	chromatin, subfamily a, member 2
SMARCA4 (BRG1)	SWI/SNF related, matrix associated, actin dependent regulator of chromatin, subfamily a, member 4
S-phase	DNA synthesis phase
ssDNA	single-stranded DNA
SUMO	small ubiquitin-like modifier
SWI/SNF	SWItch/Sucrose NonFermentable
TAP	tandem affinity purification
Tat	transactivator
TBE	TRIS-borate-EDTA
TBS	TRIS-buffered saline
TE	TRIS buffered EDTA
TEMED	tetramethylethylenediamine
TGF-ß	transforming growth factor ß
THBS1	Thrombospondin-1
THW	threonine-histidine-tryptophan
TP53	tumour protein p53
TRIS	tris(hydroxylmethyl)aminomethane
TSS	transcriptional start site
TV	transcript variant
UBC	ubiquitin C
v/v	volume per volume
VEGF	vascular endothelial growth factor
w/v	weight per volume
Wb	Western blot
WDR5	WD-repeat domain 5
wt	wild type
X-gal	5-bromo-4-chloro-3-indolyl-β-D-galactopyranoside
XPC	xeroderma pigmentosum complementation group C

In order to distinguish between genes, transcripts and proteins the following nomenclature was used in this study:

Genes and transcripts, e.g.	*PRMT6*	(human)
	Prmt6	(mouse)
Proteins, e.g.	PRMT6	(human)
	Prmt6	(mouse)

8.3 List of academic teachers

My academic teachers at the Julius Maximilian University of Würzburg were:

Berberich, PD Dr. I.

Bringmann, Prof. Dr. G.

Buchner, Prof. Dr. E.

Büttner, Dr. K.

Fischer, Prof. Dr. U.

Goebel, Prof. Dr. W.

Gross, Prof. Dr. R.

Hacker, Prof. Dr. J.

Hedrich, Prof. Dr. R.

Heisenberg, Prof. Dr. M.

Hentschel Humeida, Prof. Dr. U.

Hock, Priv.-Doz. Dr. R.

Kreft, Prof. Dr. J.

Kreß, Dr. W.

Krohne, Prof. Dr. G.

Moll, Prof. Dr. H.

Ohlsen, Dr. K.

Rdest, Dr. U.

Riederer, Prof. Dr. M.

Rommel, Dr. E.

Rössler, Prof. Dr. W.

Rühl, Prof. Dr. E.

Scheer, Prof. Dr. U.

Schmid, Prof. Dr. M.

Schneider-Schaulies, Prof. Dr. J.

8.4 Ehrenwörtliche Erklärung

Ich erkläre ehrenwörtlich, dass ich die dem Fachbereich Medizin Marburg zur Promotionsprüfung eingereichte Arbeit mit dem Titel "Functional analysis of the histone arginine methyltransferase PRMT6" im Institut für Molekularbiologie und Tumorforschung unter Leitung von Prof. Dr. Rolf Müller mit Unterstützung durch Prof. Dr. Uta-Maria Bauer ohne sonstige Hilfe selbst durchgeführt und bei der Abfassung der Arbeit keine anderen als die in der Dissertation aufgeführten Hilfsmittel benutzt habe. Ich habe bisher an keinem anderen in- oder ausländischen Medizinischen Fachbereich ein Gesuch um Zulassung zur Promotion eingereicht, noch die vorliegende oder eine andere Arbeit als Dissertation vorgelegt.

Teile der vorliegenden Arbeit wurden in folgendem Publikationsorgan veröffentlicht:

Stein C*, **Riedl S***, Rüthnick D, Nötzold RR, Bauer UM. (2012).
The arginine methyltransferase PRMT6 regulates cell proliferation and senescence through transcriptional repression of tumor suppressor genes. Nucleic Acids Res. 40(19):9522-33. (*joint first authors)

Marburg, den 15.12.2014

Stefanie Riedl